May 2015

Conceptual Design of Wind Farms Through Novel Multi-Objective Swarm Optimization

Weiyang Tong
Syracuse University

ABSTRACT

Wind is one of the major sources of clean and renewable energy, and global wind energy has been experiencing a steady annual growth rate of more than 20% over the past decade. In the U.S. energy market, although wind energy is one of the fastest increasing sources of electricity generation (by annual installed capacity addition), and is expected to play an important role in the future energy demographics of this country, it has also been plagued by project underperformance and concept-to-installation delays.

There are various factors affecting the quality of a wind energy project, and most of these factors are strongly coupled in their influence on the socio-economic, production, and environmental objectives of a wind energy project. To develop wind farms that are profitable, reliable, and meet community acceptance, it is critical to accomplish balance between these objectives, and therefore a clean understanding of how different design and natural factors jointly impact these objectives is much needed.

In this research, a *Multi-objective Wind Farm Design* (MOWFD) methodology is developed, which analyzes and integrates the impact of various factors on the conceptual design of wind farms. This methodology contributes three major advancements to the wind farm design paradigm: (I) provides a new understanding of the impact of key factors on the wind farm performance under the use of different wake models; (II) explores the crucial tradeoffs between energy production, cost of energy, and the quantitative role of land usage in wind farm layout optimization (WFLO); and (III) makes novel advancements on mixed-discrete particle swarm optimization algorithm through a multi-domain diversity preservation concept, to solve complex multi-objective optimization (MOO) problems.

A comprehensive sensitivity analysis of the wind farm power generation is performed to understand and compare the impact of land configuration, installed capacity decisions, incoming wind speed, and ambient turbulence on the performance of conventional array layouts and optimized wind farm layouts. For array-like wind farms, the relative importance of each factor was found to vary significantly with the choice of wake models, i.e., appreciable differences in the sensitivity indices (of up to 70%) were observed across the different wake models. In contrast, for optimized wind farm layouts, the choice of wake models was observed to have no significant impact on the sensitivity indices.

The MOWFD methodology is designed to explore the tradeoffs between the concerned performance objectives and simultaneously optimize the location of turbines, the type of turbines, and the land usage. More importantly, it facilitates WFLO without prescribed conditions (e.g., fixed wind farm boundaries and number of turbines), thereby allowing a more flexible exploration of the feasible layout solutions than is possible with other existing WFLO methodologies. In addition, a novel parameterization of the Pareto is performed to quantitatively explore how the best tradeoffs between energy production and land usage vary with the installed capacity decisions. The key to the various complex MO-WFLOs performed here is the unique set of capabilities offered by the new Multi-Objective Mixed-Discrete Particle Swarm Optimization (MO-MDPSO) algorithm, developed, tested and extensively used in this dissertation.

The MO-MDPSO algorithm is capable of dealing with a plethora of problem complexities, namely: multiple highly nonlinear objectives, constraints, high design space dimensionality, and a mixture of continuous and discrete design variables. Prior to applying MO-MDPSO to effectively solve complex WFLO problems, this new algorithm was tested on a large and diverse suite of popular benchmark problems; the convergence and Pareto cov-

erage offered by this algorithm was found to be competitive with some of the most popular MOO algorithms (e.g., GAs). The unique potential of the MO-MDPSO algorithm is further established through application to the following complex practical engineering problems: (I) a disc brake design problem, (II) a multi-objective wind farm layout optimization problem, simultaneously optimizing the location of turbines, the selection of turbine types, and the site orientation, and (III) simultaneously minimizing land usage and maximizing capacity factors under varying land plot availability.

CONCEPTUAL DESIGN OF WIND FARMS THROUGH NOVEL MULTI-OBJECTIVE SWARM OPTIMIZATION

By

Weiyang Tong

B.E., Beihang University, 2005

M.S., Beihang University, 2009

M.S., Syracuse University, 2011

Dissertation
Submitted in Partial Fulfillment of the Requirements for the Degree of
Doctor of Philosophy in Mechanical Engineering
in the Graduate School of Syracuse University

Syracuse University
Syracuse, New York
May, 2015

DEDICATION

I dedicate this thesis to my maternal grandmother, Yushan Wang, who raised me, loved me, and always believed in me.

I also dedicate this thesis to my paternal grandmother, Anqi Yang, who was a great woman of endless patience, eternal kindness, and boundless love.

ACKNOWLEDGMENT

I would like to express my deepest appreciation towards my advisor, Prof. Achille Messac, for his immense help throughout my doctoral studies. Prof. Messac provided me with invaluable advice and technical supervision that formed the foundation of the research presented in this dissertation and in the several well regarded journal articles that I have authored/co-authored thereof. He also inculcated in me a spirit of professionalism that greatly contributed to my professional growth. I am thankful for his devotion to my future. Without his guidance, and persistent support, this dissertation would not have been possible.

I would also like also to thank my co-advisor, Dr. Souma Chowdhury. Souma has been a tremendous mentor, an excellent colleague, and a great friend. I am thankful for the superb example he set as an outstanding scholar and former student of Prof. Messac's. The enthusiasm, inspiration, and sharp insights he has on research will always remain an excellent source of motivation for me in my future career.

I would like to thank my doctoral committee members, Prof. Utpal Roy, Prof. John Dannenhoffer, Prof. Jeongmin Ahn, Prof. Benjamin Akih-Kumgeh, and my committee chair Prof. Can Isik, for their valuable advice and comments, as well as their willingness to serve on my committee. Special thanks to Prof. Roy and Prof. Dannenhoffer, who have been supportive in many ways within the MAE department in Syracuse University.

I wish to extend my warmest thanks to my former and present colleagues, Dr. Jie Zhang, Dr. Junqiang Zhang, Samuel Notaro, and my dear friend Ali Mehmani, who have helped me in many different ways at the Multidisciplinary Design and Optimization Laboratory. I greatly appreciate their friendship, and their contributions to my research and this

dissertation. I am also grateful to my closest friends, Xiaomeng Li, Ang Gao, Jia Li, Xu Meng, Zi Wang, Bensong Yu, and Zhen Liu, who cheered me up even in the worst of times and made my life (far away from home) fun. Special thanks to "Fly Empire" and "Starkville Soccer Group", you gave me a lot of happiness and helped through the tough times.

Sponsorship of this work by the National Science Foundation awards CMMI-1100948, and CMMI-1437746 is also gratefully acknowledged.

These acknowledgements would not be complete without thanking the wonderful staff at Syracuse University, including Kathleen Datthyn-Madigan, Kimberly Drumm-Underwood, Kristin Shapiro, Linda Manzano, and Deborah Brown at the MAE department, and Cathy Mentor at the Sluztker Center, for all their efforts.

Finally, my deepest thanks go to my family; I would like to express my sincere gratitude to my parents, Lian Yu and Jun Tong, whose love and encouragement have always been my greatest strength; and I am also grateful to my uncle Fu Tong and my aunt Xiulian Zheng, who have always been supportive of all my academic endeavors.

CONTENTS

LIST OF TABLES

LIST OF FIGURES

LIST OF ACRONYMS

AEP Annual Energy Production

COE Cost of Energy

GAs Genetic Algorithms

LAMI land area per MW installed

LAT land area per turbine

LCOE Levelized Cost of Energy

MDPSO Mixed-Discrete Particle Swarm Optimization

MOWFD Multi-Objective Wind Farm Design

MOMDO Multi-Objective Mixed-Discrete Optimization

MO-MDPSO Multi-Objective Mixed-Discrete Particle Swarm Optimization

MOO Multi-Objective Optimization

MO-WFLO Multi-Objective Wind Farm Layout Optimization

NC Nameplate Capacity

NSGA-II Non-dominated Sorting Genetic Algorithm II

PSO Particle Swarm Optimization

SA sensitivity analysis

SAA Simulated Annealing Algorithm

SBR smallest bounding rectangle

UWFLO Unrestricted Wind Farm Layout Optimization

WFLO Wind Farm Layout Optimization

WTDCS Wind Turbine Design Cost and Scaling

PART I

Technical Preliminaries

CHAPTER 1

Research Motivation and Objective

In this chapter, the research motivation and objectives are presented. An outline for the dissertation is also provided.

1.1 Overview of Wind Farm Development

Wind energy is one of the most cost-effective and renewable sources of clean electricity generation. A total of nearly 35 GW of new wind capacity was installed around the world in 2013. The global cumulative installed wind capacity reached 318.1 GW by the end of 2013, resulting in a cumulative market growth of 12.5% [1]. As shown in Fig. 1.1(a) the global cumulative installed wind capacity between the years of 1996 and 2013, although it is the first time for nearly 20 years that the global annual market for wind energy shrank in 2013, the trend of cumulative market growth (as shown in Fig. 1.1(b)) indicates an increasing need of wind energy.

Despite of the precipitous drop in U.S. wind energy installation in 2012 (in the wake of uncertainty regarding Product Tax Credit), U.S. was ranked number one in the world in 2013 in terms of wind energy production [2]. In the last year, wind power added significantly more new electricity than any other resource. Based on the data from the U.S. Energy Information Administration (EIA), renewable energy sources (including hydropower) delivered more than 13% of all electricity in America in 2014; whereas wind contributed 4.4% of the total [2, 3]. Additionally, an increasing geographic diversity was observed with the boom in wind farm development − wind energy provided more than 15 percent of electricity in a total of seven

states, more than 10 percent in a total of nine states, and more than five percent in a total of 19 states [2]. However, significant improvements to wind energy technologies and cost declines are needed to convincingly march towards the targeted "20% Wind Scenario" – whereby wind energy will provide 20% of U.S. electricity needs by 2030 [4].

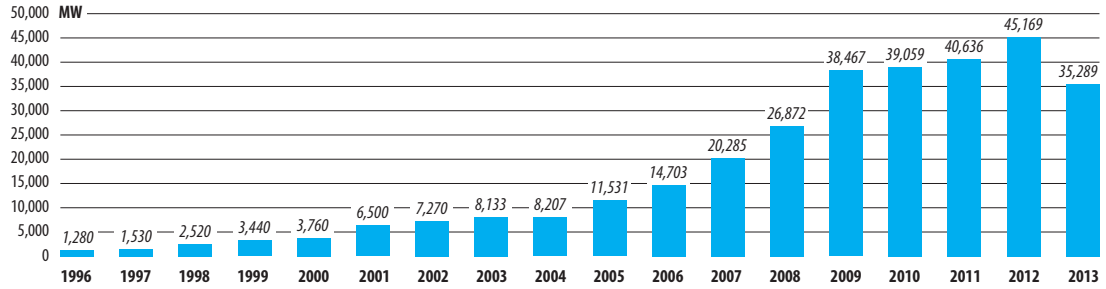

(a) Global Annual Installed Wind Capacity

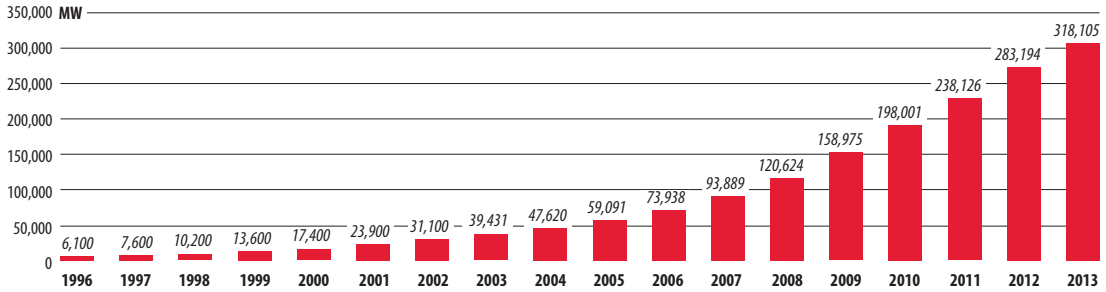

(b) Global Cumulative Installed Wind Capacity

Figure 1.1: Trend of Global Installed Wind Capacity 1996-2013 [1]

Sections 1.1.1 – 1.1.3 briefly introduces the economic, engineering, and environmental aspects of wind farm development.

1.1.1 Economic Aspect

The economic feasibility of a wind energy project is decided based on several factors. The underlying correlation between these factors needs to be analyzed to acquire a quantitative understanding of the challenges in wind farm design.

Generally, there are four cost factors strongly affecting the economics of energy sys-

tems [5]: (i) capital cost, (ii) operation and maintenance cost, (iii) fuel cost, and (iv) external cost. Here, the fuel cost and external cost are sensitive to the type of fuels. In addition, market and policy parameters (e.g., Incentive Program, Production Tax Credit, and discount/inflation rates) have a strong influence on evaluating the economic performance of an energy system.

Key elements governing the economics of a wind energy project are listed below [6, 7]:

- Investment costs;
- Operation and maintenance cost;
- electricity production cost (or capacity factor);
- Operational lifetime; and
- Capital cost.

Wind is capital intensive due to the requirement of high initial investment. However, on the upfront wind energy project costs can be lower than that of most new conventional energy installations, which makes wind energy one of the most cost-effective clean energy technologies. Table 1.1 summarizes the brakedown of the total installed capital cost for typical onshore/offshore wind energy projects [8–10]. In fact, the price of U.S. wind energy has reduced dramatically (90%) since early 1980s, benefitting from the technological and U.S.-based manufacturing improvements.

The *Levelized Cost of Energy (LCOE)* is the primary metric for describing and comparing the underlying economics of wind energy (or other renewable energy) projects. The LCOE represents the cost (generally in $\$/kW \cdot h$) for building, operating, and maintaining a wind farm over an estimated financial lifetime with financial flows discounted to a common

Table 1.1: Capital Cost Breakdown for Typical Onshore/Offshor Wind Energy Projects in 2011 [11]

Shares	Onshore (%)	Offshore (%)
Wind turbine cost[1]	64-84	30-50
Grid connection cost[2]	9-14	15-30
Construction cost[3]	4-10	15-25
Other capital cost[4]	4-10	8-30

1: Wind turbine costs generally include manufacture, transportation, and installation of the turbine rotor, blades, and gearbox.
2: Grid connection costs generally include cabling, substations, and buildings.
3: Construction costs generally include transportation and installation of the turbine rotor, tower, and foundation, as well as road access and infrastructures required for the construction.
4: Other capital costs generally include regulatory (e.g., consulting and permitting) costs, and costs of engineering development and monitoring systems.

year [7,12]. The widely used formula to calculate the LCOE of renewable energy is given by:

$$LCOE = \frac{\sum_{t=1}^{n} \frac{I_t + M_t + F_t}{(1+r)^t}}{\sum_{t=1}^{n} \frac{E_t}{(1+r)^t}} \tag{1.1}$$

where:

I_t = investment expenditures in the year t

M_t = operation and maintenance expenditures in the year t

F_t = fuel expenditures in the year t

E_t = electricity generation in the year t

r = discount rate

n = economic life of the system

It is observed from Table 1.1 that the wind turbine is the largest single cost component of the total installed cost of a wind farm. For the wind turbine, the largest costs components are then the rotor blades, the tower, and the gearbox. Together, the contribution of these three components to the total cost of a turbine can be up to 60% [7]. The electricity

production cost is also a principal parameter, which strongly depends on wind resource. If the wind speed is 10% lower, owing to the high sensitivity of the energy production to the changes of wind speed, the energy production will fall short by more than 20% [13]. More importantly, many wind farm planning activities and tasks affect the cost and financial analysis of the project, generally including site analysis, wind resource assessment, turbine type selection, and wind farm layout design. It is important to understand how the mutually-correlated factors affect the trade-off between economic performance and other concerned performance objectives (e.g., energy production, land footprint, and impact on surroundings).

1.1.2 Engineering Aspect

As wind flows across a turbine, the power available (P_0) in the wind is given by

$$P_0 = \frac{1}{2}\rho A U_\infty^3 \tag{1.2}$$

where ρ is the air density; A is the rotor swept area; and U_∞ is the incoming wind speed at hub height (assuming uniform velocity profile).

The power generated from the turbine is given by

$$P = (p_1 - p_2)AV \tag{1.3}$$

where p_1 and p_2 are the pressure immediately in front of and behind the turbine, respectively; V is the velocity through the turbine.

Assuming the air flow is incompressible, from continuity equation and Bernoulli's equa-

tion, we have

$$\begin{aligned} \rho A_\infty U_\infty &= \rho A V = \rho A_d U_d \\ (p_1 - p_2) &= \tfrac{1}{2}\rho(U_\infty^2 - U_d^2) = \rho V (U_\infty - U_d) \end{aligned} \tag{1.4}$$

where U_d is the downstream wind speed; A_∞ and A_d represent the cross sectional area of the incoming wind flow and the downstream flow in the stream tube, respectively.

From Eq. 1.4, we have

$$V = \frac{1}{2}(U_\infty + U_d) \tag{1.5}$$

which means that the velocity through the turbine is the mean of the upstream and downstream velocities (in the stream tube).

Therefore, the turbine power coefficient, C_p, can be given by

$$C_p = \frac{P}{P_0} = \frac{1}{2}(1-d)(1+d)^2 \tag{1.6}$$

where $d = U_d/U_\infty$. It is apparently to shown that the maximum power coefficient can be achieved when $U_d/U_\infty = 1/3$. Therefore, this maximum achievable efficiency of a wind turbine is known as the *Betz limit*.

To extract as much energy as possible from the wind, engineering activities directly determine the performance of a wind energy project. These activities can be further categorized into activities at the wind turbine, wind farm, and wind regime levels.

The main activity in the wind regime level is wind resource assessment. From the wind farm developer's perspective, the wind resource on sites can be analyzed from a top level, i.e., the regional level, to a micro-scale with the use of both numerical data (wind atlas) and meteorological data [14]. In general, wind resource assessment comprises: (i) on-site wind conditions (e.g., wind speed, direction, temperature, and pressure) measurement; (ii)

correlations between on-site meteorological towers to fill in the missing data; (iii) correlations between long term weather stations and short term on-site meteorological towers; (iv) wind speed estimation at hub height using power law or log law vertical shear profiles; (v) modeling of wind condition distributions (speed, direction, and air density); (vi) energy production prediction based on a wind turbine's power curve, or wind farm power generation models [15]. An accurate prediction of wind conditions can help procure funding, and therefore better analyze the project economics.

Wind turbine design, on the other hand, is the primary activity at the wind turbine level. In order for the turbine to properly extract energy from wind, the turbine as well as its necessary systems need to be designed in such a way that all the technical requirements are satisfied, which include the designs of turbine blades, control systems, generator, tower, foundation, and cable connection systems. In additional, the design criteria also needs to meet the economic and environmental standards.

At the wind farm level, the wind farm planning activities are systematically integrated through wind farm layout design. In general, a wind farm comprises a group of turbines. However, the power generated from a wind farm is significantly less than the sum of the power extracted from each individual turbine when operating as a standalone entity under the same wind resource, which can be expressed as

$$P_{farm} < \sum_{i}^{N} \hat{P}_i \tag{1.7}$$

In Eq. 1.7, P_{farm} represents the power generation of an N-turbine wind farm; whereas $\hat{P}_i$ is the power generated from Turbine-i when operating as a standalone entity under the same wind resource. This energy loss can be mainly attributed to the wake effects. To

minimize the wake-induced energy losses, the *Wind Farm Layout Optimization (WFLO)* is performed, where the location of turbines, the turbine types, and the site configuration are optimized under a given/asssessed wind resource.

It is to be noted that the major contribution of the research presented in this dissertation is to develop a framework at the wind farm level that is capable of accounting for multiple objectives in the conceptual design of wind farms. This capability will allow wind farm developers and other stakeholders (investors and local landowners) to better understand the tradeoffs between their individual interests.

1.1.3 Environmental Aspect

Factors associated with the environmental impact must be considered in the design process of a wind farm – from the planning stage to the operation stage. In general, efforts to mitigate the environmental impact or the net impact on surroundings will adversely affect the productivity of a wind farm. Therefore, the environmental impact of a wind energy project and its balance with respect to the economics and productivity of the project need to be assessed at an early stage in the wind farm development.

Generally, the environmental impact of a wind farm involves noise impact, visual impact, impact on wildlife, and public concerns (e.g., participation of local landowners and social acceptance).

Noise

Wind turbines in operating often produce significant amount of noise. Due to the features of the sound, most of the turbine noise is masked by the sound of the wind itself. However, the noise can still propagate along the direction of the wind and cause annoyance in local communities downstream from the wind farm. Hence, proper siting of turbines and

using noise insulating materials in the nacelle is required to restrict the noise to an acceptable level [16, 17].

Visual Impact

Utility-scale wind turbines are generally installed in exposed locations. Hence, wind turbines are highly visible, thereby impacting the aesthetics view of the natural landscape. One strategy used to partially offset visual impact is to site fewer turbines at any one location and another strategy involves using today's larger and more efficient models of wind turbines [18]. These strategies thus require optimal siting and selection of wind turbines.

Impact on Local Wildlife

Impact on local wildlife generally includes the fatalities of birds and bats caused by wind turbines, loss of habitat, and interference with the natural behavior of resident or migratory fish or wildlife species [16, 18, 19]. Therefore, both site selection and turbine micro-siting need to mitigate the impact on local wildlife. In addition, latest data revealed that larger turbines appear to cause fewer raptor fatalities than smaller turbines [19]. Hence, choosing proper turbine configurations can also mitigate the risk of fatalities of birds and bats, as well as other adverse impact on the local ecosystem.

Public Concern

Compared to conventional power plants that rely on combustion of fossil fuels, electricity generated from wind involves no polluting or greenhouse gas. Public concerns in the case of wind farms are mostly related to [17–19] (i) blade movement, which may cause safety issue; (ii) potential electromagnetic interference with local radar and telecommunication infrastructure; (iii) shadow flicker; and (iv) other perceived impact on public health.

1.2 Conceptual Design of Wind Farms

1.2.1 Wind Farm Development Process

Conceptual design is the very first phase of wind farm development, where a utility-scale wind farm may consist of hundreds of turbines. The development of a wind energy project can be divided into three stages: early-stage (planning), mid-stage (initial development), and late stage (construction). The wind farm planning at the early stage is a complex process, where the consideration of key aspects, namely, technical, socio-economic, permitting and legal, and environmental aspects [17, 20, 21], is needed. A general process of wind farm development is listed below (the actual process will vary based on the project-specific requirements or policies): [13, 17, 20–22]:

1. EARLY STAGE (Planning)
    - Wind Resource Assessment
    - Site Evaluation
        - Land Acquisition
        - Wind Farm Layout Design
    - Planning Application
        - Permitting Basics
    - Preliminary Feasibility Analysis
        - Economics and Financing
        - Grid and Transmission
        - Ecology and Environment
        - Public Consultation

2. MID STAGE (Initial Development)

    - Economic Analysis
    - Transmission Capacity Study
    - Wind Farm Design
    - Regulatory Framework
        - Environmental Study
        - Land Owner Agreements
        - Power Contract
        - Turbine Contract

3. LATE STAGE (Construction)

    - Financing
    - Complete Permitting
    - Lease Purchase

It is to be noted that the activities involved in wind farm planning span multiple disciplines. More importantly, most of these activities are mutually-correlated. Particularly at the early stage, it is challenging to precisely gauge the performance of the proposed wind energy project, mainly attributed to the lack of information. For instance, the preferred land plots for building a wind farm may not be finally approved (made available, e.g. via leasing) by the landowners due to their unwillingness to participate. Conceptual design often precedes the conclusion of such negotiations. Therefore, conceptual design is desired at the very first stage of wind farm development, where the proposed wind energy project can be described in terms of a set of integrated ideas, concepts, and models. However, owing to

the lack of transparency in the planning process, it is difficult for wind farm developers and stakeholder to reach an agreement on various aspects of the project. This is one of the major cause of delays, which makes the planning stage of wind farm development undesirably time-consuming. As shown in Fig. 1.2, the wind farm development time frame can range from few months up to several years.

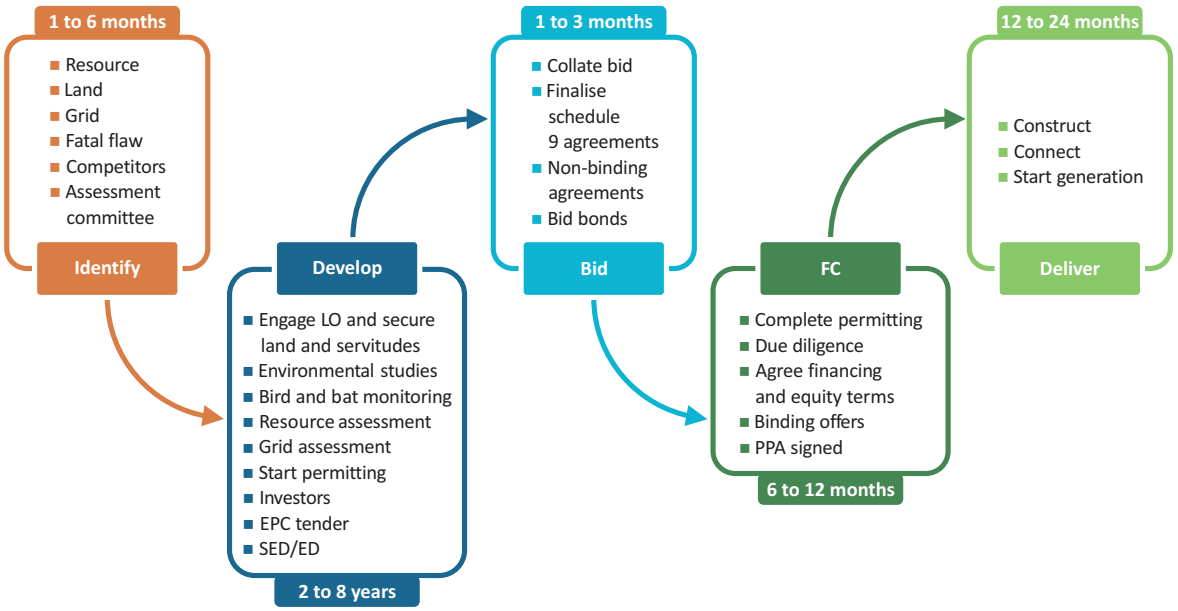

ED = economic development; FC = financial close; LO = landowner;
PPA = power purchase agreement; SED = socio-economic development

Figure 1.2: Timeframe of Wind Farm Development Process in South Africa (from a wind farm developer's perspective) [21]

1.2.2 Role of Land Resource

Land usage is one of the most important considerations in wind farm development. From the design perspective, wind farm developers need to secure the land that provides the most productive wind resources. In addition, the greater the land area used for turbine installation, the lower is the wake induced energy losses, leading to greater energy extraction from a given site. Unfortunately, land is also a limited resource, which also generally has

other alternative human usage or natural requirement [23]. To successfully site a wind energy project, there are a few key factors that must be considered with respect to land usage [24]:

Leasing This requires wind farm developers to secure the land rights from landowners. Whether landowners are willing to participate in the wind energy project strongly depends on the compensation (or incentives) offered to them by wind farm developers. One of the standard compensation routes involves leasing the land over the duration of project.

Grid transmission For large wind farms, it is necessary to account for existing transmission lines, transformers, and infrastructure. Particularly for offshore wind farms, setting up local cable connections often encounter different challenges [25]. Besides, the costs of cable installation and grid connection could be significant if the site is far away from major transmission lines, since high voltage cables and transformers can be costly.

Environmental concerns As previously mentioned, proper siting is required to mitigate the net environmental impact of a wind energy project on its surroundings, where the amount of land usage is directly related to the degree of impact, e.g., noise impact and habitat loss for local wildlife.

Land configuration Land configuration is generally related to land area, land shape, site orientation, soil property and terrain. Land area guides the overall number of turbines that can be installed; land shape and site orientation guide the turbine arrangement, and hence indirectly affect how much energy can be extracted from the local wind resource; and property of local soil also needs to be considered, to determine if the land is suitable for supporting wind turbines, and what type of turbine foundations

are necessary for the site.

Permitting After identifying site(s) with strong wind resource, developers must consult with permitting authorities to obtain the required permits and licenses for building wind power facilities at the site. These requirements may differ from state to state [16]. Investigating the related laws early in the development process can help avoid unnecessary delays.

It is to be noted that, in the early stage of wind farm development, a substantial portion of the planning activities are land orientated, since land usage strongly impacts the economic, technical, and environmental aspects (objectives) of the project. Hence, a carefully formulated land usage model is desired, which can appropriately reflect the environmental impact, landowner considerations, and land-based constraints on turbine installation.

1.3 Multi-Objective Mixed-Discrete Optimization Problems

Optimization problems that involve both continuous and discrete design variables can be called mixed-discrete optimization problems. Practical engineering optimization problems also often involve more than one objective. A mixed-discrete optimization problem with the consideration of two or more objectives can be called a Multi-Objective Mixed-Discrete Optimization (MOMDO) problem. Most mixed-discrete optimization problems are computationally challenging to solve even with a single objective function [26]. When multiple objective functions are involved, the problem complexity is significantly increased, in order to search for the *Pareto frontier*. In MOO, a candidate solution is considered to be a *Pareto optimal solution if any improvement of the solution in one objective can only take place at the cost of worsening at least one other objective* [27].

A generic form of a constrained MOMDO problem can be expressed as

$$\begin{aligned} & \min_{x^j \in \vec{x}} [\vec{f}^1(\vec{x}), \vec{f}^2(\vec{x}), \ldots, \vec{f}^N(\vec{x})] \\ & \vec{x} = (x_d^1, x_d^2, \ldots, x_d^m, x_c^1, x_c^2, \ldots, x_c^n) \\ s.t. & \\ & g_p(\vec{x}) \leq 0, \ p = 1, 2, \ldots, P \\ & h_q(\vec{x}) = 0, \ q = 1, 2, \ldots, Q \end{aligned} \tag{1.8}$$

where m denotes the number of discrete design variables (x_d), and n denotes the number of continuous design variables (x_c); the generic f^k denotes the k^{th} objective function, and the generic g_p and h_q denote the p^{th} inequality constraint and the q^{th} equality constraint, respectively; P and Q respectively represent the number of inequality and equality constraints.

1.3.1 Swarm-based Algorithms

Swarm-based algorithms or Swarm Intelligence (SI) based algorithms are originally inspired by natural evolution and collective behavior in animals, such as schools of fish, flocks of birds, and colonies of ants. In nature, such swarm behaviors are used to effectively forage for food, evade preys, or relocate colonies.

Owing to the characteristics of swarm behaviors, including decentralization, self-organization, and emergence, swarm-based algorithms are most useful for solving problems with a complex search domain but continuous. The exploration and exploitation features allow them to efficiently and effectively search for the optimal solution(s). Popular swarm-based algorithms include: (i) Particle Swarm Optimization (PSO) [28], (ii) Ant Colony Optimization (ACO) [29], and (iii) Artificial Bee Colony (ABC) [30].

1.4 Research Goals and Impact

1.4.1 Research Motivation

The quality of a wind energy project is generally determined by several performance criteria. Factors affecting the performance criteria play essential roles through the entire process of wind farm development, and most of these factors are mutually-correlated. To develop wind farms that are profitable, reliable, and meet community acceptance, it is necessary to seek a balance between the socio-economic, technical, and environmental aspects of the concerned wind farm.

However, owing to the lack of information on potential impacts in each aspect in wind farm development, several design alternatives often need to be considered to explore the balance point between the concerned performance objectives. More importantly, owing to the lack of decision-making transparency in wind farm planning, the evaluation of design alternatives can be undesirably time-consuming. As a result, before a wind energy project can be approved and proceed to construction, it might have gone through years of planning [21,31].

In order to help wind farm developers and stakeholders make more time-efficient decisions on the optimal configuration of a wind energy project, i.e., to help streamline the concept-to-installation process, a systematic exploration of the trade-offs between the multiple objectives is needed; such exploration should also consider the role of land resource at the early stage of planning. In addition, WFLO used in the planning process should be capable of dealing with problems that are highly nonlinear, high dimensional, constrained, and involves both continuous and discrete design variables. Therefore, a powerful multi-objective mixed-discrete optimization solver is imperative to providing the foundation of a time-efficient and effective optimal wind farm planning process.

1.4.2 Research Objectives

This research is aimed to develop a sensitivity-integrated approach to conceptual design of wind farms, which understands of the impact of various factors on wind farm performance, and leverage such understanding towards providing unprecedented facility in decision making. Specific research objectives are described below:

1.4.2.1 Analyzing the Sensitivity of Wind Farm Power Output to Key Factors

The expected power generation (or energy production) is one of the most important considerations in planning a wind energy project. Analytical wake models are generally used to estimate the wake-induced power losses, which is the major cause of wind farm inefficiency. A quantitative understanding of the relative impact of each of key natural and design factors is paramount to reliable estimation of wind farm power generation, and planning a high-quality wind energy project. However, such an understanding is not readily evident in the current wind farm design paradigm. To fill this important gap in wind farm planning, a comprehensive sensitivity analysis (SA) of wind farm power estimation is performed in this research. More specifically, this dissertation aims to investigate the sensitivity of the maximum farm output potential to the following crucial factors: the incoming wind speed, the number of turbines, the ambient turbulence, and the land configuration; the impact of the choice of wake models on the relative sensitivity is to be explored as well.

1.4.2.2 Multi-Objective Wind Farm Design Framework

WFLO is essentially multi-objective, where the performance objectives are generally conflicting (e.g., energy production vs. land usage). This research aims to develop a multi-objective framework for conceptual design of wind farms. WFLO is to be performed without limiting prescribed conditions (e.g., prescribed land configuration or fixed turbine choice).

More specifically, we aim to explore how the tradeoffs between multiple objectives are related to site-scale decisions, such as installed capacity.

1.4.2.3 Land Use Related Considerations

Land usage plays an important role at the early stage of wind farm planning. Most of the early planning activities involve analysis and consideration directly related to land usage. However, in the state of the art in wind farm design, a wind farm is generally assumed to have a rectangular shape and fixed boundaries. Such assumptions are unrealistic. In practice, wind farm siting should explore the maximum energy potential of the candidate sites under different land resource availability. Hence, this research aims to develop an optimal land usage model, to explore how optimal land shapes are related to site-scale decisions (e.g., installed capacity and unit land area), to landowner participation, and to the nature of the local wind resource.

1.4.2.4 Multi-Objective Mixed-Discrete Particle Swarm Optimization

To address the combination of complex characteristics inherent in multi-objective WFLO, namely highly nonlinear criteria functions, constrained high dimensional design space, and involving a mixture of discrete and continuous variables, this research aims to develop, test, and implement a multi-objective mixed-discrete PSO algorithm that also retains the natural computational efficiency of the fundamental swarm dynamics. The objective is to make important advancements to a mixed-discrete PSO algorithm, by developing and exploring the potential of a novel multi-domain diversity preservation concept. More specifically, these advancements include: **(i) the sets of local and global Pareto solutions are used to incorporate the Pareto dominance-based search strategy, which is critical to retain the original dynamics of the basic PSO, (ii) the selection mech-**

anism for local and global leaders is modified for multi-objective application, and (iii) a novel multi-domain diversity preservation technique is formulated to mitigate the premature particle stagnation issue while maintaining a desirably even distribution of the Pareto optimal solutions.

1.4.3 Research Impact

The research subject of this dissertation provides the foundation for building a time-efficient transparent decision-making platform for multi-objective wind farm development at the conceptual design phase. Significant research work has been done in the wind farm design literature. However, the majority of such research work is focused on single objective optimizatoin with prescribed conditions, e.g., the number of turbines and the wind farm size are assumed to be fixed. In contrast, this dissertation introduces a novel approach to allow the WFLO to be performed without prescribing the number of turbines or the wind farm boundaries. This approach was achieved by integrating the consideration of land usage and a novel Pareto shifting technique. The land usage model determines the usage for any given layout of turbines as a post optimization process; whereas the Pareto shifting technique is capable to "visualize" the tradeoffs between multiple objectives under different values of installed capacity (within the specified range of interest).

Heuristic algorithms are suitable for solving WFLO problems. Such problems are normally constrained, highly nonlinear, high dimensional, and multi-objective. PSO has been shown to be a powerful single objective optimization solver for continuous design variables. It is well known for its ease of implementation and fast convergence. Many research projects have been done based on converting PSO to a MOO solver. However, the primary drawback of PSO is often not adequately addressed, where it suffers from premature stagnation issue

due to loss of population diversity. Additionally, very few multi-objective versions of PSO (MOPSO) in the literature are capable of dealing with discrete design variables. In this dissertation, we address the traditional limitations of MOPSO. The new MOPSO developed in this research is capable of addressing the major complex attributes in WFLO. It is also important to note that the new MOPSO keeps the dynamics of the basic PSO, so that the original advantages of PSO can be retained. Overall, the new MOPSO can be a reliable MOO solver, and provide an option for handling complex MOO problems.

From a broader perspective, the research in this dissertation is expected to have an impact on both the respective academic fields and the related practical engineering applications. The theoretical contribution of this research lies in the novel Pareto shifting technique that enables the parameterization of tradeoffs between multiple objectives. Application of this technique is not restricted to wind farm design; it also provides an approach to solving a complex engineering system with a changeable number of design variables. The case study presented in this context illustrates the major implementation procedure of this technique, and shows a strategy for integrating optimization and regression modeling techniques.

The multi-objective swarm based strategy allows the wind farm design framework developed in this research to provide time-efficient solutions of complex engineering optimization problems. The concepts and ideas (the multi-domain diversity preservation technique and leader selection mechanism) introduced in this framework not only benefit the wind energy community, but are also expected to contribute to the algorithms in general that are motivated by *Swarm Intelligence* and related decision-making techniques.

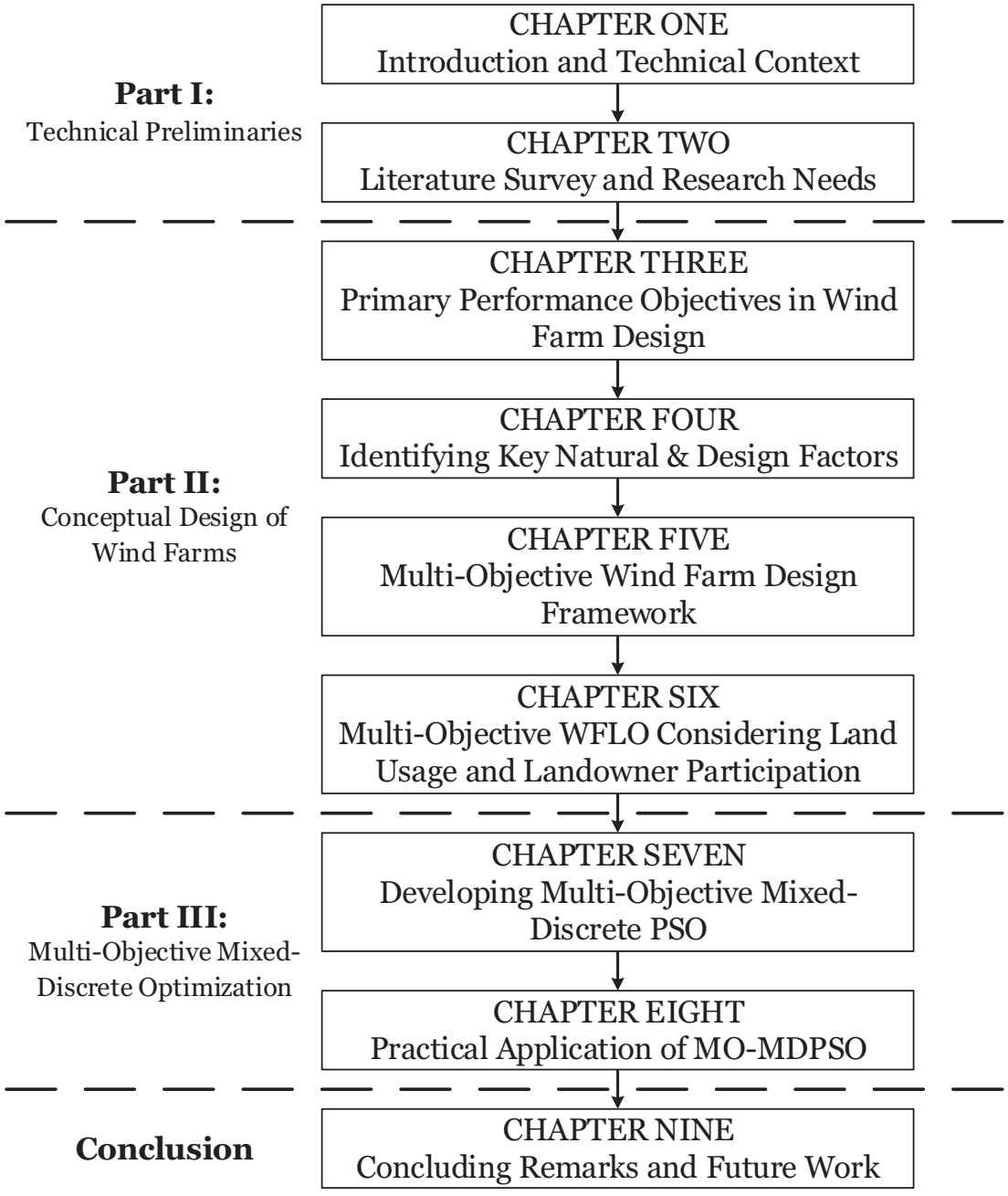

Figure 1.3: Thesis structure

1.5 Dissertation Outline

The dissertation is presented in four parts. The graphical structure of the document is shown in Fig. 1.3. Each part is expanded into several chapters as listed below:

- **Part I** includes two chapters. Chapter 1 briefly introduces the technical context of this research, including overviews of wind energy and the conceptual design of wind farms, as well as the discussion on multi-objective mixed-discrete optimization problems. The research motivation, objectives, and research impact are then provided. Chapter 2 provides a comprehensive literature on pertinent topics, including the modeling of wake effects in WFLO, the state of the art of the WFLO, and multi-objective search strategies in multi-objective PSO.

- **Part II** presents the development of the multi-objective wind farm design (MOWFD) methodology. Chapter 3 introduces the primary performance objectives considered in this research, including (i) Annual Energy Production (AEP), (ii) Cost of Energy (COE), and (iii) unit land footprint. The model of each performance objective is also provided. A SA of of wind farms with array-like and optimized layout was performed in Chapter 4, to identify the key natural and design factors affecting the wind farm performance. Chapter 5 provides the implementation of MOWFD methodology through a case study. Case studies related to land usage and varying land plot availability are conducted in Chapter 6.

- **Part III** describes the development of the MOO solver used in this research. Chapter 7 provide the development procedure of the MO-MDPSO algorithm. In Chapter 8, MO-MDPSO is implemented to solve practical complex engineering optimization problems.

- **Part IV** summarizes the concluding remarks in this research. Future work of this research is then discussed.

CHAPTER 2

Literature Survey

This chapter provides a comprehensive literature survey of the modeling of wake effects in WFLO, the state of the art of WFLO, and multi-objective search strategies in multi-objective PSO. Section 2.1 describes the role of wake effects in WFLO and four analytical wake models that are widely used (to estimate/simulate the wake-induced energy losses) in the literature of WFLO. Section 2.2 reviews the literature on WFLO framework, the performance objectives generally considered, and the optimization algorithms used in WFLO, thereby providing an overview of the the state of the art. Section 2.3 reviews the search strategies used in multi-objective PSO. Key observations from the reviewed literature and research needs are provided at the end of this chapter.

2.1 The Wake Effects

The wake effects have a huge impact on many wind energy projects. Utility-scale wind farms should consider the impact of turbines wakes on turbine arrangement. In this section, we discuss the role of wake effects in wind farm power estimation and describe four analytical wake models that are widely used in WFLO to estimate the wake-induced power/energy losses.

2.1.1 The Role of Wake Effects in Wind Farm Power Estimation

As wind flows across a turbine, the wind speed reduces and the turbulence intensity increases. Thus, a wake is formed behind the turbine, which affects the performance of downstream turbines. The wake not only progresses along the streamwise direction, it also

Table 2.1: Comparison of computation time of wake simulation for two turbines in line [32]

Wake model	Computation time	Model type
Jensen model [33, 34]	5 seconds	Analytical
Actuator disk model [35]	25 seconds	Actuator disk
Dynamic Wake Meandering model [36]	8 minutes	Analytical+Actuator disk
SOWFA [37, 38]	30 hours	3D CFD

expands laterally. As a result, downstream turbines that are not coaxially downstream can be also affected by upstream turbine wakes. Collectively, this is called *the wake effects*. There are two major impacts of the wake effects on the entire wind farm: (i) it causes a deficiency in the overall energy output due to the velocity deficit in the wakes, and (ii) it causes a reduction of the turbine lifetime due to the additional turbulence induced structural loading. Factors affecting the wake behavior can be classified into two categories: natural factors and design factors.

Natural factors are primarily the variation in wind conditions (including wind speed, wind shear, and ambient turbulence) at the concerned wind farm site. These factors cannot be controlled through design or optimization. Design factors, on the other hand, are generally regulated by design decisions, such as turbine locations, turbine features (e.g., turbine rotor diameter and hub height), land configuration, and installed capacity (number of turbines). It is important to realize that these factors regulating the behavior of turbine wakes in turn affect the quality of a wind energy project. Therefore, the reliability of wind farm power estimation relies on the accuracy of the wake model used and on the assumptions associated with the natural and design factors.

2.1.2 Analytical Wake Models

In the context of WFLO problems, the computational efficiency of a particular analytical wake model often presents a higher priority compared to the specific applicability.

Table 2.1 shows a comparison of the computation time of each wake model for a two turbines scenario [32]. It is readily evident that analytical wake models are the most suitable for WFLO problems. Hence, analytical wake models are preferred in WFLO problems, and have been used by different researchers (e.g., Jensen model [39–41] and Frandsen [42, 43]).

Several studies/projects emphasize the validation of wake models through comparisons with test cases, to understand the limitations and define clear guidelines of how each of the wake models should be applied [44–47]. For example, Jensen model has been proven to be reliable for long-term power predictions in small to medium size wind farms [33, 34]; Refs. [45, 48, 49] show that the accuracy of a wake model decreases when wind direction sectors are smaller than 10 degrees. Additionally, model validation also highly depends on the quantity and quality of the wind data acquired from real wind farm sites (e.g., anemometer data may be inadequate) [47].

Four popular analytical wake models are discussed in the following part: Sections 2.1.2 – 2.1.2 provide the mathematical description of each of these wake models.

Jensen Model

The analytical wake model developed by Jensen [33] and further advanced by Katic [34] is one of the most popular analytical wake models. The key assumption in the Jensen model is that the wake behind the wind turbine has a linear expansion. Hence, the velocity deficit is only dependent on the distance downstream of a turbine, which is given by

$$u_f = U_\infty \left[\frac{1 - \sqrt{1 - C_T}}{(1 + 2ks)^2} \right] \tag{2.1}$$

where C_T is the turbine thrust coefficient; k is the wake decay constant, which regulates how the wake breaks down in terms of the growth of the vertical wake width per unit length in

the downstream direction; and s is the normalized downstream distance defined as the ratio of streamwise distance between two turbines to the turbine rotor diameter D. The wake growth, D_w, is then formulated as

$$D_w = D(1 + 2ks) \tag{2.2}$$

The recommended k values for onshore and offshore wind farms are 0.075 and 0.04, respectively [50].

Frandsen Model

The Frandsen model was originally used to predict the wind speed deficit in large offshore wind farms with rectangular plots and array-like turbine layouts [51]. Based on the inner flow patterns, this model assumes that turbine wakes inside a wind farm have three regimes. The first regime considers the development of turbine wakes, where the wake growth and velocity deficit are respectively formulated as

$$D_w = D\left(\beta^{k/2} + \alpha s\right)^{1/k} \tag{2.3}$$

and

$$u_f = \frac{U_\infty}{2}\left(1 \pm \sqrt{1 - 2\frac{A}{A_{wake}}C_T}\right) \tag{2.4}$$

where α defines the initial wake speed deficit that must be determined experimentally; k is the shape parameter, where $k = 2$ (square root shape) [51, 52]; A_{wake} is the effective influence area of the wake with respect to the wake width at the current location; and the

wake expansion parameter β is given by

$$\beta = \frac{1+\sqrt{1-C_T}}{2\sqrt{1-C_T}} = \left(\frac{D_{eff}}{D}\right)^2, \quad s = x/D \tag{2.5}$$

For the "$\pm$" sign in Eq.(2.4), the "+" applies to cases in which the induction factor $a \leq 0.5$; while the "$-$" applies to $a > 0.5$.

It is noted that the Eq.(2.5) uses an effective rotor diameter, D_{eff}, to account for the near wake approximation, which is given by

$$D_{eff} = D\sqrt{\frac{1+\sqrt{1-C_T}}{2\sqrt{1-C_T}}} \tag{2.6}$$

Larsen Model

The Larsen wake model was first introduced in [53], and later reported in the European Wind Turbine Standards II (EWTS II) [54]. The Prandtl's mixing length theory is applied in this model, and the wake flow is assumed to be incompressible, stationary, and axisymmetric. Differing from the Jensen model, the velocity deficit in Larsen model depends on both the streamwise distance downstream of a turbine (x) and the radial distance (r) from the hub. The first-order formulation of the velocity deficit in Larsen model is given by

$$\begin{aligned} u_f &= \frac{U_\infty}{9}\left[C_T A(x+x_0)^{-2}\right]^{\frac{1}{3}} \left\{ r^{\frac{3}{2}}\left[3c_1^2 C_T A(x+x_0)\right]^{-\frac{1}{2}} \right. \\ &\quad \left. - \left(\frac{35}{2\pi}\right)^{\frac{3}{10}} (3c_1^2)^{-\frac{1}{5}} \right\}^2 \end{aligned} \tag{2.7}$$

The wake growth in the Larsen model is given by

$$D_w = 2\left(\frac{35}{2\pi}\right)^{\frac{1}{5}}\left(3c_1^2\right)^{\frac{1}{5}}\left[C_T A(x+x_0)\right]^{\frac{1}{3}} \tag{2.8}$$

In Eqs.(2.7) and (2.8), c_1 is a constant that represents the non-dimensional mixing length, related to the Prandtl's mixing length; and x_0 denotes the turbine's position with respect to the reference coordinate system. Equations used to estimate these two constants are given by [54], as shown below:

$$c_1 = \left(\frac{D_{eff}}{2}\right)^{\frac{5}{2}}\left(\frac{105}{2\pi}\right)^{-\frac{1}{2}}\left(C_T A x_0\right)^{-\frac{5}{6}} \tag{2.9}$$

$$x_0 = \frac{9.5D}{\left(\frac{2R_{9.5}}{D_{eff}}\right)^3 - 1} \tag{2.10}$$

Here, $R_{9.5}$ represents the wake radius at a relative distance of 9.5 rotor diameters ($9.5D$) downstream from the turbine, which is defined based on an empirical equation expressed as

$$R_{9.5} = 0.5\left[R_{nb} + min\left(H, R_{nb}\right)\right] \tag{2.11}$$

where R_{nb} is an empirical parameter related to the ambient turbulence at the hub height (I_a), as given by

$$R_{nb} = max\left[1.08D, 1.08D + 21.7D\left(I_a - 0.05\right)\right] \tag{2.12}$$

Ishihara Model

The Ishihara model is developed using wind tunnel data for a scaled model of a Mitsubishi wind turbine. An important feature of this model is its ability to account for the effect of turbulence on the wake recovery, considering both the ambient turbulence and the

turbine-induced turbulence. Experiments have shown that, for onshore farm sites, the rate of the wake recovery is generally higher due to the existence of sufficient turbulence in the wake. In the case of offshore farm sites, a relatively low ambient turbulence intensity is prevalent; the wake recovery is therefore more dependent on the turbine-induced turbulence. Similar to the Larsen model, the predicted wake velocity in the Ishihara model depends on both the streamwise distance (x) and the radial distance (r), and is assumed to have a Gaussian profile. The velocity deficit is given by [55]

$$u_f = \frac{\sqrt{C_T}U_\infty}{32}\left(\frac{1.666}{k_1}\right)^2\left(\frac{x}{D}\right)^{-p}\exp\left(-\frac{r^2}{{D_{wake}}^2}\right) \tag{2.13}$$

where the wake growth is formulated as

$$D_{wake} = \frac{k_1 {C_T}^{\frac{1}{4}}}{0.833} D^{1-\frac{p}{2}} x^{\frac{p}{2}} \tag{2.14}$$

The parameter p in Eqs.(2.13) and (2.14) is a function of two forms of turbulence, as given by

$$p = k_2(I_a + I_w) \tag{2.15}$$

where I_a and I_w represent the ambient turbulence and the turbine-induced turbulence, respectively.

The turbine-induced turbulence can be expressed as

$$I_w = \frac{k_3 C_T}{max(I_a, 0.03)}\left\{1 - \exp\left[-4\left(\frac{x}{10D}\right)^2\right]\right\} \tag{2.16}$$

In Eqs.(2.13) $-$ (2.16), the coefficients k_1, k_2, and k_3 are respectively set to 0.27, 6.0, and 0.004, as recommended in the literature [55, 56].

2.2 The State of the Art in Wind Farm Layout Optimization

Since the pioneering article reported by Mosetti et al. [57] in 1994, WFLO has seen continuously increasing attention. WFLO is performed primarily to avoid wake-induced energy losses by optimally arranging the turbine locations, thus maximizing the expected wind farm performance and minimizing the adverse impacts. A generic formulation of the WFLO problem can be expressed as

$$\begin{aligned} & \min_{\vec{V}} \vec{f}_{farm}(\vec{V}) \\ s.t. & \\ & \vec{g}_{farm}(\vec{V}) \leq 0 \\ & \vec{h}_{farm}(\vec{V}) = 0 \end{aligned} \tag{2.17}$$

where $\vec{V}$ is a vector of design variables (normally the coordinates of turbines); $\vec{f}_{farm}$ represents the performance objective(s) of the concerned wind farm, which are generally the AEP, the COE, the turbine operation lifetime, and the net impact on surroundings (e.g., the noise impact and the impact on local wildlife); and $\vec{g}_{farm}$ and $\vec{h}_{farm}$ represent the inequality and equality constraints, respectively, that are imposed on the wind farm site.

The following provides a comprehensive survey of WFLO, providing an overview of the state of the art, including the existing WFLO frameworks, performance criteria considered in WFLO, and the optimization algorithms that are widely used in WFLO. Through this survey, a better understanding of the existing issues and research needs in WFLO. In addition, several commercial software programs for wind farm design are also introduced.

2.2.1 Overview of Wind Farm Layout Optimization Frameworks

Existing WFLO frameworks in the literature can be classified into two types: (i) the discrete model and (ii) the continuous model.

In discrete models, the wind farm site is discretized into uniform grids that represent potential positions to install wind turbines. Consequently, the location of turbines is restricted to these grids. The WFLO framework used in the pioneering article by Mosetti et al. [57] use the discrete model. In their work, the wind farm was discretized into 10 $\times$ 10 square cells. Grady et al. [58] followed the same framework but improved on Mosetti's work in terms of the optimization algorithm used. It is to be noted that some researchers assume an array-like layout wind farm [59]. where the lateral spacing between arrays is to be optimized. However, this scheme restricts the turbine locations to arrays instead of grids, which can still be considered discrete model. More WFLO frameworks using the discrete model can be found in Refs. [23, 40–42, 59–72].

In continuous models, on the other hand, the location of turbines is not restricted to "grids", and turbines can be placed arbitrarily within the specified wind farm boundaries. Ozturk and Norman [73] allowed the turbines to be placed in a continuous space. Later, Kusiak and Song [39] extended the analytical framework by Lackner and Elkinton [74] and developed a continuous model based WFLO framework. Chowdhury et al. [43] motivated by Kusiak's approach, developed one of the most advanced WFLO frameworks in the literature, called the Unrestricted Wind Farm Layout Optimization (UWFLO) framework [43, 75]. In discrete models, the feasible solutions of potential positions to install turbine positions are limited due to the predefined grids; while continuous models are more likely to find the global optimum. Over the past few years, continuous models have received increasing attention. Recent reported work using continuous models can be found in Refs. [76–83].

2.2.2 Performance Criteria in WFLO

Production Consideration

Wind farm Annual Energy Production (AEP) is one of the most important performance criteria used to evaluate the quality of a wind energy project. More than one third of the work reviewed in Ref. [84] used AEP or wind farm power generation as the objective function.

A utility-scale wind farm can consist of a group of turbines, and the potential power generation of a single turbine is determined by the available power in the wind. This available power in the wind is expressed as the product of the wind mass flow rate ($\rho A U_\infty$) and the kinetic energy of the wind ($\frac{1}{2}U_\infty^2$), as shown in Eq. 1.2. The actual power generated from a wind turbine is derived from the mechanical power conversion, which is given by the product of the wind turbine power coefficient (C_p) and the available power in the wind. Here, the power coefficient is an intricate function that is determined by many factors, including the incoming wind conditions (e.g., freestream wind speed and turbulence intensity) and turbine features (tip speed ratio, turbine rotor diameter, etc.). In the literature, two metrics are generally used to evaluate how much energy a wind farm can extract from the wind: (i) wind farm efficiency (η) and (ii) wind farm capacity factor (CF). Wind farm efficiency is defined as the ratio of the actual wind farm power generation to the ideal power generation without considering the wake-induced power losses, i.e., the sum of the power generated by each of the installed wind turbines when operating as a standalone entity. The efficiency of a N-turbine wind farm is given by

$$\eta = \frac{P_{farm}}{\sum_i^N P_{0i}} \tag{2.18}$$

where P_{farm} is the actual power generated by the wind farm; and P_{0i} is the ideal power generation of Turbine-i when operating as a standalone entity.

The wind farm capacity factor is given by

$$CF = \frac{P_{farm}}{P_{NC}} \tag{2.19}$$

where P_{NC} is the nameplate capacity of the concerned wind farm.

In the early research projects, Mosetti et al. [57] and Grady et al. [58] considered wind farm energy production as the objective function. Other reviewed work considering AEP or wind farm power generation can be found in Refs. [23, 39, 40, 42, 43, 60, 63, 64, 67, 68, 71–73, 76–78, 78–82, 85, 86].

Economic Consideration

The economic performance is another important performance criterion in WFLO, which can be related to the wind farm COE, the Net Present Value (NPV), the Financial Balance (FB), or the wind farm operation and maintenance cost.

Research on economic performance can be found in Refs. [41, 43, 58–60, 62–67, 70, 71, 74, 76, 82, 86, 87].

Other Considerations

Other considerations in wind farm design include noise impact [72], land usage related considerations [23, 82, 88], landowner participation [41], risk management [87], and transmission capacity [69].

2.2.3 Optimization Algorithms in WFLO

In this part, we discuss the algorithms and optimization solvers used to perform WFLO.

2.2.3.1 Genetic Algorithms

Genetic Algorithms (GAs) are are adaptive heuristic search algorithm based on the evolutionary ideas of natural selection and genetics. In the context of WFLO problems, the basic idea of GAs is to maintain a large number of random chromosomes, each of which represents a candidate wind farm layout. These chromosomes then evolve over generations following the selection process and the reproduction process. In the selection process, each candidate layout is assigned with a fitness value (e.g., the objective function value), which is used to determine if the candidate solution is eligible to "evolve"; whereas the reproduction process is to apply genetic operators, i.e., the crossover and mutation, which enables new patterns of wind farm layouts to be generated. Owing to the genetic feature of GAs, they are capable to efficiently and effectively explore an initially unknown complex design space. Mosetti et al. [57] first used GAs to perform the WFLO, and since then GAs have gained a particular preference in WFLO. More WFLO work using GAs can be found in Refs. [42, 57, 58, 60, 63–65, 67, 69].

2.2.3.2 Particle Swarm Optimization Algorithms

Particle Swarm Optimization (PSO) algorithm [28] is a population-based optimization solver inspired by the social behavior of birds in a flock or fishes in a school. In PSO, candidate solutions are represented by the positions of a swarm of "particles", distributing over the entire design space. Each particle is assigned with a "velocity", which guides the particle's movement toward its local best position (local leader), as well as the best position in the swarm (global leader). The local best is updated based on each particle's own experience, while the global best is updated by socially exchanging the information with other local bests in the swarm. In the context of WFLO problems, each particle represents

a candidate layout. Initially, PSO starts with a population of randomly generated layouts. Particles are dynamically guided by local and global leaders in the design space searching for solutions that have the best wind farm performance.

However, PSO has a primary drawback of pre-stagnation, which causes the swarm to converge to a sub-optimal solution. This is mainly attributed to the loss of diversity during the fast convergence [89]. This scenario occurs especially when the problem is complex and multimodal, as the case in WFLO.

Relevant research using PSO to solve WFLO problems can be found in Refs. [43,78,86].

2.2.3.3 Simulated Annealing Algorithm

Simulated Annealing Algorithm (SAA) is characterized as a metaheuristic algorithm for global optimization. Initially, the idea of SAA was inspired by the simulation of cooling a material in a heat bath to decrease defects; thus minimizing the system energy. Later this method was proposed as an optimization problem solver by Kirkpatrick et al. [90]. At each iteration of SAA, a new point is randomly generated. The distance of the new point from the current point is based on a probability distribution with a scale proportional to the temperature. SAA accepts all new points that are lower than the objective function; but also, with a certain probability, point that raise the objective function. An annealing schedule is selected to systematically decreases the temperature as the algorithm converges to a minimum.

Rivas et al. [91] applied SAA to optimize turbine locations for a large offshore wind farm. Bilbao and Alba [66] also applied SAA in their work to maximize the wind farm annual profit.

2.2.3.4 Other Algorithms

Other algorithms used to solve WFLO problems include: Evolutionary Algorithms (EA) [39, 61, 71, 72], Greedy Heuristic Algorithm [60, 73], Mixed Integer Programming [68], Patter Search [40], Monte Carlo Simulation [62], and Ant Colony Algorithm [77].

2.2.4 Commercial Software

There are several commercial software programs used to optimize and design wind farms. Below is a summary of the most widely used programs:

1. **WAsP** The Wind Atlas Analysis and Application Program (WAsP developed by the Risø National Laboratory (`www.wasp.dk`), is considered the industry-standard software for bankable wind resource assessment and wind farm micro-siting. WAsP provides different analysis regarding the wind farm production, the wind power potential, the wind climate estimation, and micro-sitting. Although it lacks an optimization tool for wind farm design, its powerful packages are normally incorporated by other WFLO frameworks (e.g., TOPFARM [92]) or software programs (e.g., WindPRO and WindFarmer).

2. **WindSim** (`www.windsim.com`) is a powerful wind farm design tool based on computational fluid dynamics (CFD) that is mainly used for wind data analysis and WFLO. The wind flow modeling approach is based on a 3D Reynolds-Averaged Navier-Stokes (RANS) solver, which is complemented with different types of turbulence models (e.g., standard $k-\varepsilon$, RNG $k-\varepsilon$ and the standard $k-\omega$). The Park Optimizer module in WindSim can determine the areas where is not advisable for turbine placement due to poor resource or bad wind quality based on IEC criteria. Hence, wind farm developers are able to identify the suitable positions for turbine installation.

3. **Wind Farm** (`http://www.resoft.co.uk`) developed by ReSoft is a general commer-

cial system for wind farm development. Its capabilities in wind farm design include: (i) WFLO for maximizing energy production or minimizing COE, subject to environmental (noise, visual impact, and shadow flicker) and physical (forests, trees, hedges, etc) constraints, (ii) long-term wind speed prediction, (iii) 3D visualizations of multiple wind farms and the landscape, and (iv) option to calcuate energy yields using multiple anemometers.

4. **WindPRO** (http://www.emd.dk/windpro) is a robust tool developed by EMD International A/S. Several different modules are included in WindPRO for the simulation and quantification of the wind farm energy production. In addition, it containts modules for the electrical layout design and its optimization (including the quantification of power losses) and a robust financial balance model. WindPro optimizes the wind farm layout using the AEP as a performance criterion while accounting for several environmental impacts (not accounted during the optimization procedure), including noise impact, visual impact, and shadow flicker effect . The optimization framework is incorporated from the WAsP engine. Different WFLO strategies are available in WindPRO: (i) a stochastic and gradual placement of turbines into the wind farm until the pre-specified number of turbines are all installed; (ii) an array-layout based strategy; (iii) an iterative addition of turbines into the available land plots; and (iv) minimizing the noise impact for fixed wind farm layouts.

5. **WindFarmer** (www.dnvgl.com/services/windfarmer-3766) developed by DNV-GL is a state-of-the-art software tool for designing, optimizing and analysing wind farms. The optimization procedures in WindFarmer are based on greedy heuristics, which

[1]visual phenomenon occasionally caused by rotating blades; excessive shadow flicker may be considered a nuisance and wind energy projects should reduce the impact of shadow flicker

can either maximize the AEP or the financial balance of the project, while considering several major environmental effects, including noise impact, visual impact, shadow flicker, and impact on local radar stations. It is worth mentioning that the energy production can be analyzed with a high degree of precision in WindFarmer. The energy production in WindFarmer incorporates the WAsP engine and accounts for the effects of turbulence, terrain, and variable air density at every turbine.

2.3 Multi-Objective Particle Swarm Optimization (MOPSO)

2.3.1 Overview of MOPSO

Evolutionary Algorithms (EAs) and Particle Swarm Optimization (PSO) are among the most popular nature-inspired algorithms for solving highly nonlinear optimization problems. EAs that are used for solving MOO problems (known as MOEAs), include Vector Evaluated Genetic Algorithm (VEGA) developed by Schaffer [93, 94], Non-dominated Sorting Genetic Algorithm II (NSGA-II) developed by Deb et al. [95], Strength Pareto Evolutionary Algorithm (SPEA) [96, 97], SPEA2 [98], Predator-Prey Evolutionary Strategy (PPES) [99], and Modified Predator Prey (MPP) [100]. Some of these MOEAs are also capable of handling integer and discrete design variables, e.g., NSGA-II.

PSO on the other hand is well-known for its fast convergence and ease of implementation, particularly in solving single objective, unconstrained, and continuous optimization problems. Since 1999, there has been an increasing thrust towards translating the key advantages of PSO into solving MOO problems. Figure 2.1 provides an overview of the areas of application of multi-objective PSO reported in the literature. Popular multi-objective versions of the PSO algorithm (MOPSO) include: (i) the early study of MOPSO by Parsopulos and Vrahatis [102], (ii) the MOPSO developed by Coello et al. [103], (iii) the Dynamic

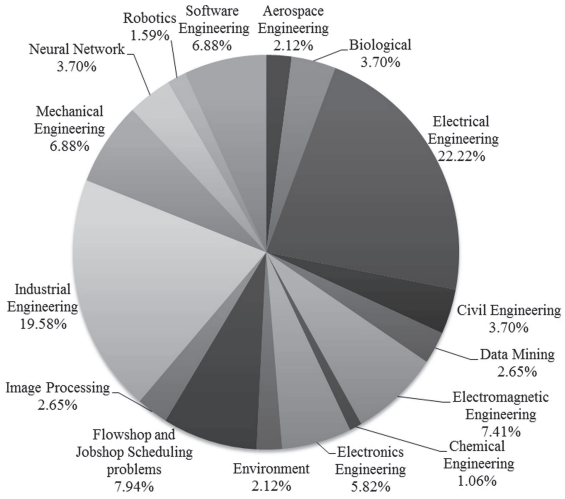

Figure 2.1: Publications of MOPSO by field of engineering applications [101]

Neighborhood PSO algorithm (DNPSO) [104, 105], (iv) the Non-dominated Sorting PSO (NSPSO) developed by Li [106], and (v) the MOPSO that uses crowding distance (MOPSO-CD), developed by Raquel and Naval, Jr. [107].

The numerous variants of MOPSO, developed over the past few decades, primarily focus on the search strategy in the multi-objective space. Mechanisms have also been developed to handle constraints and select individuals. Unfortunately, there exists only a handful of studies in MOPSO where mixed-discrete variables are considered [108–114], and even fewer studies where diversity preservation is also considered [103, 106, 115, 116].

2.3.2 Search Strategies in MOPSO

In MOO problems, the selection of individual particles must account for the tradeoffs among the multiple objective functions. One of the following three common search strategies is generally used for finding the Pareto optimal solutions in MOPSO [117, 118]: (i) aggregating function, (ii) single objective-based, and (iii) Pareto dominance principle.

Aggregating function is one of the most common multi-objective search strategies employed in PSO, due to its simplicity of implementation. Baumgartner et al. [119] used the

weighted sum approach to solve MOO problems and vector optimization problems, where the basic PSO was used as the single objective optimizer for the aggregating function. Parsopolous and Vrahatis [102] applied aggregating function to solve MOO problems, where they tested three different aggregating approaches: conventional weighted sum, dynamic weighted sum, and Bang-Bang weighted sum (abruptly changing inertia weight). However, the aggregating function based strategies suffer from the typical drawbacks that have over years made them less popular compared to MOEAs; e.g., no well-defined approach to assign weights, need for objective scaling, and poor capture of non-convex Pareto frontier. In addition, the aggregating function strategy is computationally expensive, since only one Pareto optimal solution can be obtained in each optimization run.

Single objective-based strategies optimize one objective at a time. In the DNPSO algorithm proposed by Hu et al. [104], bi-objective optimization problems were solved using the lexicographic ordering scheme. This scheme compares a particle only with its two neighbors, where the performance of optimization is likely to be sensitive to the assigned ordering of importance of objectives [117]. Similarly, in a multi-swarm variant of PSO called Vector Evaluated PSO (VEPSO) method, developed by Parsopoulos et al. [120], the evaluation of each sub-swarm is based on one assigned objective (local search); while the global search depends on the information exchange between multiple sub-swarms. It is noted that both lexicographic ordering scheme and the multi-swarm based approach are generally applicable for only bi-objective problems.

One of the MOPSO algorithms that uses the Pareto dominance search strategy to compare solutions is the MOPSO developed by Coello et al. [103]. In this MOPSO, an external repository is used to store the non-dominated solutions, and the search space is divided into hypercubes that are adaptively controlled by the number of particle enclosed

by them. There also exist MOPSO algorithms that combine multiple approaches to search in the multi-objective space. Ray and Liew [121] proposed a "swarm metaphor" algorithm, where they introduced a non-dominance based sorting in PSO, and where the selection of individuals was driven by a probabilistic crowding radius. The NSPSO developed by Li [106] also applied the concept of non-dominance sorting. The selection of individuals in this algorithm is based on two criteria, the niche count and the crowding distance.

In the basic PSO, the comparison of individual particles is based on the objective function value. For multi-objective problems, the principle of non-dominance comparison is applied in the Pareto dominance strategy. The search strategy in this paper is therefore motivated by the Pareto dominance strategy, since it retains the original dynamics of PSO. However, a majority of the existing MOPSO algorithms using the Pareto dominance strategy do not explicitly seek to generate evenly distributed Pareto solutions, which is one of the core measures of goodness of the Pareto optimal solutions offered by a MOO algorithm. The commonly-observed failure to evenly capture the entire Pareto frontier can be mainly attributed to a loss of population diversity in parts of the design variable space as the swarm converges to the global Pareto solutions. In this paper, we formulate the multi-domain diversity preservation technique that allows the swarm to maintain the diversity during convergence and generate a desirably even distribution of Pareto solutions.

2.4 Research Observations and Needs

2.4.1 Key Observations

Majority of the relevant work in WFLO is focused on solving single objective function. This is mainly attributed to the complexity of WFLO problems. The design of a wind farm spans multiple disciplines. It is challenging to systematically evaluate the performance

objectives and constraints subject to these disciplines (e.g., wind farm power generation). In addition, WFLO may include a large number of design variables that may contain a mixture type of both continuous and discrete (e.g., turbine selection and land plot availability). Therefore, problems addressed in WFLO are constrained, highly nonlinear, high dimensional, multimodal, and involve a mixture of both continuous and discrete design variables.

It is observed from the literature that much of the literature reported results using prescribed wind farm boundaries and installed capacity. In practice, the size of a wind farm and the installed capacity (or the number of turbines) are normally limited by the maximum potential energy that can be sold, the land plot availability, and the transmission capacity. Mathematically, using prescribed conditions may reduce the number of feasible solutions with the implication of restricting possible wind farm layouts and thus the quality of the wind energy project.

The fact that WFLO problems are generally constrained, highly nonlinear, and high dimensional makes heuristic algorithms a suitable solver. Therefore, heuristic algorithms are preferred in WFLO literature, owing to the capability of exploring complex unknown design space. Among the reviewed algorithms, GAs and PSO were the most popular. GA is specifically applied to discrete models, while PSO is a general solver for continuous models. Continuous models have recently received increasing attention. The shortcoming of discrete approaches is evident: the location of turbines is restricted to the predefined grid points, thus the performance of WFLO may not be globally optimal. However, discrete models are preferred in problems where specific land plot-based constraints are imposed. This is because that, due to the discretization of land plots, discrete models are less sensitive to the location of turbines. Chen and McDonald [41] used discrete land plots to consider the landowner participation.

Due to the computational cost in the evaluation of performance objectives and constraints considered in WFLO, the desired MOO for solving WFLO problems should be computationally efficient and robust. To this end, PSO seems to be a suitable choice for this purpose. However, most of the MOPSO variants are unable to well-preserve the original advantages of PSO, and the capability of dealing with mixed-discrete design variable was rarely reported in MOPSO literature.

2.4.2 Research Needs

2.4.2.1 Research Needs in Wind Farm Power Estimation

The complex relationship between the wind farm power and the factors regulating the power estimation raises important questions in the context of wind farm analysis and optimization, as summarized below:

1. What is the relative importance of each natural and design factor in the context of power output potential of a wind farm?

2. Which of these factors can be neglected and/or assumed to be practically fixed in the process of WFLO?

3. How does the impact of these factors on the wind farm power output vary under the use of different wake models?

A comprehensive and coherent exploration of these questions is missing from the WFLO literature. An extensive sensitivity analysis of the wind farm power estimation is hence desired, seeking to address the above questions. This analysis should investigate how sensitive the wind farm power estimation to critical farm-scale factors (e.g., incoming wind speed and inter-turbine spacing) to explore how the impact of these factors (on the wind farm power output) vary with the implementation of different wake models.

2.4.2.2 Research Needs in Wind Farm Design

Problems in WFLO are naturally multi-objective. Therefore, a carefully formulated multi-objective framework for wind farm design is desired, in which different performance criteria, constraints, and factors affecting them can be systematically evaluated. Performance criteria considered in this framework include: (i) the annual energy production, (ii) the cost of energy, and (iii) the net impact on surroundings.

On the other hand, appropriate strategies need to be developed, which allow the WFLO to be performed without prescribing wind farm boundaries or the number of turbines. This development is particularly important for conceptual design of wind farms. Since at the conceptual design phase, most of the information regarding the proposed wind energy project is uncertain. Undesirable delays may occur if assuming fixed wind farm size and/or the installed capacity.

In addition, to allow the consideration of land usage, which is related to many planning activities at the early stage, a land usage model is also needed. This model should be capable to account for land-based constraints and environmental impact.

2.4.2.3 Research Needs in the Multi-Objective Optimization Solver

Considering the fast convergence need for solving WFLO problems, a multi-objective version of PSO is desired in this research to address the major complex attributes in multi-objective WFLO. Important modifications need to be made to retain the original advantages of the basic PSO and mitigate its pre-stagnation issue.

Given that developing a utility-scale wind farm may include a large number of both continuous and discrete design variables, the desired new MOPSO should also be capable of dealing with mixed-discrete design variables.

PART II

A Novel Approach to the Conceptual Design of Wind Farms

CHAPTER 3

Primary Performance Objectives in Wind Farm Design

This chapter provides the detailed descriptions of models used to evaluate the primary performance objectives. Specifically, (i) the annual energy production of a wind farm is computed using the energy production model offered by the Unrestricted Wind Farm Layout Optimization methodology; (ii) the wind farm cost of energy is estimated using the Wind Turbine Design Cost and Scaling model developed by National Renewable Energy Laboratory; and (iii) the layout based land usage model developed in this research is used to quantify the land usage based on a given farm layout of a wind farm.

3.1 Annual Energy Production

Annual Energy Production (AEP) is one of the most important performance criteria in wind energy development. The energy production model used in this research is adopted from the UWFLO framework developed by Chowdhury et al. [43], which is one of the most advanced frameworks in WFLO. This energy production model quantifies the wind farm power output as a function of the turbine features, the location of turbines, and the incoming wind conditions [43]. A *generalized power curve* is used to evaluate the power output of each turbine. This *generalized power curve* is scaled back to represent the approximated power response of a particular commercial turbine, using the corresponding manufacturer specifications. For Turbine-i, the power generation, P_i, can be evaluated using the following

equations:

$$\frac{P_i}{P_r} = \begin{cases} P_n\left(\frac{U_i - U_{in}}{U_r - U_{in}}\right), & \text{if } U_{in} < U_i < U_r \\ 1, & \text{if } U_r < U_i < U_{out} \\ 0, & \text{if } U_{out} < U_i \text{ or } U_i < U_{in} \end{cases} \tag{3.1}$$

where U_i is the velocity immediately in front of Turbine-i. Estimation of U_i accounts for wake merging scenarios and the possibility of partial wake-rotor overlap. U_{in}, U_{out}, and U_r are respectively the turbine cut-in, cut-out, and rated speeds, reported by the turbine manufacturer. The function P_n represents a polynomial fit for the *generalized power curve*, generated using the power curve data reported for the "GE 1.5 MW xle" turbine [122], which can be expressed as

$$\begin{aligned} P_n = \; & 10.3686\left(\tfrac{U_i - U_{in}}{U_r - U_{in}}\right)^5 - \left(\tfrac{U_i - U_{in}}{U_r - U_{in}}\right)^4 + 24.2977\left(\tfrac{U_i - U_{in}}{U_r - U_{in}}\right)^3 \\ & -7.5166\left(\tfrac{U_i - U_{in}}{U_r - U_{in}}\right)^2 + 1.5967\left(\tfrac{U_i - U_{in}}{U_r - U_{in}}\right) + 0.0034 \end{aligned} \tag{3.2}$$

This power generation model also allows for a variable induction factor. According to the 1-D flow assumption [123, 124], the induction factor a and the power coefficient, C_p, can be related by

$$C_p = 4a(1-a)^2 \tag{3.3}$$

where the power coefficient itself can be expressed as a function of incoming wind speed and turbine characteristics, as given by

$$C_p = \frac{P_i}{P_0} = \frac{P_i}{\frac{1}{8}\rho\pi D_i^2 U_\infty^3} \tag{3.4}$$

In Eq.(3.4), P_0 represents the power available from the wind; and U_∞ is the incoming wind speed at the hub height.

Subsequent solution of the non-linear equation, Eq.(3.3), gives the induction factor for each turbine based on the estimated approaching wind conditions. Thereafter, the overall power output of a N-turbine wind farm, $P_{farm}(U^j, \theta^j)$, can then be given by

$$P_{farm}(U^j, \theta^j) = \sum_{i=1}^{N} P_i \tag{3.5}$$

where U^j and θ^j represent the j^{th} wind condition defined by incoming wind speed U and wind direction θ. Assuming the wind farm operates continuously throughout the year (all 365×24 hours), the AEP of this wind farm, E_{farm} (in kWh/yr), can be expressed as

$$\begin{aligned} E_{farm} &= (365 \times 24) \sum_{j=1}^{N_p} P_{farm}(U^j, \theta^j) p(U^j, \theta^j) \Delta U \Delta\theta, \\ \text{where} \\ \Delta U \Delta\theta &= U_{max} \times 360^\circ / N_P \end{aligned} \tag{3.6}$$

In Eq. 3.6, U_{max} represents the maximum possible wind speed in the current wind distribution; $p(U^j, \theta^j)$ represents the probability of the occurrence of the j^{th} wind condition. It is important to note that the wake effects are integrated in this model, particularly in the process of determining the effective wind speed immediately in front of any turbine (U_i). Given the predicted wake growth, the location of turbines, and the turbine features, an influence matrix is created to determine whether a turbine is in the wakes of other upstream turbines for a given wind direction. As a result, the velocity immediately in front of each turbine is dynamically evaluated using a wake model, and in the same order in which the turbines encounter the wind coming from a particular direction. The Katic model [34] is used here to account for the wake merging and partial wake-rotor overlap. If Turbine-i is in the influence of multiple wakes created by K upstream turbines, the corresponding velocity

deficit, v_i, is given by

$$v_i = \sqrt{\sum_{k=1}^{K} \frac{A_{ki}}{A_i} (u_f^{ki})^2} \tag{3.7}$$

where u_f^{ki} represents the velocity deficit in the wake (created by Turbine-k) at the location of Turbine-i; and A_{ki} is the effective influence area of the wake (created by Turbine-k) on Turbine-i. If Turbine-i is completely in the wake of Turbine-k, $A_{ki} = A_i$; otherwise, A_{ki} denotes the overlapping area between the wake of Turbine-k and Turbine-i, estimated by standard geometrical intersection formula.

3.2 Wind Farm Cost of Energy

Wind farm cost of energy (COE) is measured by the LCOE, which is given by

$$COE = \frac{FCR \times ICC + LRC}{AEP} + LLC + O\&M \tag{3.8}$$

where

ICC – Initial Capital Cost ($/kWh)

LRC – Levelized Replacement Cost ($/kWh)

LLC – Land Lease Cost ($/kWh)

$O\&M$ – Operation and Maintenance Cost ($/kWh)

AEP – Annual Energy Production (kW)

FCR – Fixed Charge Rate

In Eq.(3.8), the Wind Turbine Design Cost and Scaling (WTDCS) model developed by National Renewable Energy Laboratory [125] is used to estimate the initial capital cost, the levelized replacement cost, the land lease cost, and the annual operation and maintenance cost. The initial capital cost is the sum of the turbine system cost and the balance of station cost, which can be quantified as a function of the turbine rated power, the rotor diameter, the hub height, and the type of drive train. Primary cost elements considered in this term are as follows [125]:

- Rotor
  - Blades
  - Hub
  - Pitch mechanisms and bearings
  - Spinner, nose cone
- Drive train nacelle
  - Low-speed shaft
  - Bearings
  - Gearbox
  - Mechanical brake, high-speed coupling, and associated components
  - Generator
  - Variable-speed electronics
  - Yaw drive and bearing
  - Main frame

  - Electrical connections
  - Hydraulic and cooling systems
  - Nacelle cover
- Control, safety system, and condition monitoring
- Tower
- Balance of station
  - Foundation/support structure
  - Transportation
  - Roads, civil work
  - Assembly and installation
  - Electrical interface/connections
  - Engineering permits

It is important to note that turbines used in this model are subject to the assumption of a specified type: three bladed, upwind, pitch-controlled, variable-speed with active yaw, and mounted on steel tubular towers.

In this research, the AEP is computed by integrating the power generation over a wind distribution in terms of a series of sampling wind conditions, using the energy production model in the UWFLO framework [43]. Therefore, the annual levelized replacement cost is given by [125]

$$\text{Annual } LRC = \$10.7/\text{kW} \times P_r \tag{3.9}$$

where P_r is the turbine rated power. Based on the report in Ref. [125], the annual operation and maintenance cost (land-based) and the annual land lease cost are represented as linear functions of AEP, which are \$0.00108/kWh and \$0.007/kWh, respectively. In addition, the fixed charge rate is assumed to be 11.85% constantly.

3.3 Land Usage

Land configuration is an important consideration in wind energy development. From the design perspective, land configuration can be represented in terms of land area, land shape, and site orientation. The design of a wind farm layout is generally optimized to reduce the wake-induced energy losses and maximize the energy production. However, the maximum energy that can be extracted from a certain wind farm land shape (defined by specific boundaries) could significantly differ from that given by another farm site. Besides, the size and the ground property of a wind farm site determine how many turbines and what type of turbines can be placed in this site, thus regulating the scale of the proposed wind energy project. However, in the case of conventional WFLO, land area and the installed capacity (the number of turbines) are prescribed, so the optimal farm layouts and the corresponding maximum energy production that can be obtained under a certain wind resource depend on the pre-defined installed capacity and the boundaries of the wind farm. In fact, at the early stage of wind energy development, the boundaries of a wind farm governing turbine installations are themselves subject to planning and need not be fixed.

On the other hand, large utility-scale wind energy projects demand greater land area for wind farms, since the reduction of wake-induced energy losses necessitates larger inter-turbine spacing. Therefore, the energy production is also strongly related to the allowed land area [88]. Particularly, large utility-scale wind energy projects are more likely to have

concerns regarding permitting framework, the net environmental impact on surroundings (e.g., noise impact and impact on local wildlife), and potential landowner participation related issues [126,127]. Specifically, in the context of the ISO-9613-2 [128], the noise impact of a wind farm on its surroundings is primarily a function of the distance away from the source, i.e., the installed wind turbines. Besides, the reported rates of bird, raptor, and bat mortality are measured by the wind farm nameplate capacity [129] – the available land resource subsequently reflects the scale of the wind farm. In other words, a wind farm's net impact on surroundings is strongly related to its land usage. Therefore, wind energy projects in turn demand minimization of the land footprint of wind farms, **assuming that minimizing the land usage will reduce the degree of impact of the wind farm on its immediate surroundings**.

In this research, a wind farm land usage model was developed to determine the land area taken by the installed turbines without prescribing farm boundaries. In this model, the land usage of a wind farm is determined by the wind farm layout or turbine arrangement. For any given optimal farm layout, the "2D convex hull" enclosing all turbines is determined. The Graham scan algorithm [130] is applied to find turbines that comprise the facets of the 2D convex hull. Considering wind farms generally have a rectangular shape, and that land is sold on leased as rectangular plots, the land shape in this paper is then determined by **the smallest bounding rectangle (SBR)** enclosing all turbines, which is computed using the rotating calipers algorithm [131]. A buffer zone, equivalent to one rotor diameter, is then added to each side to yield the final land usage estimate. As shown in Fig. 3.1, the region enclosed by the solid line box represents the SBR, and the layout-based land usage ("including buffer area") is denoted by the dash line. As a result, we quantify the land usage

of an N-turbine wind farm as a function of the turbine coordinates, given by

$$\begin{aligned} A_{land} &= f(\vec{X}^N, \vec{Y}^N) \\ S_{land} &= g(\vec{X}^N, \vec{Y}^N) \end{aligned} \tag{3.10}$$

where A_{land} and S_{land} represent the land area and the land shape of the wind farm; and $(\vec{X}^N, \vec{Y}^N)$ represents the turbine coordinates.

If the optimal layout, $(\vec{X_*}^N, \vec{Y_*}^N)$, is given, the optimal land area (A^*_{land}) and land shape (S^*_{land}) of the wind farm can be expressed as

$$\begin{aligned} A^*_{land} &= f(\vec{X_*}^N, \vec{Y_*}^N) \\ S^*_{land} &= g(\vec{X_*}^N, \vec{Y_*}^N) \end{aligned} \tag{3.11}$$

It should be also noted that the land shape can be regulated by the smallest bounding circle, eclipse, triangle, or any other 2D convex polygon.

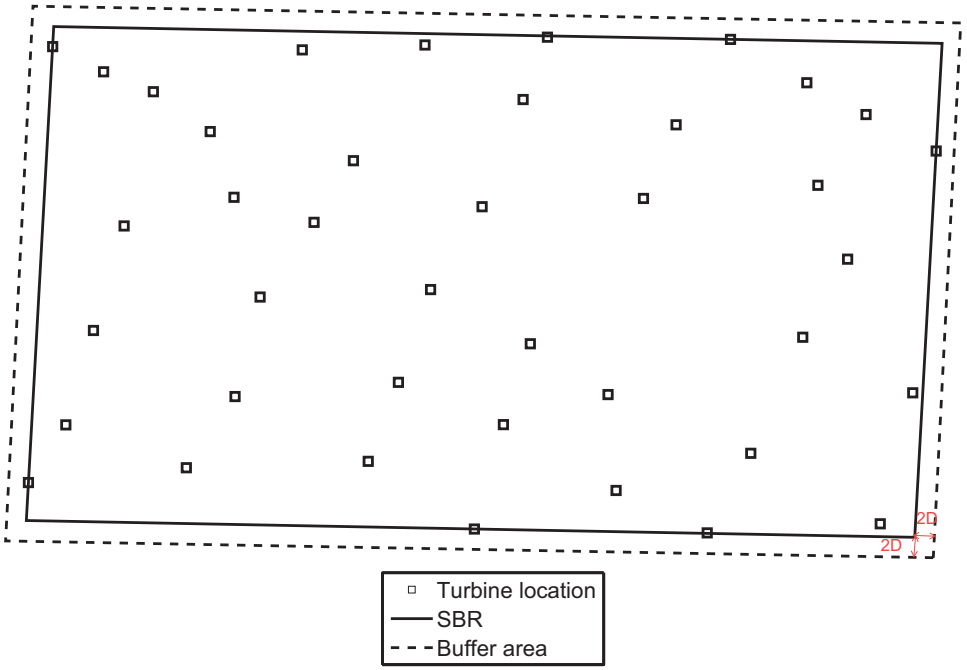

Figure 3.1: Illustration of the wind farm layout

CHAPTER 4

Identifying Key Factors Influencing Wind Farm Performance

This chapter provides the sensitivity analysis work to identify the relative impact of different natural and design factors on the wind farm performance objectives. Section 4.1 explores how different the wind farm power estimation would be if using different wake models. Section 4.2 investigates the sensitivity of both array-like and optimized wind farm outputs to the following key factors: (i) incoming wind speed, (ii) ambient turbulence, (iii) land configuration, and (iv) nameplate capacity. The impact of the choice of wake models on the relative impact of different natural and design factors is also explored. Four analytical wake models are implemented and compared for the purpose of quantifying wake-induced power losses.

4.1 Impact of Different Analytical Wake Models on Wind Farm Power Estimation

This section investigates the impact of using different analytical wake models (I) on the wake behavior downstream of turbines, and (II) on the relationship of wind farm power generation to land area and Nameplate Capacity (NC). Careful numerical experiments are designed to illustrate the variation in wake behavior and the variation of the wind farm power generation with unit land area and incoming wind speed. Four analytical wake models are investigated, namely, Jensen, Frandsen, Larsen, and Ishihara wake models. Table 4.1 lists the general input parameters considered in each wake model.

Table 4.1: Analytical wake model inputs

Input to wake model	Jensen	Frandsen	Larsen	Ishihara
Incoming wind speed	✓	✓	✓	✓
Streamwise distance from hub	✓	✓	✓	✓
Radial distance from hub			✓	✓
Rotor diameter	✓	✓	✓	✓
Hub height			✓	
Turbulence intensity			✓	✓

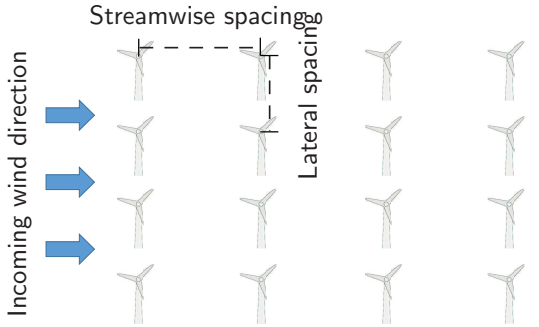

Figure 4.1: An array-like farm layout with 16 "GE 1.5 MW xle" turbines

4.1.1 Numerical Settings

We assume a rectangular wind farm with 16 "GE 1.5 MW xle" turbines arranged in a 4×4 array-like layout as shown in Fig. 4.1. The power characteristics of "GE 1.5 MW xle" turbine is shown in Fig. 4.2, and Table 4.2 lists the turbine specifications. The range of incoming wind speed is varied between the turbine cut-in speed and cut-out speed. The land area per MW installed (LAMI), A_{MW}, is used to represent the unit land area. The range of A_{MW} is specified as

$$10\frac{D^2}{P_r} < A_{MW} < 30\frac{D^2}{P_r} \tag{4.1}$$

where P_r is the turbine rated power in MW.

This range of LAMI spans from a very stringent (small) land footprint to practically average land footprint which is the range of interest for future wind farms, considering that a generous land footprint has an undesirable impact on surroundings. This range was used for a land area-energy production analysis by Chowdhury et al. [132], and motivated by the

land area of currently operational US wind farms, reported by [133]. For a "GE 1.5 MW xle" turbine, the rated power is 1.5 MW. Since identical turbines are considered, the numerical range of the LAT, A_T, is given by

$$70,000 \text{ m}^2 \leq A_T \leq 200,000 \text{ m}^2 \tag{4.2}$$

We also assume that all turbines are uniformly arranged, and the land aspect ratio is fixed at 7/3. Hence, the effective inter-turbine spacing is regulated by the LAT. We also assume a unidirectional wind condition, a constant ambient turbulence intensity over the farm site, and a uniform incoming velocity profile over the rotor area. The ratio of the longitudinal (or streamwise) spacing and the lateral spacing between turbines is also maintained at 7/3.

Here, we used the wind farm capacity factor (CF) to measure the wind farm power generation performance. The wind farm capacity factor is defined as the ratio of the actual power generation of the wind farm to the installed capacity of the wind farm. As shown in Eq. 2.19, P_{NC} is the nameplate capacity of the concerned wind farm; and P_{farm} is the actual power generated by the wind farm, as estimated by the UWFLO power generation model. Jensen wake model is used to account for the wake-induced power losses. The results from the two different numerical experiments, i.e., the single wake test and the wind farm power analysis, are discussed in the following subsections.

4.1.2 Single Wake Analysis

The single wake test provides important insights into the distinguishing characteristics of the wake behavior, simulated by different wake models. The "GE 1.5 MW xle" turbine is used in this test (Table 4.2). Additionally, since far wake scenarios are mostly considered

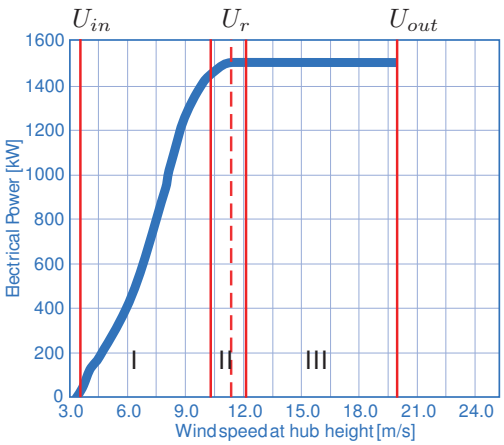

Figure 4.2: Power curve of "GE 1.5 MW xle" turbine [122]

Table 4.2: Specifications of "GE 1.5 MW xle" turbine [122]

Specifications	Value
Rated power (P_r)	1.5 MW
Turbine rotor diameter (D)	82.5 m
Hub height (H)	80 m
Cut-in speed (U_{in})	3.5 m·s^{-1}
Cut-out speed (U_{out})	20 m·s^{-1}
Rated speed (U_r)	11.5 m·s^{-1}

(i.e., turbines are unlikely to be located within each other's near wakes), the simulation of wake behaviors starts at two rotor diameters downstream from the turbine. Figures 4.3(a) and 4.3(b) present the wake expansions and the wake speeds behind the "GE 1.5 MW xle" turbine, as estimated by the four analytical wake models. It is observed that, along the entire flow field, the Frandsen model predicts the highest wake speed, and the Larsen model predicts the largest wake diameter. It is also observed that the Ishihara model predicts the lowest wake speed; however, it also yields the highest rate of wake recovery. This phenomenon can be attributed to the greater mixing of the turbine wake with the upper layers of the atmospheric boundary layer, which is facilitated by the turbine-induced turbulence specifically accounted for in the Ishihara model. It is important to note (from Fig. 4.3(a)) that, in the practically popular range of farm inter-turbine spacing (of 7D − 10D), the difference in the wake speeds

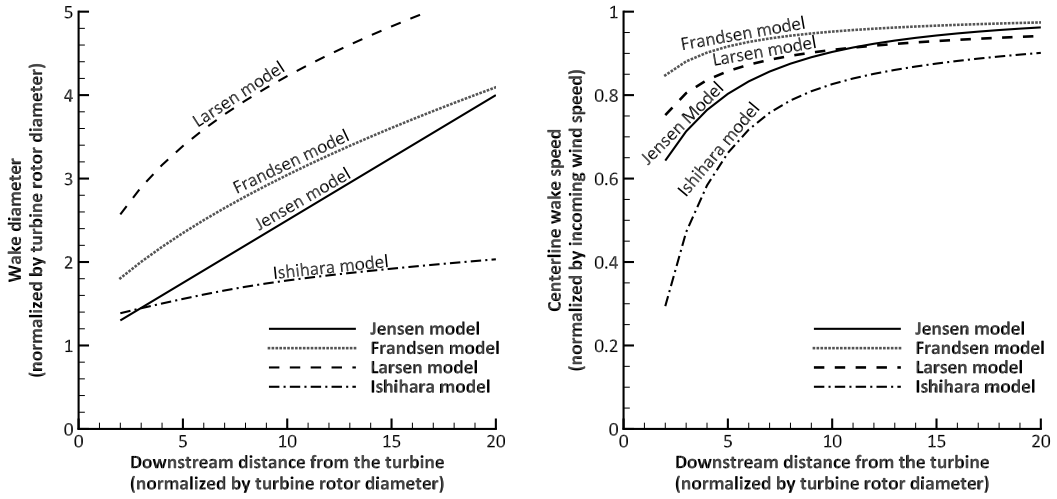

(a) Wake diameter behind a "GE 1.5 MW xle" turbine (b) Wake speed behind a "GE 1.5 MW xle" turbine

Figure 4.3: Single wake test

estimated by the four wake models is approximately $15 - 20\%$.

4.1.3 Wind Farm Power Generation Analysis

4.1.3.1 Power Variation with the Land Area per Turbine

Figures 4.4(a) – 4.4(d) show the variation of the wind farm capacity factor with the LAT, estimated at different values of incoming wind speed. Among the four analytical wake models, the Frandsen model predicts the largest capacity factor while the Ishihara wake model predicts the smallest; this trend holds true over the entire range of LAT studied and the different incoming wind speeds considered. **Three scenarios** are observed based on the flow patterns inside the wind farm.

Scenario one: When the incoming wind speed is close to the turbine cut-in speed, the downstream turbines most likely do not start generating power, since the wake speed they encounter is lower than the turbine cut-in speed. As shown in Fig. 4.4(a), when the incoming wind speed is 4 $\text{m}\cdot\text{s}^{-1}$, the capacity factor predicted using the Frandsen

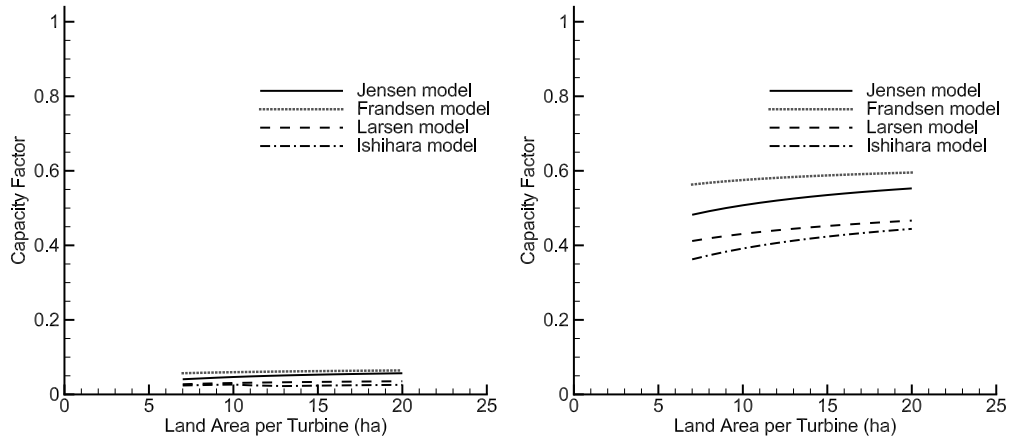

(a) Incoming wind speed = 4 m·s^{-1} (slightly above the turbine cut-in speed)

(b) Incoming wind speed = 8 m·s^{-1} (in between the turbine cut-in and rated speeds)

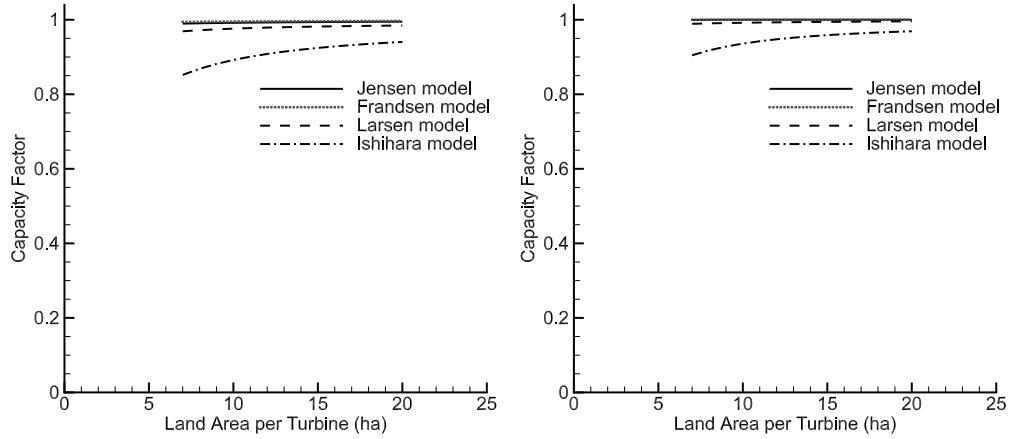

(c) Incoming wind speed = 11.5 m·s^{-1} (at the turbine rated speed)

(d) Incoming wind speed = 12 m·s^{-1} (slightly above the turbine rated speed)

Figure 4.4: Variation of the capacity factor with the LAT

model or the Jensen model shows some variation with the LAT. This is attributed to their relatively high predicted wake speeds, as shown in Fig. 4.3(a). For the cases using Larsen model and Ishihara model, due to their relatively lower wake speed estimates, the predicted capacity factors show almost no variation with the LAT (within the specified ranges).

Scenario two: The wake speed in front of the downstream turbines is expected to be higher

than the turbine cut-in speed in this case. The flow pattern inside the wind farm now becomes more complex owing to the combined influence from the wake effects and the inter-turbine spacing regulated by the LAT. As shown in Fig. 4.4(b), the capacity factors predicted using all four wake models are varying with the LAT. A trend is observed that the capacity factor improves as the LAT increases. However, as the incoming wind speed is approaching the turbine rated speed, the variation of the predicted capacity factor with the LAT becomes less prominent.

Scenario three: This scenario is observed when turbines in the first row reach the rated power. As shown in Fig. 4.4(c), the capacity factor predicted using the Frandsen model, the Jensen model, or the Larsen model shows marginal to no variation with LAT (the predicted value is slightly below 100% due to the wake effects). However, this is not the case with the Ishihara model due to its relatively lower wake speeds estimation. As the incoming wind speed continues to increase, the velocity in front of all the downstream turbines also exceeds the turbine rated speed. Therefore, all downstream turbines are then able to reach the rated power, leading to a 100% capacity factor. In Fig. 4.4(d), the capacity factor predicted using the Jensen model or the Frandsen model has reached 100%. If the incoming wind speed continued to increase beyond 12 $m \cdot s^{-1}$, the Larsen model and the Ishihara model will also lead to 100% capacity factor.

4.1.3.2 Power Variation with the Incoming Wind Speed

The variations of the capacity factor with incoming wind speed are investigated at selected values of LAT, as shown in Fig. 4.5(a) – 4.5(c). The "normalized power curve" (indicted by a light grey curve) represents the polynomial fit for the *generalized power curve* normalized with respect to the turbine rated power. Among the four analytical wake models,

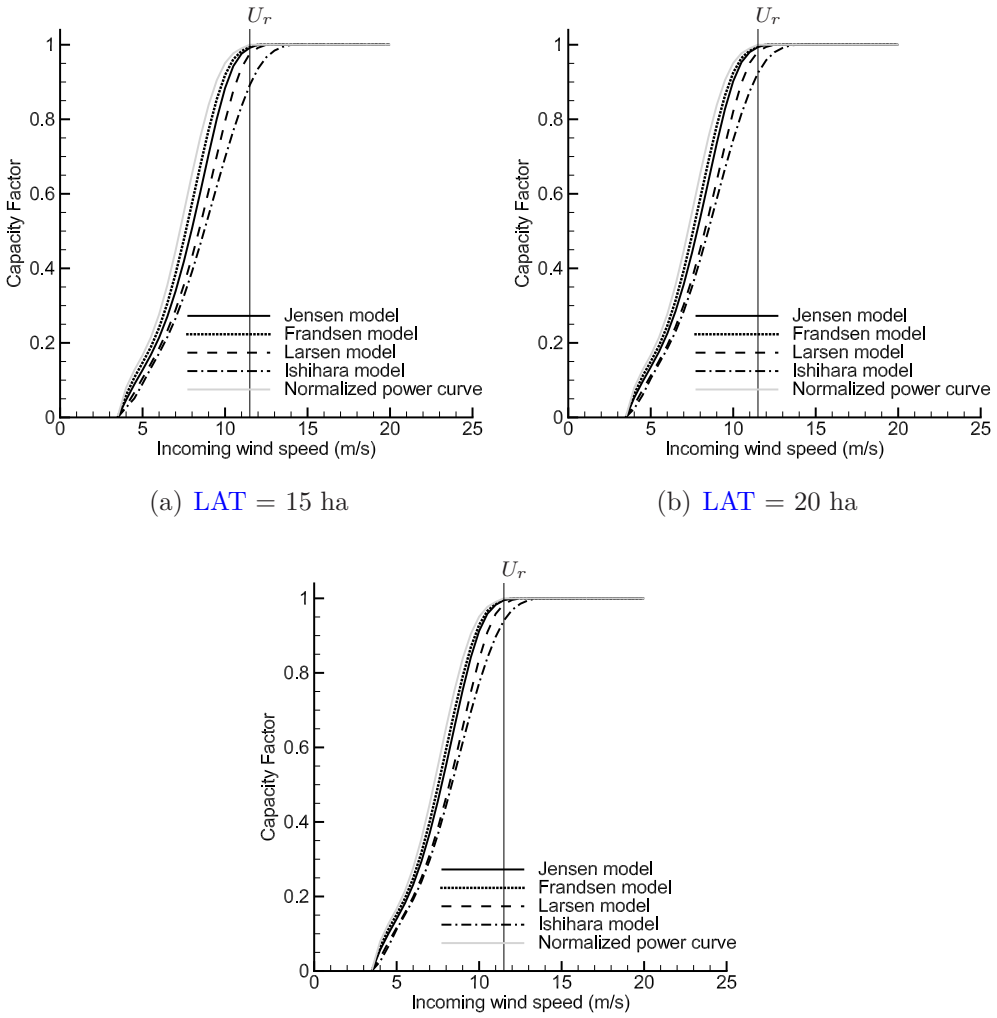

(a) LAT = 15 ha

(b) LAT = 20 ha

(c) LAT = 25 ha

Figure 4.5: Variation of the capacity factor with the incoming wind speed

we observe that the Frandsen model predicts the highest capacity factor, while the Ishihara wake model predicts the lowest capacity factor. It is observed that, owing to the wake effects, all the predicted capacity factor curves asymptotically approach the normalized power curve when the LAT increases. In addition, the difference between the capacity factors predicted using different wake models slightly decreases as the LAT increases.

Table 4.3: Upper and lower bounds of natural factors

Natural factors	Case 1 (Region I)		Case 2 (Region II)		Case 3 (Class IV)	
	Lower bound	Upper bound	Lower bound	Upper bound	Lower bound	Upper bound
Incoming wind speed	3.5 m·s^{-1}	10.35 m·s^{-1}	10.35 m·s^{-1}	12.1 m·s^{-1}	7.0 m·s^{-1}	7.5 m·s^{-1}
Ambient turbulence	10%	25%	10%	13%	14%	16%

Table 4.4: Upper and lower bounds of design factors

Design factors	Lower bound	Upper bound
Land area/MW installed	10 ha/MW	50 ha/MW
Land aspect ratio	0.1	10
Nameplate capacity	15 MW	150 MW

4.2 Sensitivity Analysis of Wind Farm Power Output

In this section, we analyze the sensitivity of wind farm output to five key factors, which include (i) incoming wind speed (U_∞), (ii) ambient turbulence (I_a), (iii) land area per MW installed (A_{MW}), (iv) land aspect ratio (a_r), and (v) nameplate capacity (P_{NC}). Two numerical experiments are conducted to perform the SA using the "GE 1.5 MW xle" turbines (Table 4.2). Numerical Experiment I examines the sensitivity of the power output of an array-like wind farm to the first four input parameters. The wind farm is assumed to have 16 turbines installed on a 4×4 array-like layout. In Numerical Experiment II, we investigate the sensitivity of the maximized wind farm output to all five input parameters. The maximized wind farm output is obtained by WFLO, which is performed using the single objective Mixed-Discrete Particle Swarm Optimization (MDPSO) algorithm (from the UWFLO framework) [43,134]. The assumptions made in the case of these two numerical experiments are summarized below:

i. Wind shear effect is not considered in this paper; the incoming velocity is assumed to be uniform over the entire rotor area (rotor-averaged velocity);

ii. Identical turbines are considered;

iii. The wind farm has a rectangular shape; and

iv. The ambient turbulence over the farm site is constant everywhere.

The Extended Fourier Amplitude Sensitivity Test (eFAST) is used to perform the SA. An overview of the eFAST method is provided in the following subsection.

4.2.1 Overview of the Extended Fourier Amplitude Sensitivity Test

The Extended Fourier Amplitude Sensitivity Test (eFAST) developed by Saltelli and Bolado [135] is adopted in this paper. The eFAST method was developed based on the original FAST method proposed by Ckuier et al. [136–139]. The primary advantage of eFAST method is the ability to determine both the first-order and the total-order sensitivity indices. The first-order index, also known as the main effect, illustrates the variance of the model output due to each of the input parameters. To estimate the first-order index, the input parameters of a model are transformed into a frequency domain using a Fourier transformation. Hence, partitioning of variance is achieved by encoding the identity of different input parameters at different frequencies. In the original FAST method [136], for a model with n input parameters, $X = [x_1, x_2, \ldots, x_n]$, the output of the model, Y, is expressed as $Y = f(x_1, x_2, \ldots, x_n)$.

A search function is defined to allow the input parameter to oscillate periodically in the input space, by assigning a characteristic frequency ω_i, expressed as

$$x_i = G_i(sin\omega_i s), \qquad i = 1, 2, \ldots, n \tag{4.3}$$

Here G_i is a transform function, and $s \in (-\infty, +\infty)$ is a scalar.

By applying the properties of Fourier series, $E(Y)$ can be expressed as

$$Y = f(s) = A_0 + \sum_{k=1}^{+\infty} [A_k \cos(ks) + B_k \sin(ks)] \tag{4.4}$$

where $f(s) = f(x_1(s), x_2(s), \ldots, x_n(s))$, and $i = 1, 2, \ldots, n$; A_0, A_k, and B_k are the Fourier coefficients, defined as

$$\begin{aligned} A_0 &= \frac{1}{2\pi} \int_{-\pi}^{\pi} f(s) ds, \text{ and} \\ A_k &= \frac{1}{\pi} \int_{-\pi}^{\pi} f(s) \cos(ks) ds, \; B_k = \frac{1}{\pi} \int_{-\pi}^{\pi} f(s) \sin(ks) ds \end{aligned} \tag{4.5}$$

For practical problems, k must be limited to a reasonable value of the integer N, which indicates the sample size of the input data. The variance of the model output, s_Y^2, can therefore be approximated as

$$s_Y^2 = E(Y^2) - [E(Y)]^2 \approx \frac{1}{2\pi} \sum_{k=1}^{(N-1)/2} \left(A_k^2 + B_k^2\right)$$

where

$$A_k = \frac{1}{\pi} \sum_{j=1}^{N} f(s_j) \cos(s_j k), \; B_k = \frac{1}{\pi} \sum_{j=1}^{N} f(s_j) \sin(s_j k) \tag{4.6}$$

In the variance-based SA, the first-order sensitivity index of an input parameter, x_i, is defined as the conditional variance of the model output, $s^2_{E(Y/x_i)}$, with respect to the unconditional variance of the model output (s_Y^2). To measure this conditional variance, the expectation value of x_i, $E(Y/x_i)$, must be evaluated throughout the entire interval of x_i. In the FAST method, the conditional variance is approximated by summing up the spectrum

values for the basic frequency ω_i and its higher harmonics, as shown below.

$$s^2_{E(Y/x_i)} \approx \frac{1}{2}\sum_{p=1}^{m}(A^2_{p\omega_i} + B^2_{p\omega_i}) \tag{4.7}$$

In Eq.(4.7), $p \in Z$ and $p\omega_i \leq (N-1)/2$; and m indicates the order of higher harmonics that are considered [139].

Therefore, the first-order index can be formulated by combining Eq.(4.7) and Eq.(4.6), which is expressed as

$$S_i = \frac{s^2_{E(Y/x_i)}}{s^2_Y} \tag{4.8}$$

The total-order sensitivity index includes the interactions between the input parameters of any order. The eFAST method uniquely accounts for interactions by considering the complementary set of the conditional variance, corresponding to the i^{th} input [140]. Here, we use "$\neq i$" to denote "all except i". Hence, the conditional variance, $s^2_{E(Y/x_{\neq i})}$, is expressed as

$$s^2_{E(Y/x_{\neq i})} = 2\sum_{p=1}^{m}(A^2_{p\omega_{\neq i}} + B^2_{p\omega_{\neq i}}) \tag{4.9}$$

The total-order index is thus given by subtracting the variance due to all other input parameters from 1, that is

$$S_{Ti} = 1 - \frac{s^2_{E(Y/x_{\neq i})}}{s^2_Y} \tag{4.10}$$

4.2.2 Upper and Lower Bounds of Input Parameters

The process of SA of the wind farm output could become expensive even under the use of analytical wake models. It is therefore important to have a computationally efficient approach to implement the SA. As a result, the selection of the upper and lower bounds of different natural and design factors influencing the wind farm power estimation is an

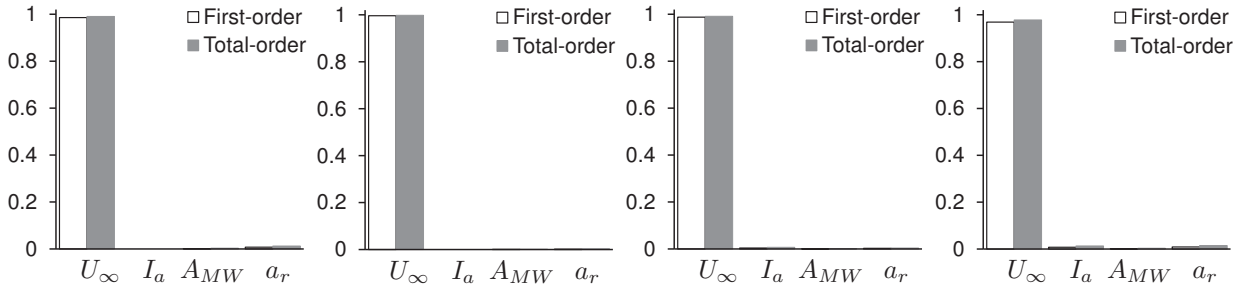

(a) Jensen model (b) Frandsen model (c) Larsen model (d) Ishihara model

U_∞: Incoming wind speed I_a: Ambient turbulence
A_{MW}: Land area/MW installed a_r: Land aspect ratio

Figure 4.6: Sensitivity analysis of the power output of a wind farm with a 4×4 array-like layout (Case 1)

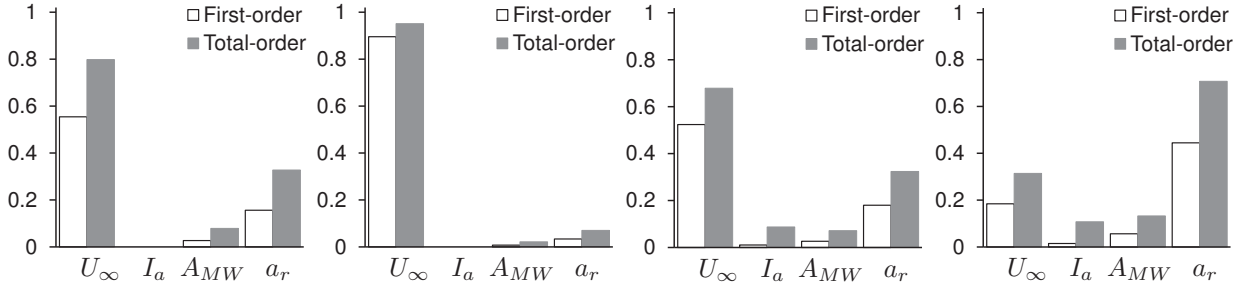

(a) Jensen model (b) Frandsen model (c) Larsen model (d) Ishihara model

U_∞: Incoming wind speed I_a: Ambient turbulence
A_{MW}: Land area/MW installed a_r: Land aspect ratio

Figure 4.7: Sensitivity analysis of the power output of a wind farm with a 4×4 array-like layout (Case 2)

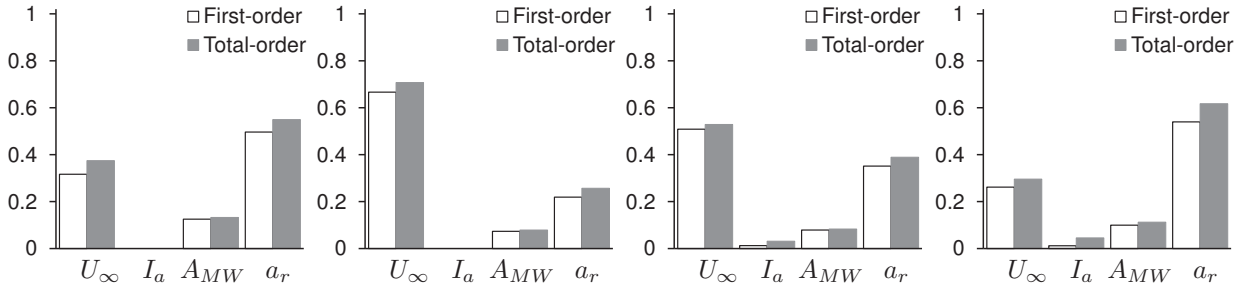

(a) Jensen model (b) Frandsen model (c) Larsen model (d) Ishihara model

U_∞: Incoming wind speed I_a: Ambient turbulence
A_{MW}: Land area/MW installed a_r: Land aspect ratio

Figure 4.8: Sensitivity analysis of the power output of a wind farm with a 4×4 array-like layout (Case 3)

important step in itself. It requires significant prior understanding of the area of WFLO. In this paper, five input parameters are investigated, including two natural factors (incoming wind speed and ambient turbulence) and three design factors (land area per MW installed, land aspect ratio, and nameplate capacity). The ranges of all input parameters are specified with the objective to focus on the variation or range that is most likely to occur in practice.

The upper and lower bounds of incoming wind speed are set as the turbine cut-in speed (3.5 $m{\cdot}s^{-1}$) and cut-out speed (20 $m{\cdot}s^{-1}$), respectively. Based on the nature of the turbine power curve, the incoming wind speed can be divided into three regions as shown in Fig. 4.2. In the first region where the incoming speed is below the turbine rated speed, the farm power output is highly sensitive to the incoming wind speed. The second one is a transient region, where the power output may be variably sensitive to the incoming wind speed depending on the degree of the wake-induced power losses. This is because the wake-induced losses can drive the incoming wind from Region II to Region I for the downstream rows of turbines. Hence, the incoming wind speed in this region is ranged from 10% below to 5% above the turbine rated speed. In the third region, the power output of the farm is weakly or not sensitive to the incoming wind speed variations. This is because, in this case even after wake losses, the wind speed approaching the downstream turbines within the farm remain above the rated speed, unless the farm comprises a very large number of turbines (that would then lead to substantial cumulative wake losses). Therefore, SA is only performed in the first two regions (defined in Fig. 4.2, i.e. Case I and Case 2, respectively. Additionally, a new case (Case 3) is defined to investigate the variation of incoming wind speed in the range representing wind speed Class IV (between 7 $m{\cdot}s^{-1}$ and 7.5 $m{\cdot}s^{-1}$). The purpose of Case 3 is to better understand the impact of the four input parameters other than wind speed, as these impacts are otherwise grossly overshadowed by the influence of wind speed in Case 1

and Case 2.

The variation range of the ambient turbulence in this paper is specified from 0.1 to 0.25, which is determined based on the representative turbulence intensity given by IEC 61400-1 (Edition 3) [141].

The land aspect ratio, a_r, is varied between 0.1 and 10. The range of LAMI is set between 10 ha/MW and 50 ha/MW, based on the reported average unit land usage of US commercial wind farms in 2009 (34.5 ± 22.4 ha/MW) [133]. The number of turbines is ranged from 10 to 100. Since identical turbines are considered, the nameplate capacity therefore varies between 15 MW and 150 MW. Owing to the computational constraints, the nameplate capacity is limited to 150 MW, which is the level of a mid-scale wind farm. The trends obtained are however expected to hold for wind farms with larger number of turbines.

Tables 4.3 and 4.4 list the detailed upper and lower bounds specified for the natural and design input parameters, respectively. It is important to note that the upper and lower bounds of the natural input parameters are specified differently for each case, whereas those for the design input parameters are fixed across all three cases.

4.2.3 Numerical Experiment I: Sensitivity Analysis of the Power Output of Wind Farms with Array-Like Layouts

In this part, the sample size of each input parameter is set at 1000. Figure 4.6 presents the sensitivity of wind farm power output to the four input parameters. In this case, the incoming wind speed is between 3.5 m·s^{-1} and 10.35 m·s^{-1} (Case 1). How the choice of wake models affect the sensitivity of the estimated power output to the input parameters is shown in Figs. 4.6(a) – 4.6(d). It is observed that the impact of incoming wind speed on the wind farm power output is dominant, irrespective of the choice of wake models. Both

the first-order and the total-order sensitivity indices of the incoming wind speed are close to 1.

Figures 4.7(a) – 4.7(d) show the SA performed in Case 2, where the variation of incoming wind speed is limited to a small range around the turbine rated speed (between 10.35 $m \cdot s^{-1}$ and 12.1 $m \cdot s^{-1}$). In Case 2, it is observed that the relative impact of the input parameters varies appreciably with the choice of wake models. Under all the four wake models, the incoming wind speed still remains the decisive factor affecting the power output. On closer observation, the power output predicted using the Frandsen model (Figs. 4.7(b)) is found to be the most sensitive to the incoming wind speed, which can be attributed to the tendency of the Frandsen model to yield relatively high wake speeds (Fig. 4.3(b)).

In contrast, the land aspect ratio appears to be the most important input parameter when using the Ishihara model (Fig. 4.7(d)); this is an important observation considering that the role of land shape (or aspect ratio) in wind energy production has not been comprehensively investigated either in the turbulence/ABL community or in the wind farm design community. It is also interesting to note that, irrespective of the choice of wake models, the land aspect ratio has a relatively stronger impact than the land area per MW installed. Overall, in Case 2 it is observed that the total-order sensitivity index of each input parameter is substantially higher than the corresponding first-order index, when compared to the results obtained in Case 1. This observation indicates that the influences of different factors on the farm are highly coupled, which is indirectly also representative of the high nonlinearity of the wind farm power output function. This in turn implies that, in estimating wind farm power generation, one needs to carefully consider the interactions between the input factors, which has not always been the case in conventional wind farm design.

Case 3 considers the standard wind class IV as the defined range of incoming wind

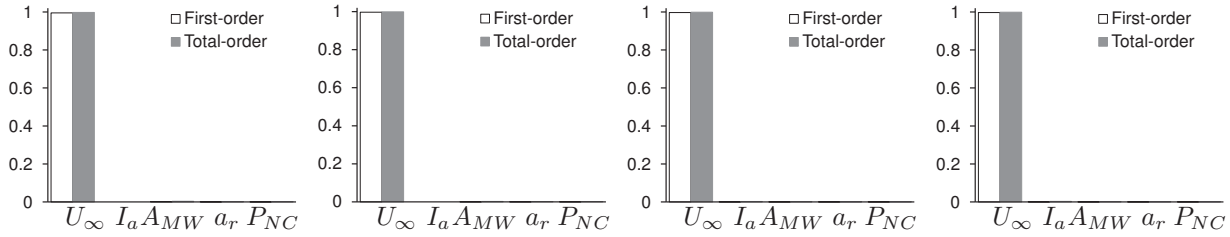

(a) Jensen model (b) Frandsen model (c) Larsen model (d) Ishihara model

U_∞: Incoming wind speed I_a: Ambient turbulence
A_{MW}: Land area/MW installed a_r: Land aspect ratio P_{NC}: Nameplate capacity

Figure 4.9: Sensitivity analysis on the maximized wind farm capacity factor with optimized layouts (Case 1)

speed. This case is intended to illustrate the relative importance of the input parameters other than wind speed. The sensitivity results of Case 3 are shown in Figs. 4.8(a) – 4.8(d). It is observed that the relative importance of the input parameters varies significantly with the choice of wake models. When using Frandsen model and Larsen model (Figs. 4.8(b) and 4.8(c)), the wind farm power output is still the mostly sensitive to incoming wind speed; while under Jensen model and Ishihara model (Figs. 4.8(a) and 4.8(d)), land aspect ratio is the most decisive input parameter that regulates the power output. Comparing these results with the single wake test, we can readily identify that the relative influence of incoming wind speed (in terms of wake model choice) on the wind farm power estimation follows the same order as that of the wake speeds estimated by the different wake models.

4.2.4 Numerical Experiment II: Sensitivity Analysis on Maximized Farm Output with Optimal Layouts

In the second numerical experiment, the sensitivity of the maximized farm output is analyzed with respect to five input parameters, including nameplate capacity in additional to those considered in Numerical Experiment I. The sample size of each input parameter is again set to 1000. Conditions under Cases 1 and 2 (Tables 4.3) are also explored in this

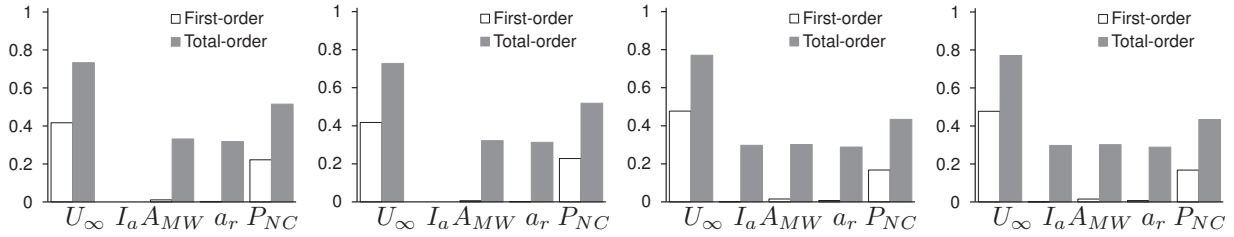

(a) Jensen model (b) Frandsen model (c) Larsen model (d) Ishihara model

U_∞: Incoming wind speed I_a: Ambient turbulence
A_{MW}: Land area/MW installed a_r: Land aspect ratio P_{NC}: Nameplate capacity

Figure 4.10: Sensitivity analysis on the maximized wind farm capacity factor with optimized layouts (Case 2)

Numerical Experiment.

The WFLO takes each combination of the sample input parameters as given conditions. Since identical turbines are considered, the number of turbines to be installed is readily determined based on the given sample value of the nameplate capacity. However, as the number of turbines for each WFLO may be different, the wind farm capacity factor (as defined in Eq.(2.19)) is used to represent the farm output (to be maximized). Therefore, the WFLO problem is formulated as

$$\begin{aligned} & \max \ CF(V) \\ & V = \{x_1, x_2, \cdots, x_{N_s}, y_1, y_2, \cdots, y_{N_s}\} \\ \textit{subject to} & \\ & g(V) \leq 0 \end{aligned} \tag{4.11}$$

where N_s is the number of turbines for the s^{th} combination of sample input parameters; $CF(V)$ is the capacity factor computed using the power generation model in the UWFLO framework [43]; V is the design vector, which denotes the location of turbines; and $g(V)$

defines the minimum inter-turbines spacing constraint ($2D$), as given by

$$g(V) = \sum_{\forall i \neq j} \max\{(2D - d_{ij}, 0\}\}$$
$$\text{where} \tag{4.12}$$
$$d_{ij} = \sqrt{(x_i - x_j)^2 + (y_i - y_j)^2}$$
$$i, j = 1, 2, \ldots, N_s$$

Figures 4.9(a) – 4.9(d) illustrate the sensitivity of maximized wind farm capacity factor to all the five input parameters, when the variation of incoming wind speed is located in Region I. Similar to Case 1 in Numerical Experiment I, the impact of incoming wind speed is again the dominant factor influencing the maximized wind farm output, irrespective of the choice of wake models.

A completely different scenario evolves when the variation of incoming wind speed restricted to that in Region II (Case 2). The corresponding results are shown in Figs. 4.10(a) – 4.10(d). It is observed (from Fig. 4.10) that the choice of wake models has a significantly smaller impact on the relative influence of each input parameter compared to that observed for an array-like layout (Fig. 4.7). For the array-like layout, the order of influence of the different input parameters varies across the different wake models. In contrast, for the optimized layout, the order of influence of the different input parameters remains consistent across all four wake models. For example, Figs. 4.10(a) – 4.10(d) show that wind speed and nameplate capacity are the strongest and the second strongest influencing factors across all four wake models; and land aspect ratio and the unit land area have a similar degree of influence irrespective of the choice of wake models.

In addition, large values of the total-order indices of all the input parameters are observed. This observation again indicates that the input factors are strongly coupled in

their influence on the maximized wind farm capacity factor. It also illustrates that the number of turbines, which is often fixed in conventional WFLO, has a significant impact on the maximized farm output potential, compared to other design factors; especially when the incoming wind speed is close to the turbine rated speed.

Figs. 4.11(a) – 4.11(d) illustrate the optimized layouts resulting from the use of the four different wake models; the corresponding maximized values of capacity factor is reported in the figure captions. Input parameters used to generate these layouts are: (i) $U = 7.5$ m·s^{-1}, (ii) $I_a = 10\%$, (iii) $A_{MW} = 35$ ha/MW, (iv) $a_r = 7/3$, and (v) $P_{NC} = 30$ MW (20 turbines). It is interesting to note that, using the Jensen or Frandsen wake model, most of the optimally located turbines lie on the left (upstream) and right (downstream) edges of the farm, with very few turbines on the inside of the farm site; while using the Larsen or Ishihara wake model, optimally located turbines are placed both inside and on the edges of the wind farm site. One possible cause of this difference in optimal layout pattern is as follows In Larsen or Ishihara wake model, the velocity deficit is affected by both the downstream and the radial distances from the turbine hub. Using Larsen or Ishihara wake model, downstream turbines are therefore not required to be primarily placed at greater distances from the upstream turbine to escape the impact of wakes, as is the case promoted by Jensen and Frandsen wake models.

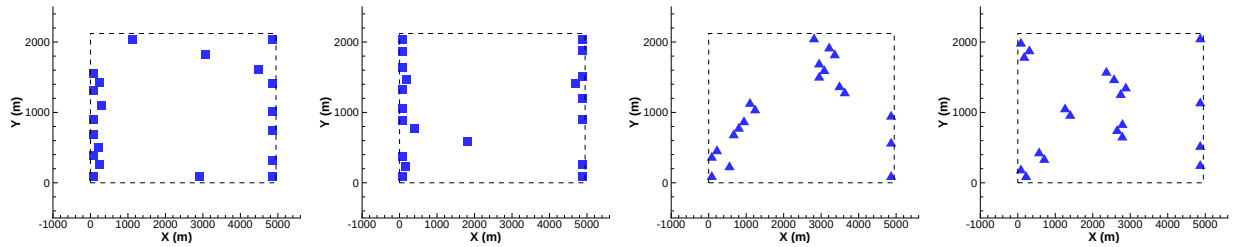

(a) Jensen model ($CF = 54.34\%$) (b) Frandsen model ($CF = 54.00\%$) (c) Larsen model ($CF = 54.15\%$) (d) Ishihara model ($CF = 54.69\%$)

Figure 4.11: Illustration of optimized layouts using different wake models

4.3 Chapter Summary

In this chapter, we explored the sensitivity of wind farm power output to five key natural and design factors, using the eFAST method. Important findings of this research are summarized below:

1. When the incoming wind speed is lower than the turbine rated speed, the clearly dominant impact of wind speed on the wind farm power generation is not affected by the choice of wake models.

2. When the incoming wind speed has a relatively small variation range, the relative impact of each input parameter is dependent on the spatial arrangement of wind turbines:

   (a) For array-like wind farms, the relative importance of each input parameter varies with the choice of wake models, and significant differences in the sensitivity indices are observed across different wake models. The maximum difference can be up to 70%; where the first-order index of the incoming wind speed reached approximately 90% for the Frandsen model, and only 19% for the Ishihara model.

   (b) For wind farms with optimized layouts, the relative importance of each input parameter is less sensitive to the choice of wake models, i.e., layout optimization has a smoothing effect.

   (c) All input parameters show a high value of the total-order sensitivity indices, which implies that the farm output is strongly sensitive to the coupled impact of these key factors. Hence, assuming fixed values of certain factors during WFLO, e.g., ambient turbulence or land area, will limit the feasibility of the optimal layouts obtained.

3. The incoming wind speed in general drives most of the variance in the wind farm capacity factor as expected, while the nameplate capacity is the most decisive input among all the design factors.

This work has ventured into an untrodden (but critical) area of understanding the impact of natural/design factors on wind farm performance, by specifically investigating the SA of wind farms with optimized layouts. The upper bound of nameplate capacity was limited to 150 MW in this study due to the high computational expense of SA. Future work should implement more computationally efficient approaches (e.g., using parallel computing or meta-models) to analyze the sensitivity of wind farms with GW size installed capacity. Since different wake models make different assumptions, thereby limiting their applicability to distinct scenarios, a straightforward comparison (as performed here) may not yield comprehensive insight into their suitability for WFLO.

CHAPTER 5

Developing the Multi-Objective Wind Farm Design Methodology

In this chapter, we present the development of the Multi-Objective Wind Farm Design (MOWFD) framework. Section 5.1 presents the implementation steps of MOWFD methodology. This framework is implemented in Section 5.2 through a case study.

5.1 Implementation of MOWFD Methodology

The previous chapter helps us understand that key design factors affecting the wind farm performance are primarily the installed capacity and the land configuration (e.g., land area, land shape, and land aspect ratio) [142]. To integrate the effects of these key design and natural factors in wind energy development, the Multi-Objective Wind Farm Design (MOWFD) methodology is developed in this dissertation. Together with a Pareto shifting technique, the MOWFD methodology allows an efficient and effective exploration of the best tradeoffs between multiple performance objectives subject to the variation of critical site-scale decisions (e.g., the installed capacity).

The MOWFD methodology is described by the following two steps:

Step One: Multi-Objective Wind Farm Layout Optimization (MO-WFLO). At this step, information regarding the wind conditions (wind speed and direction), the interested ranges of land area and installed capacity, and the available candidate turbine types, is provided. Based the given information, a series of MO-WFLOs are to be performed. The number of design variables for each of these MO-WFLOs is determined by the sample installed capacity that is generated within the specified range. As a result,

each MO-WFO will generate a set of Pareto optimal solutions, representing the tradeoff between the multiple objectives considered.

Step Two: By collecting all the Pareto optimal solutions obtained from each MO-WFLO performance with a sample installed capacity, regression models are applied to select the appropriate function form that fits all the tradeoffs by different values of installed capacity. By parameterizing the tradeoffs using the installed capacity, we now are able to quantitatively explore how the best tradeoffs between the multiple objectives considered vary with the installed capacity decisions.

More details of the MOWFD methodology is illustrated using a case study presented in the following section.

5.2 Case Study: Multi-Objective Wind Farm Design

In this case study, the interested range of installed capacity is from 30 MW to 100 MW. The corresponding range for the number of turbines is from 13 to 67, assuming identical turbines are used [122]. Five sample installed capacity decisions are generated, as shown in Table 5.2. Two objectives considered in this case study are (i) maximizing the wind farm capacity factor and (ii) minimizing the unit land footprint (represented by the LAMI). This bi-objective optimization problem can be solved by performing a constrained single objective

optimization, which is formulated as:

$$\begin{aligned} & \max\ CF \\ & \textit{subject to} \\ & g_1(\vec{x},\vec{y}) \geq 2D \\ & g_2(\vec{x},\vec{y}) \leq A^*(\vec{x},\vec{y}) \\ & x_{min} \leq x_i \leq x_{max} \\ & y_{min} \leq y_i \leq x_{max} \\ & \text{where} \\ & i = 1, 2, \ldots, N \end{aligned} \tag{5.1}$$

where CF is the wind farm capacity factor given by Eq.(2.19); N is the number of turbines to be installed; g_1 represents the constraint that the minimum spacing between turbines (distance measured from hub to hub) should not be less than two rotor diameters; g_2 gives the constraint of the area of layout, A^*, calculated based on the SBR determined by the layout; $\vec{x}$ and $\vec{y}$ are design vectors that represent the turbine coordinates as given by

$$\begin{aligned} \vec{x} &= x_1, x_2, \ldots, x_N \\ \vec{y} &= y_1, y_2, \ldots, y_N \end{aligned} \tag{5.2}$$

The mixed-discrete PSO is applied to perform the WFLO. The parameter setup of this layout optimization problem is shown in Table 5.1.

From each run of WFLO with the sample installed capacity decision, a set of Pareto optimal solutions can be obtained. The trend of these tradeoffs between the capacity factor and the unit land footprint can be observed in Fig. 5.1. Here, model selection technique is used to select the best function form; and based on the model selection result, the power

Table 5.1: User-defined parameters in MDPSO

Parameter	Value
W	0.5
β_g	1.4
β_l	1.4
γ	1.0
γ_0	$1e-10$
Population size	$10 \times N$
Max. allowable function calls	$500,000$

function form can best fit these *CF-LAMI* curves. The relationship between the capacity factor and the LAMI can be expressed as

$$CF = aA_{MW}^{b} + c \tag{5.3}$$

where A_{MW} is the LAMI.

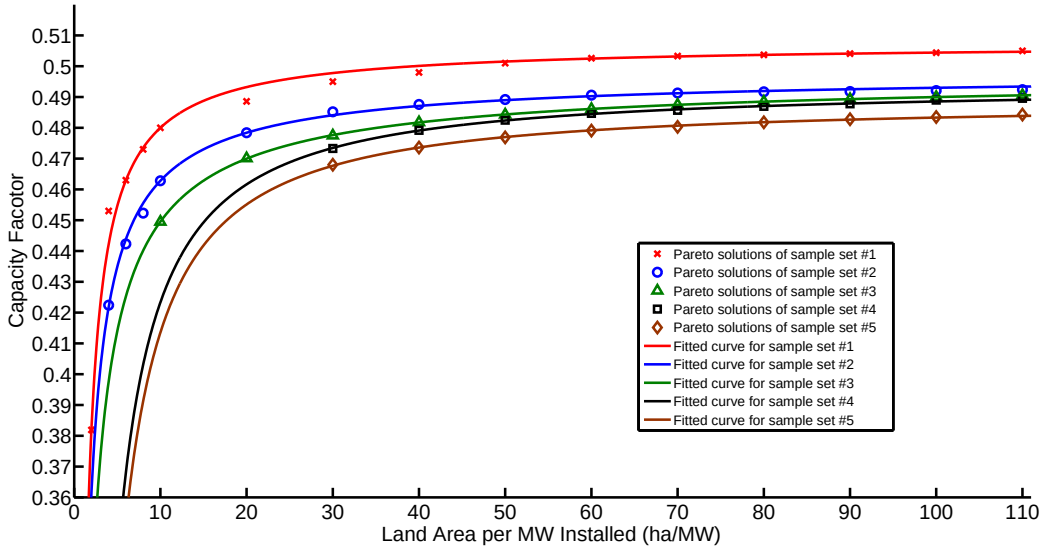

Figure 5.1: *CF-LAMI* Tradeoff Curves

5.2.1 Pareto Shifting Technique

Figure 5.1 shows the curves fitted by using power functions. The coefficients for the power functions are listed in Table 5.2.

Table 5.2: Parameterization of *CF-LAMI* Tradeoff

Sample set	No. of Turbines	Coef. a	Coef. b	Coef. c
1	13 turbines	-0.2415	-0.9424	0.5076
2	20 turbines	-0.2453	-0.8423	0.4981
3	40 turbines	-0.3027	-0.7985	0.4976
4	60 turbines	-0.9575	-1.133	0.4937
5	67 turbines	-1.107	-1.170	0.4884

It is observed that, for a certain allowable land area, the predicted capacity factor decreases as the installed installed capacity increases. This trend is also similar to that presented by Chowdhury et al. [132]. Another observation is that the predicted CF becomes less sensitive to the LAMI when the LAMI is beyond the range of the average land usage. By following the above two rules, each coefficient shown in Eq. 5.3 can be fitted as a function of the installed capacity, which provides an approach to parameterize the *CF-LAMI* tradeoff by installed capacity. Hence, Eq. 5.3 can be modified by

$$CF = a(NC)A_{MW}^{b(NC)} + c(NC) \tag{5.4}$$

where NC is the NC of the wind farm.

The equations for the three coefficients expressed in the power function are given by:

$$\begin{aligned} a &= -6 \times 10^{-5} NC^2 - 3.7 \times 10^{-3} NC - 0.1432 \\ b &= -1 \times 10^{-5} NC^2 - 1.4 \times 10^{-3} NC - 0.9099 \\ c &= 5 \times 10^{-7} NC^2 - 2 \times 10^{-4} NC + 0.5091 \end{aligned} \tag{5.5}$$

Therefore, the *CF-LAMI* tradeoff can be quantified by the installed capacity decisions. For any given installed capacity decision within the specified range, the corresponding Pareto frontier can be generated, which provides a time-efficient exploration to wind farm developers. The correlation between the CF and the unit land area subject to a certain installed capacity decision can be expressed as

$$\begin{aligned} CF = \quad & (-6\times10^{-5}NC^2 - 3.7\times10^{-3}NC - 0.1432)A_{MW}^{-1\times10^{-5}NC^2-1.4\times10^{-3}NC-0.9099} \\ & +5\times10^{-7}NC^2 - 2\times10^{-4}NC + 0.5091 \end{aligned} \tag{5.6}$$

5.2.2 Result and Discussion

Figure 5.2 shows the optimal layout obtained from the case of 40 turbines. It is observed that turbines tend to be placed very close to each other when the allowable area of layout is small. Subsequently, the capacity factor predicted is relatively low due to the power reduction caused by the wake effect. When turbines have more space, i.e., a larger allowable area, a better capacity factor can be predicted. However, the capacity factor becomes less sensitive to the land area when the LAMI exceeds 30 ha/MW. It is also interesting that the actual land use of the optimal layouts shown in Fig. 5.2 have similar geometric shapes, which indicates that such layouts can best capture the wind energy over the particular wind distribution assumed in this paper.

Eq. 5.6 can be helpful for wind farm developers to explore the *CF-LAMI* trade-off by selecting a certain value of installed capacity in the 20 MW to 100 MW range. For a particular land resource, $LAMI^*$, an optimal installed capacity decision can be decided to reach the maximum capacity factor. Therefore, the optimal layout can be efficiently solved

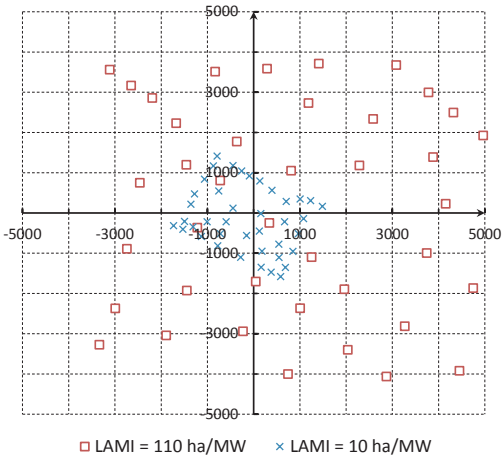

Figure 5.2: Optimal Layouts of 40 turbines with different allowable areas

by using the following formulation:

$$
\begin{aligned}
&\max \ CF \\
&\textit{subject to} \\
&\qquad g_1(\vec{x},\vec{y}) \geq 2D \\
&\qquad g_2(\vec{x},\vec{y}) \geq CF_{max} \\
&\qquad g_3(\vec{x},\vec{y}) \leq A^*_{MW} \\
&\qquad x_{min} \leq x_i \leq x_{max} \\
&\qquad y_{min} \leq y_i \leq x_{max} \\
&\text{where} \\
&\qquad i = 1, 2, \ldots, N^*
\end{aligned}
\tag{5.7}
$$

where CF_{max} is the maximum capacity factor obtained by optimizing Eq. 5.6 with given LAMI; A_{MW} is the unit land area; and N^* represents the optimal number of turbines to be installed, which can be determined by solving the optimization problem as addressed in Eq. 5.6.

5.3 Chapter Summary

This chapter presented the development of MOWFD methodology that provides an approach to explore how the trade-off between the capacity factor and the unit land footprint vary with the installed capacity decisions. A case study was conducted to show the implementation procedure of MOWFD methodology. With this methodology, for a certain wind resource, wind farm developers are able to "visualize" the balance between the capacity factor and the unit land footprint by shifting the installed capacity decisions, allowing to make time-efficient decisions over the concerned objectives.

CHAPTER 6

Multi-Objective Wind Farm Design Considering Land Usage

In this chapter, a visualization platform is developed for Co-operative Decision-Making in wind farm planning. This platform enables the major parties involved in the wind energy project to acquire an upfront understanding of how various co-related factors collectively affect the overall wind farm performance and local impact. Specifically, the wind farm performance in this work is represented by the wind farm Capacity Factor (CF) and the Land Area per MW Installed (LAMI). Therefore, we perform a multi-objective (bi-objective) wind farm layout optimization to explore the CF-LAMI trade-off *for different nameplate capacities. In addition, we also explore the variation of the land shapes associated with the best* CF-LAMI trade-offs *by applying the optimal layout-based land usage in the optimization. A* GUI-based land shape chart *estimation is finally developed to provide information regarding the interplay of the following planning elements: (i) CF, (ii) LAMI, (iii) nameplate capacity, (iv) optimal land shape, and (v) the average energy production potential. For example, the involved parties can now readily visualize how different LAMI and nameplate capacity decisions impact the estimated land portion/plots that need to be used and the maximum energy production that could be extracted under such decisions.*

6.1 Developing a Consolidated Visualization Platform for Co-operative Decision-Making in Wind Farm planning

Two objectives considered are: (i) maximizing the wind farm Capacity Factor, (ii) and minimizing the unit land footprint (represented by land area per MW installed). In this work,

this bi-objective optimization problem is solved by performing multiple constrained single-objective optimizations. Each of these constrained single-objective optimization problems is formulated as

$$\begin{aligned} & \max CF(V) \\ & V = \{x_1, x_2, \cdots, x_N, y_1, y_2, \cdots, y_N\} \\ \textit{subject to} & \\ & g_1(V) \geq 2D \\ & g_2(V) \leq A^i_{MW} \end{aligned} \tag{6.1}$$

where $CF(V)$ represents the wind farm CF computed using the power generation model offered by UWFLO, and Jensen wake model is used to compute the wake behavior; V is the design variable that represents the location of turbines; N is the total number of turbines installed; D is the rotor diameter of the turbine used; and $g_1(V)$ represents the inner-turbine spacing, which given by

$$\begin{aligned} & g_1(V) = \sum \max\left\{\left(d_{ij} - 2D\right), 0\right\} \\ \text{where} & \\ & d_{ij} = \sqrt{(x_i - x_j)^2 + (y_i - y_j)^2} \\ & i, j = 1, 2, \ldots, N, \ \textit{and} \ i \neq j \end{aligned} \tag{6.2}$$

In Eq. 6.1, $g_2(V)$ represents the constrained land area based on the nameplate capacity (number of turbines), A^i_{MW}. By specifying multiple values of A^i_{MW}, the trade-off between CF and LAMI can be obtained and the comparison of CF for the same LAMI is also enabled. The Mixed-Discrete Particle Swarm Optimization (MDPSO) algorithm is used in this work to perform the layout optimization. For each given A^i_{MW}, the algorithm is run at least 5 times. The optimal solution (farm layout) is then selected as the best solution out of

the 5 runs. Detailed information of the MDPSO algorithm can be found in the paper by Chowdhury et al. [134]. The Sobol's quasi-random sequence generator [143] is applied to provide the initial set of farm layouts.

6.2 Numerical Experiment

In this Section, numerical experiments are conducted to generate the *CF-LAMI trade-off* and the *GUI-based land shape chart*, for a set of representative wind resource scenarios. Three different wind patterns (shown in Fig. 6.1) generated using the same wind distribution are used to allow a general appreciation of the benefits of such a wind farm layout optimization-based visualization platform.

Table 6.1: GE 1.5 MW xle Turbine [122]

Specifications	Value
Rated capacity	1500 kW
Cut-in	3.5 m/s
Cut-out	20 m/s
Rated speed	11.5 m/s
Rotor diameter	82.50 m
Hub height	80 m

6.2.1 Description and Settings

In the wind diagrams in Fig. 6.1, the angular coordinate, showing the direction wind is flowing from, is measured clockwise from North. According to the wind patterns, three cases are considered in this paper:

Case 1: The wind pattern in Case 1 (as shown in Fig. 6.1(a)) comprises one dominant wind direction at an angle of 45°.

Case 2: The wind pattern in Case 2 comprises two dominant directions that are opposite to each other at angles of 45° and −135°, as shown in Fig. 6.1(b).

Case 3: The wind pattern in Case 3 also comprises two dominant directions, which are however orthogonal to each other at angles of 45° and −45° as shown in Fig. 6.1(c).

These three patterns are generated from the same wind distribution fitted using simulated wind data, to ensure that they have equal *wind power density* (WPD).

$$\begin{aligned} WPD &\simeq \sum_{i=1}^{N_p} \tfrac{1}{2}\rho U_i^3 f(U_i,\theta_1)\Delta U \\ &= \sum_{i=1}^{N_p} \tfrac{1}{2}\rho U_i^3 [\tfrac{1}{2} f(U_i,\theta_1) + \tfrac{1}{2} f(U_i,\theta_2)]\Delta U \\ &= \sum_{i=1}^{N_p} \tfrac{1}{2}\rho U_i^3 [\tfrac{1}{2} f(U_i,\theta_1) + \tfrac{1}{2} f(U_i,\theta_3)]\Delta U \end{aligned} \tag{6.3}$$

$$where$$

$$\Delta U = U_{max}/N_p$$

Here θ_1, θ_2, and θ_3 represent the angles of wind directions, which are 45°, 135°, and 225° (from North to South clockwise), respectively.

For each wind pattern, 12 different combinations of nameplate capacities and the unit land footprint are considered in this experiment. For each combination, WFLO is run for 5 times to compensate for the impact of random parameters in the stochastic optimization used in this paper (which is MDPSO). Therefore, totally 60 WFLOs are required in this experiment. These optimizations were carried out parallelly on 4 workstations, and this overall framework was (macro-grained) parallelized to also fully exploit the multi cores (4/8 cores) architecture of each workstation. The total computational time is approximately 40 hours. A *GUI-based land shape chart* is then generated for each wind pattern, illustrating the variation of the optimal land shape and maximized CF with different values of LAMI and nameplate capacity.

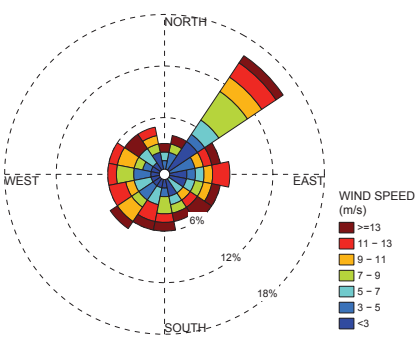

(a) Case 1: Single dominant direction

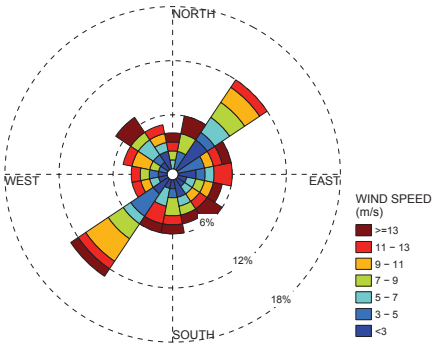

(b) Case 2: Two opposite dominant directions

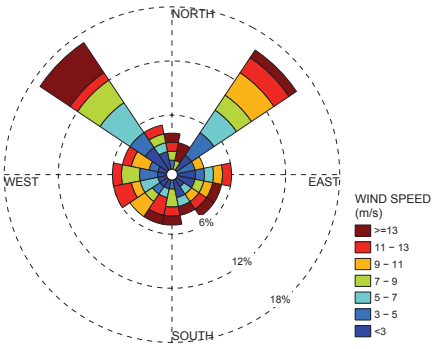

(c) Case 3: Two orthogonal dominant directions

Figure 6.1: Wind diagrams

The major assumptions made in this numerical experiment are listed below:

i. identical turbines (GE1.5 MW xle as shown in Table 6.1) are used;

ii. the incoming wind speed is uniformly distributed over the entire rotor area; and

iii. the ambient turbulence over the entire farm site is assumed constant.

6.2.2 Results and Discussion

Figure 6.2 – 6.4 represent the land shape charts for the three wind patterns. This paper focuses on the impact of land use on wind farm performance, so the outline of each optimal land shape is specifically shown as the smallest bounding rectangle. The outer x-axis and y-axis in the chart represent the LAMI and the number of turbines (nameplate

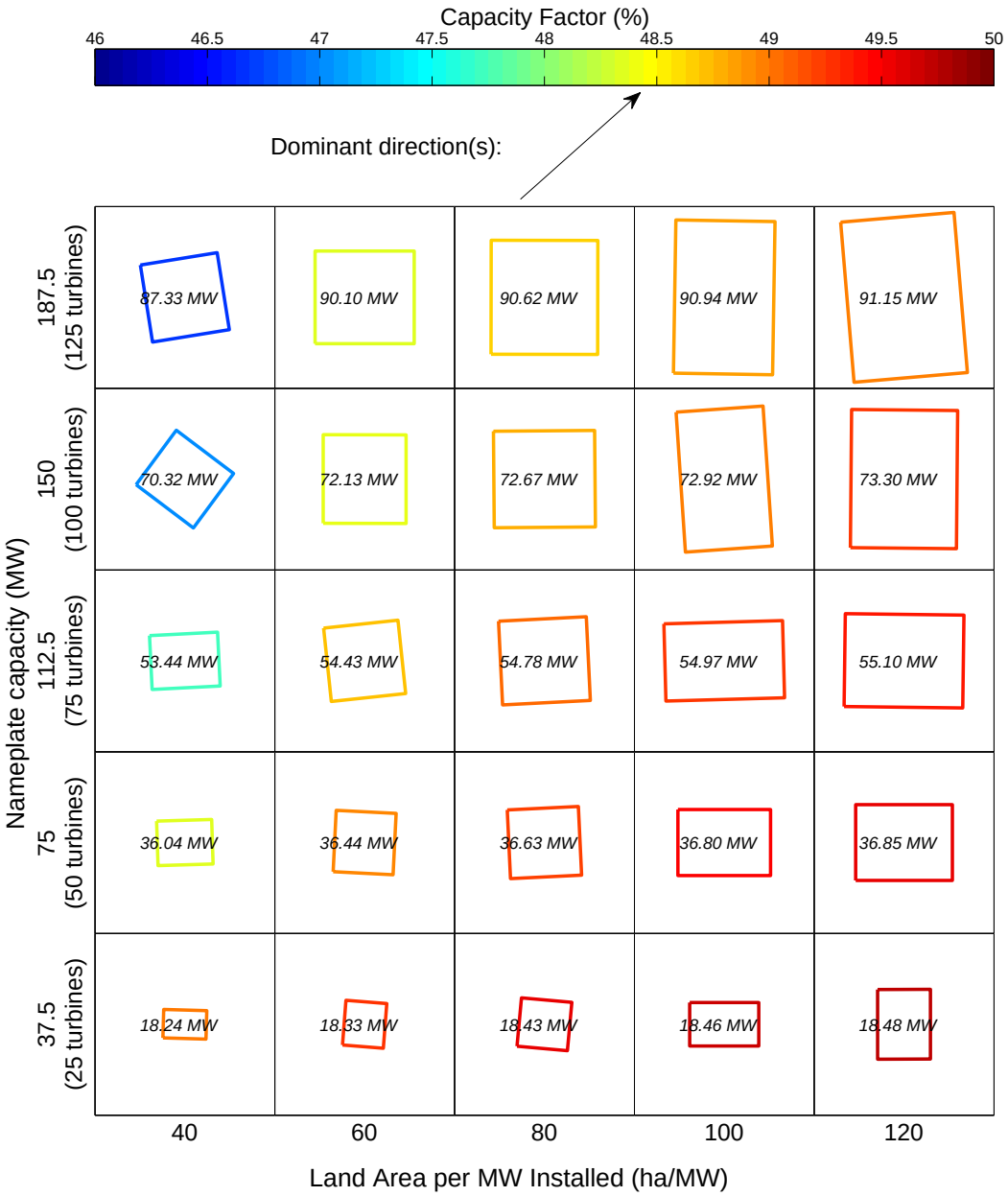

Figure 6.2: Case 1: GUI-based land shape chart under single dominant wind direction, with the average AEP potential (MW) of each layout as shown at the center of each cell

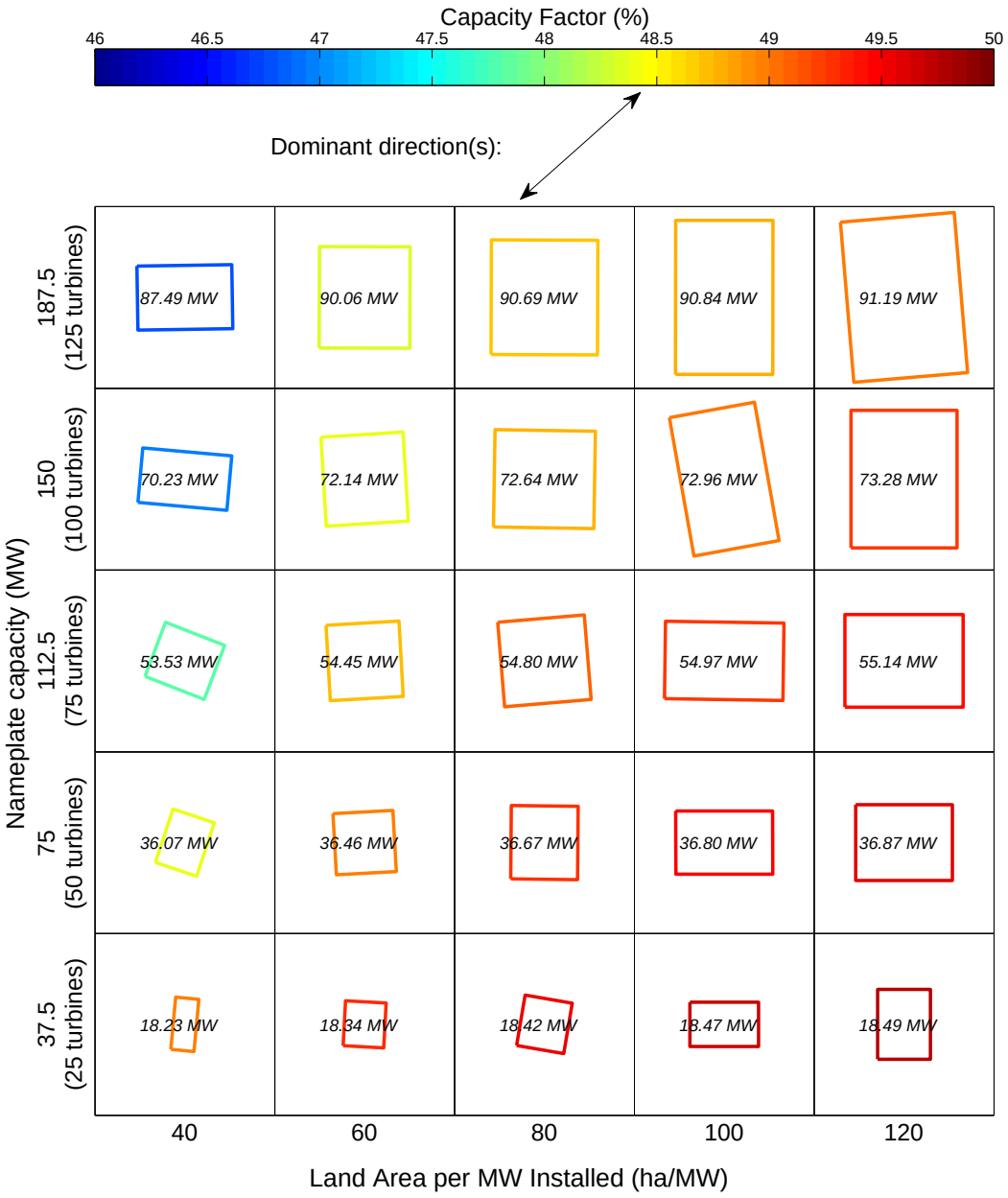

Figure 6.3: Case 2: GUI-based land shape chart under opposite dominant wind directions, with the average AEP potential (MW) of each layout as shown at the center of each cell

capacity), respectively. The CF obtained from each of the optimal farm layouts are given by the color of the estimated rectangular wind farm bounding. The average AEP potential obtained by each optimal layout is shown at the center of the estimated rectangular farm bounding.

Figure 6.2 shows the results obtained in Case 1. Expectedly, for the same number of turbines installed (along each each row), the estimated CF improves as the land area increases; and for the same allowed LAMI (along each column), the estimated maximum CF reduces as the nameplate capacity increases (indicating more crowding of turbines). Therefore, throughout the entire chart the optimal land shape located at the top-left corner yields the lowest CF; while the one at the bottom-right corner yields the highest CF. This trend is also observed in the other two land shape charts obtained in Case 2 and Case 3 (as shown in Fig. 6.3 and Fig. 6.4, respectively). This scenario is mainly attributed to the wake effect: for a given number of turbines installed, the greater the land area, the greater the inner-turbine spacing, thus leading to a reduction of wake losses. On the contrary, installing more turbines in a limited size of farm site will decrease the inner-turbine spacing, thereby causing more energy losses.

A more interesting observation is that, in Case 1, the optimal land shapes for the lowest nameplate capacity (25 turbines, shown in the first row of the land shape chart shown in Fig. 6.2) experienced the most significant change in land aspect ratio; on the other hand, the most significant change in land orientation is experienced by the optimal land shapes corresponding to the lowest allowed LAMI (40 ha/MW, in the first column of the land shape chart). A similar scenario is observed for the optimal land shapes obtained in Case 2. However, in Case 3, the optimal land shapes corresponding to either the lowest LAMI or the lowest nameplate capacity are experienced the most significant change in both the

land orientation and aspect ratio. Overall, this initial investigation indicates that, for small allowed LAMI and for wind farm with few turbines, the optimal land shape is highly sensitive to the variable factors (between LAMI and nameplate capacity).

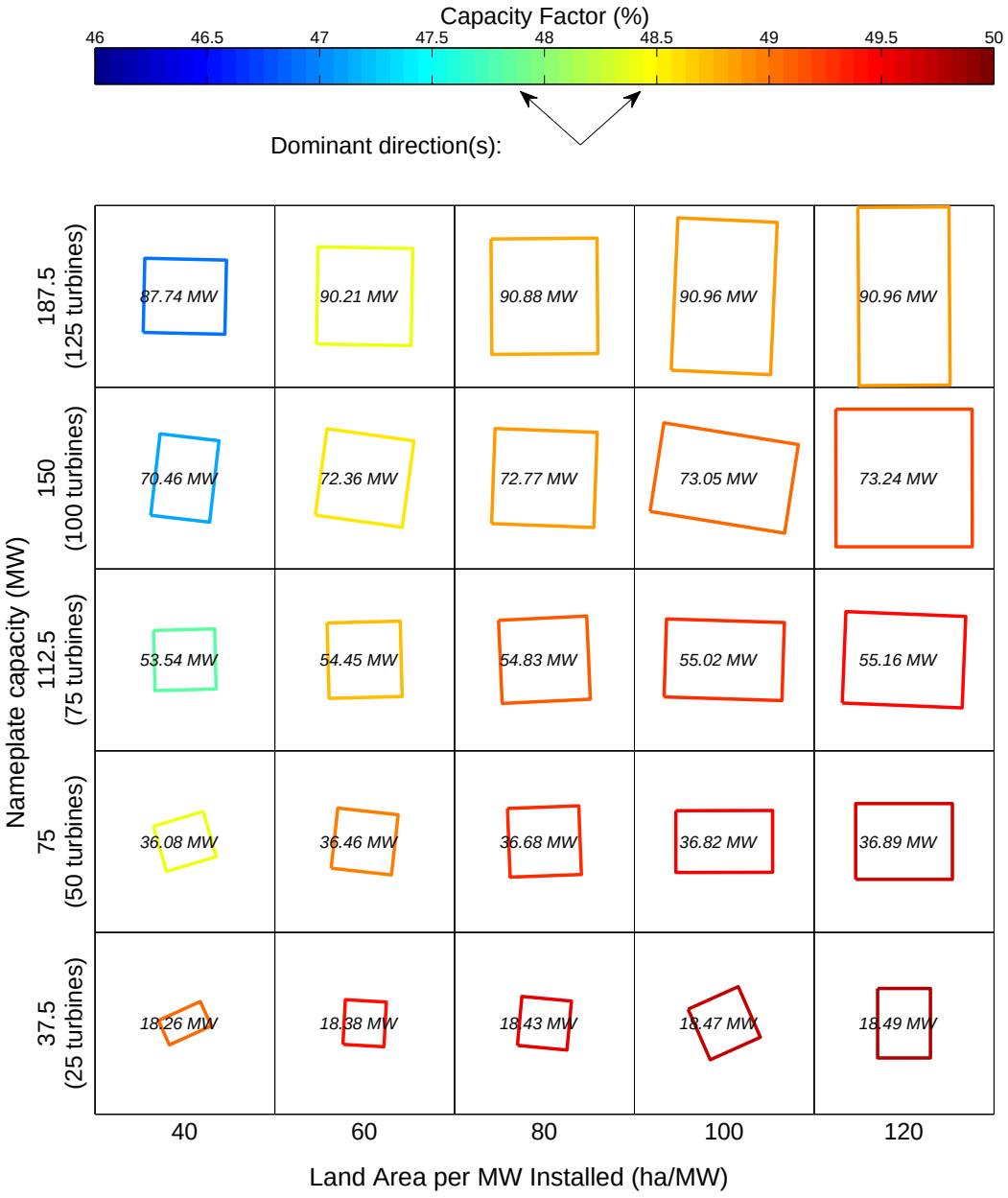

Figure 6.4: Case 3: GUI-based land shape chart under orthogonal dominant wind directions, with the average AEP potential (MW) of each layout as shown at the center of each cell

It is also observed that, under the same planned nameplate capacity and LAMI, the

optimal land shapes obtained in Case 1 and Case 2 are relatively similar (as shown in Fig. 6.2 and Fig. 6.3); the only exception to this observation occurs in the case of the smallest allowed LAMI (which is 40 ha/MW). Additionally, we observe that, under the same planned nameplate capacity and LAMI, the average AEP potential obtained in Case 1 and Case 2 are also very close to each other − the average estimated difference being 0.06% (the maximum AEP difference observed is around 1440 MWh/yr). Put this observation into perspective, it should be noted that across the range of LAMI the average AEP potential varies by 4.37%, and across the range of nameplate capacity the average AEP potential varies by 4.42%. Nevertheless, from the land shape chart shown in Fig. 6.4, it is observed that the optimal land shapes obtained in Case 3 are noticeably different from those obtained in Case 1 and Case 2 for the same nameplate capacity and LAMI. For the same nameplate capacity and LAMI, the different in the average AEP potential in Case 1 and Case 3 is equal to 0.47% on average (the maximum AEP differen observed is around 3610 MWh/yr).

Based on the response surface of wind farm capacity factor developed by Chowdhury et al. [88], it was concluded that, for a given farm site, a high capacity factor can be obtained with a relatively large land aspect ratio. However, we observed that some of the optimal land shapes have a square shape (the land aspect ratio is very close to 1). This difference can be attributed to the wind distributions used in this paper, which essentially involve one or two clearly defined dominant wind directions, unlike the complex real data-based multi-modal wind distribution used by Chowdhury et al. [88].

6.3 Chapter Summary

This chapter presented a trade-off visualization platform that is expected to promote Cooperative Decision Making platform and provide useful information guiding the wind

farm planning process. Due to the nature of the defined problem and the consideration of computational efficiency, we solve the essentially bi-objective optimization problem as multiple constrained single objective optimization problems. The subsequent application of the optimal layout-based land use (obtained using 2D convex hull and the smallest bounding rectangle concepts) enabled the WFLO to be performed without specifying farm boundaries. A novel *GUI-based land shape chart* is then developed to explore the *CF-LAMI trade-off* while also providing the optimal land shapes and the average AEP potential for different values of nameplate capacities and LAMI.

The visualization platform was applied to three distinct wind patterns: (i) single dominant direction, (ii) two opposite dominant directions, and (iii) two orthogonal dominant directions; all these cases involved the same distribution of wind speed. The results represented by the *GUI-based land shape charts* showed that the optimal land shapes are self-oriented by the dominant wind direction(s). Moreover, the optimal land shape is highly sensitive to the number of turbines in the case of small allowed LAMI and (vice versa) to the LAMI in the case of small installed capacity (few turbines installations). We also noted that, for a given number of turbines, the predicted CF improves as the LAMI increases; corollarily, the predicted CF decreases if more turbines are installed with the same LAMI. Additionally, under the same nameplate capacity and LAMI, the optimal land shape obtained in Case 1 (with single dominant wind direction) and Case 2 (with two opposite dominant wind directions) is very similar; however, the optimal land shape obtained in Case 1 and Case 3 (with two orthogonal dominant wind directions) is noticeably different. Across three cases, the difference in the estimated maximum AEP can be up to 3610 MWh/yr.

Overall, the *GUI-based land shape chart* enables the integration of various key factors and objectives in wind farm planning, and hence provides insightful information to assist

the major stakeholders in making favorable co-operative decisions.

PART III

Development of Multi-objective Mixed-Discrete Optimization Solver

CHAPTER 7

Development of the Multi-Objective Mixed-Discrete Particle Swarm Optimization Algorithm

In previous chapters, we described the details of the MOWFD methodology developed in this dissertation. Here, in this Chapter, we present the development of the MO-MDPSO algorithm that is used to solve the complex characteristics addressed in the MO-WFLO. The major contribution of this part of the dissertation is the fundamental advancements made over the single-objective MDPSO algorithm, which extends MDPSO to a multi-objective optimizer. More specifically, these advancements include: (i) the adoption of the Pareto dominance based search strategy for retaining the original dynamics of the basic PSO, (ii) the leader selection mechanism for local/global Pareto sets, and (iii) the multi-domain diversity preservation technique used to mitigate the pre-stagnation issue while maintaining a good spread in the generated Pareto optimal solutions. Numerical experiments using a suite of benchmark test problems are then conducted in Section 7.2, to investigate the performance of this MO-MDPSO, and to compare its performance with other multi-objective solvers such as NSGA, SPEA, and MPP.

7.1 Overview of the Single-Objective Mixed-Discrete Particle Swarm Optimization Algorithm

In this section, we start with an overview of the original single-objective MDPSO algorithm, followed by the description of the new MO-MDPSO.

7.1.1 Overview of Single Objective MDPSO

PSO is a population-based algorithm that was originally developed for single-objective optimization by Kennedy and Eberhart [28]. In PSO, a candidate solution is represented by the position of a particle in the design space, which is updated through a velocity vector. The particle dynamics is governed by two basic equations: (i) the position update and (ii) the velocity update. The Mixed-Discrete Particle Swarm Optimization (MDPSO) algorithm, developed by Chowdhury et al. [134], retains the fundamental structure of the original PSO. In addition, a special diverging velocity vector is introduced in the standard velocity update formulation in MDPSO. The purpose of this additional vector is to preserve population diversity, and hence prevent premature particle clustering and stagnation of solutions (a major issue in PSO). The position and velocity update equations in MDPSO are respectively given by

$$\vec{x}_i(t+1) = \vec{x}_i(t) + \vec{v}_i(t+1) \tag{7.1}$$

$$\begin{aligned} \vec{v}_i(t+1) &= w\vec{v}_i(t) + r_1 C_1 \left[\vec{P}_i^l(t) - \vec{x}_i(t)\right] \\ &\quad + r_2 C_2 \left[\vec{P}^g(t) - \vec{x}_i(t)\right] + r_3 \gamma_c \hat{v}_i(t) \end{aligned} \tag{7.2}$$

In Eqs. 7.1 and 7.2, $\vec{x}_i(t)$ and $\vec{v}_i(t)$ respectively denote the position and the velocity of Particle-i at the t^{th} iteration; w is the inertial weight that balances the local search (exploitation) and the global search (exploration); $\vec{P}_i^l$ is the local leader of Particle-i at the t^{th} iteration, which represents the best local solution found in the motion-history of Particle-i; $\vec{P}^g(t)$ is the global leader of the entire swarm at the t^{th} iteration, which is determined through a social information exchange among all local leaders and particles; C_1 and C_2 represent cognitive and social parameters, respectively; r_1, r_2, and r_3 are random real numbers between

0 and 1; and $\gamma_c \hat{v}_i(t)$ is the diversity preservation vector component.

In MDPSO, the diversity is measured by the effective spread of all candidate solutions in the design variable space, which also seeks to avoid false impression of diversity attributed to outlier particles. Diversity preservation is implemented on continuous and discrete variables separately. The diversity preservation in the continuous variable space, as defined by the last term of Eq. 7.2, includes (i) a preservation coefficient (γ_c) that is evaluated adaptively as a function of the prevailing diversity in the population at every iteration; and (ii) a diverging velocity vector ($\hat{v}_i(t)$) that is defined as the vector opposite to that directed towards the position of the current global leader, as given by

$$\hat{v}_i(t) = \vec{x}_i(t) - \vec{P}^g(t) \tag{7.3}$$

After the discrete variables are updated in the continuous domain using Eq. 7.2, the discrete component of each candidate solution is moved to one of the vertices in its neighborhood (in the discrete design space), based on a stochastic process. The stochastic update is so designed that a particle could have the opportunity to jump out of its local hypercube.

The net constraint violation concept, $f_c(\vec{x})$, is used to handle constraints in MDPSO, as given by

$$f_c(\vec{x}) = \sum_{p=1}^{P} \max(\bar{g}_p, 0) + \sum_{q=1}^{Q} \max(|\bar{h}_q| - \epsilon, 0) \tag{7.4}$$

where $\bar{g}_p$ and $\bar{h}_q$ respectively represent the normalized inequality and equality constraints, whereas P and Q are the number of constraints of each type; and ϵ is the specified tolerance for equality constraints. When comparing two particles, their net constraint violation is given preference over their objective function values.

7.1.2 Introducing the Multi-Objective Capability to Mixed-Discrete PSO

The general form of a constrained MOO problem with mixed-discrete variables is defined in Eq. 1.8, where m discrete design variables (x_d) and n continuous design variables (x_c) are included.

In MOO problems, a candidate solution is considered to be a *Pareto optimal solution* – *if any improvement of the solution in one objective can only take place at the cost of worsening at least one other objective.*

The principle of constrained non-dominance comparison [95] is applied to compare solutions in MO-MDPSO. According to this principle, candidate solution-$\vec{x}$ is said to be better than candidate solution-$\vec{y}$ if and only if one of the following scenarios occur:

I. Solution-$\vec{x}$ is feasible and solution-$\vec{y}$ is infeasible or,

II. Both solutions are infeasible and solution-$\vec{x}$ has a smaller net constraint violation than solution-$\vec{y}$ or,

III. Both solutions are feasible and solution-$\vec{x}$ dominates solution-$\vec{y}$ in terms of the objective functions.

There exists two principles of domination based on objective functions, both of which are used in different contexts in MO-MDPSO. Assuming all objectives are being minimized, Solution-$\vec{x}$ is said to *weakly dominate* solution-$\vec{y}$ if

$$f_k(\vec{x}) \leq f_k(\vec{y}) \; \forall k = 1, 2, \ldots, N \tag{7.5}$$

and $f_k(\vec{x}) < f_k(\vec{y})$ holds for at least one k.

Assuming all objectives are being minimized, Solution $\vec{x}$ is said to *strongly dominate* solution-$\vec{y}$ if and only if

$$f_k(\vec{x}) < f_k(\vec{y}) \; \forall k = 1, 2, \ldots, N \tag{7.6}$$

In Eqs. 7.5 and 7.6, N is the number of objectives.

In the new MO-MDPSO algorithm, the position update equation is the same as that defined in MDPSO (Eq. 7.2). Important modifications are made in the velocity update equation, particularly to the leader selection mechanism and the diversity preservation technique in a multi-objective space.

Leader Selection Mechanism

In MO-MDPSO, there are two types of leader selection, i.e., identifying the local leaders and the global leaders. The local leader for Particle-i is selected from a set of solutions known as the local set, $\vec{L}_i(t)$. The historical solutions of a particle are compared with each other, and the ones that are not strongly dominated by any other solution in that particle's history are stored in the local set. Hence, the eligibility of the current Particle-i ($\vec{x_i}$) to be stored in $\vec{L}_i(t)$ is defined as

$$\begin{aligned} & \vec{x}_i(t) \in \vec{L}_i(t) \\ & \text{if} \\ & f^k(\vec{x_i})(t) \not< f^k(\vec{y_i})(t), \text{ for at least one } k \\ & \text{where } \forall k = 1, 2, \ldots, N \text{ and } \forall \vec{y_i} \in \vec{L}_i(t-1) \end{aligned} \tag{7.7}$$

Then the local set is updated by applying a Pareto filter [144] to it.

The size of each local set, $|\vec{L}_i|$, is pre-defined and regulated using the concept of crowding distance [95]: the most crowding solution is eliminated when the size of a local set exceeds

the pre-defined size. The local leader of each particle is selected randomly from the following two solutions: (I) the local set solution with the shortest Euclidean distance to the concerned particle, and (II) the least crowding solution from the local set.

The global leader for each particle is selected from a set of solutions known as the global set, $\vec{G}$, defined for the entire population. The global set can be obtained by applying the Pareto filter to the solutions stored in all of the local sets. This Pareto filter is based on the rule of weak domination. The size of the global set, $|\vec{G}|$, is also pre-defined, and this definition is guided by the number of Pareto optimal solutions desired by the user. We again use the crowding distance concept to regulate the size of the global set, $\vec{G}$. If $|\vec{G}| > |\vec{G}|_{desired}$, based on the values of crowding distance, only the top $|\vec{G}|_{desired}$ solutions (in terms of least crowding) are kept in the global set. Now, since the global set, $\vec{G}$, is shared by the entire particle population at any given iteration, it is important to identify the global leader, $\vec{P}_i^g(t)$, for each Particle-i. The solution from the global set that has either the smallest or the largest Euclidean distance to Particle-i in the objective space is chosen to be the global leader of Particle-i. The choice between the closest/farthest global solution is driven by a stochastic diversity preservation process, discussed in Section 7.1.3.

Figure 7.1 shows an illustration of the leader selection mechanism in MO-MDPSO. In this case, each local set is allowed to store three local non-dominated solutions (the respective green, blue, and red symbols in Fig. 7.1). For the particle shown as a solid blue square, its local leader is represented by the blue triangle. By applying the Pareto filter, 6 candidate solutions (which includes some of the local set solutions) are selected to form the global set, marked by the red circle symbols in Fig. 7.1.

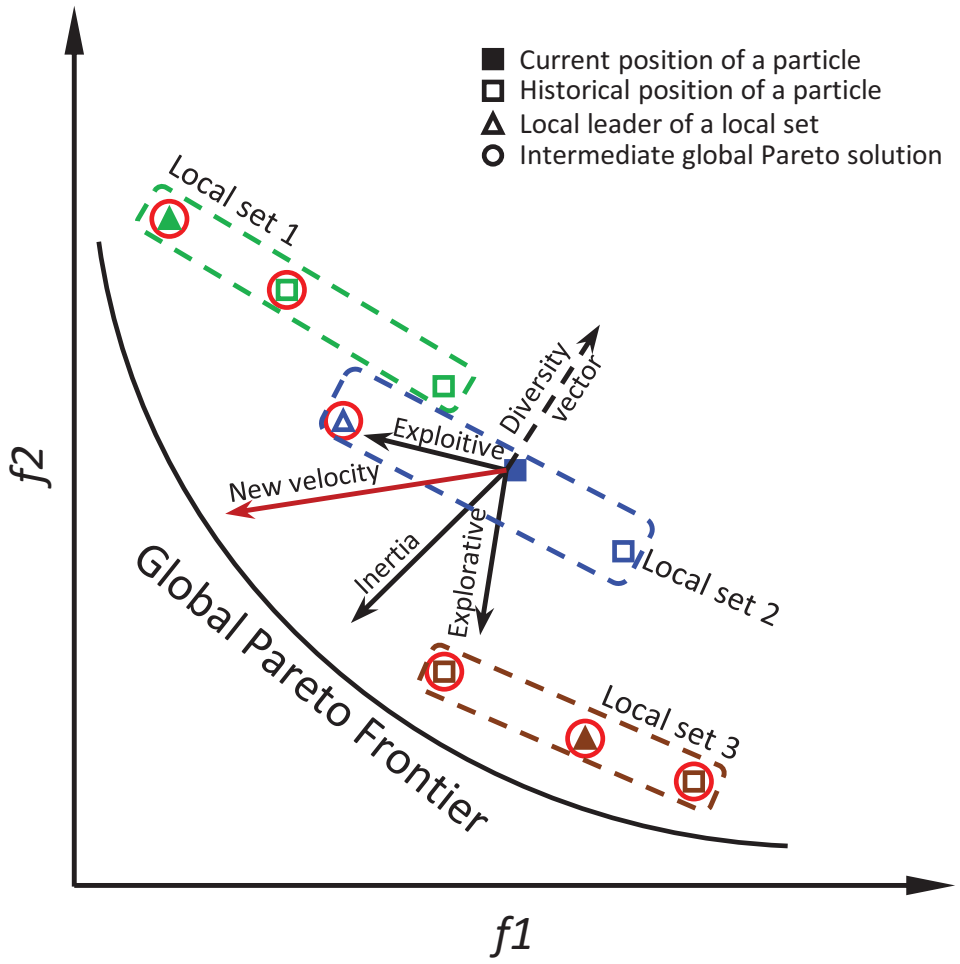

Figure 7.1: Illustration of MO-MDPSO dynamics in the objective space

Dynamics of MO-MDPSO

The position and velocity update equations for the MO-MDPSO algorithm are given by

$$\vec{x}_i(t+1) = \vec{x}_i(t) + \vec{v}_i(t+1) \tag{7.8}$$

$$\begin{aligned} \vec{v}_i(t+1) = & \; w\vec{v}_i(t) + r_1 C_1 \left[\vec{P}_i^l(t) - \vec{x}_i(t)\right] \\ & + r_2 C_2 \left[\vec{P}_i^g(t) - \vec{x}_i(t)\right] \\ & + r_3 \gamma_{c,i} \left[\vec{x}_i(t) - \vec{P}_i^g(t)\right] \end{aligned} \tag{7.9}$$

While Eq. 7.8 is similar to that defined in basic PSO, important modifications are inherent in the velocity update equation. In Eq. 7.9, $\vec{P}_i^g$ represents the global leader of Particle-i, selected from the global set $\vec{G}(t)$ at the t^{th} iteration; and $\vec{P}_i^l$ is the local leader of Particle-i selected from its local set $\vec{L}_i(t)$. The term $\gamma_{c,i}(\vec{x}_i(t) - \vec{P}_i^g)$ is the diversity preservation vector in the continuous variable space. The multi-domain diversity preservation is further described in the following subsection.

7.1.3 The Multi-domain Diversity Preservation in MO-MDPSO

In MO-MDPSO (similar to MDPSO), different diversity preservation schemes are defined for continuous and discrete variables, since the nature in which particles lose diversity in the continuous and the discrete variable spaces can be quite different.

For continuous variables, the diversity metric, D_c, is defined as the smallest hypercube enclosing all candidate solutions in the continuous variable space, as given by

$$D_c = \left[\prod_{j=1}^{n} \frac{x^{max,j} - x^{min,j}}{X^{max,j} - X^{min,j}} \right]^{\frac{1}{n}} \tag{7.10}$$

In Eq. 7.10, $x^{max,j}$ and $x^{min,j}$ are respectively the upper and lower bounds of the entire set of candidate solutions in the j^{th} dimension; $X^{max,j}$ and $X^{min,j}$ represent the defined upper and lower bounds of the j^{th} design variable, respectively. Hence, D_c essentially represents the normalized side-length of the smallest enclosing hypercube.

The generic m-dimensional discrete design space can be prescribed as a hypergrid, where each grid cell (hypercell) is defined by the allowed values of the discrete variables. The discrete space diversity metric is defined such that it mitigates the stagnation of particles within its current hypercell. The diversity metric for a discrete variable, D_d^j, is thus defined

as

$$D_d^j = \frac{x^{max,j} - x^{min,j}}{X^{max,j} - X^{min,j}} \tag{7.11}$$

where $x^{max,j}$ and $x^{min,j}$ are respectively the feasible upper and lower bounds of the current population for the j^{th} discrete variable.

It is important to note that **candidate solutions** refer to both the particles at the current iteration and the historical solutions stored in all the local sets. As a result, in Eqs. 7.10 and 7.11, D_c defines the normalized spread of solutions in the continuous domain, whereas D_d^j describes the fractional distance of solutions in the discrete space. However, owing to the potential impact of outlier candidate solutions on the measurement of diversity, a fractional domain concept is applied [134], where the fractional domain boundaries are guided by the best global particle that is generally the source of attraction. Only particles enclosed by this fractional domain are selected to represent the diversity. In MO-MDPSO, as there are multiple global leaders, we modify the fractional domain concept. Here, the boundaries of this fractional domain is determined by the location of each particle's global leader, $\vec{P}_i^g$. For Particle-i, the upper and lower bounds of the fractional domain in the j^{th} dimension are respectively given by

$$\begin{aligned} \bar{x}_i^{max,j} &= \max \left\{ \begin{array}{l} x^{min,j} + \lambda_i \delta x^j, \\ \min \left[\vec{P}_i^{g,j} + \frac{1}{2}\lambda_i \delta x^j, x^{max,j} \right] \end{array} \right\} \\ \bar{x}_i^{min,j} &= \min \left\{ \begin{array}{l} x^{max,j} - \lambda_i \delta x^j, \\ \max \left[\vec{P}_i^{g,j} - \frac{1}{2}\lambda_i \delta x^j, x^{min,j} \right] \end{array} \right\} \end{aligned} \tag{7.12}$$

where $\vec{P}_i^{g,j}$ is the value of the j^{th} variable for Particle-i's global leader; $\delta x^j = X^{max,j} - X^{min,j}$

defines the side-length of the smallest hypercube enclosing all candidate solutions; and λ is a user-defined parameter between 0 and 1, representing a fractional side-length of the smallest enclosing hypercube. If $\lambda = 1$, no outlier solutions are discarded.

Therefore, based on the number of particles enclosed by the fractional domain, the modified diversity metrics for both continuous and discrete variables are expressed as

$$\overline{D}_{c,i} = \Lambda_i D_c \tag{7.13}$$

$$\overline{D}^j_{d,i} = \Lambda_i D_{d,j} \tag{7.14}$$

where

$$\Lambda_i = \left(\lambda \frac{N_p + 1}{N_i + 1}\right)^{\frac{1}{m+n}} \tag{7.15}$$

where Λ_i is the diversity modification coefficient of Particle-i.

In Eq. 7.15, N_p is the number of candidate solutions at the current iteration, and N_i is the number of particles enclosed by the fractional domain defined with respect to the global leader of Particle-i.

The diversity preservation coefficient for continuous variables (for each particle), γ^i_c, is given by [134]

$$\begin{aligned} \gamma_{c,i} &= \gamma_{c0} \exp\left(\frac{-\overline{D}^2_{c,i}}{2\sigma_c^2}\right), \ and \\ \sigma_c &= \frac{1}{\sqrt{2 \ln 1/\gamma_{min}}} \end{aligned} \tag{7.16}$$

whereγ_{c0} and γ_{min} are user-defined scale and shape parameters for the diversity coefficient.

Table 7.1: User-defined parameters in MO-MDPSO

Parameter	Class I	Class II	Mixed-Integer optimization problems
w	0.5	0.5	0.5
C_1	1.5	1.5	1.5
C_2	1.5	1.5	1.5
γ_{c0}	1.0	1.0	1.5
γ_{min}	$1e-06$	$1e-06$	$1e-08$
γ_{d0}	NA	NA	1.0
λ	0.2	0.1	0.1
Capacity of local set $\lvert\vec{L}\rvert$	5	6	8
Capacity of global set $\lvert\vec{G}\rvert$	50	50	100
Population size N_p	$\min(2n, 100)$	$\min(2n, 100)$	$\min(5(m+n), 500)$

For discrete design variables, the diversity preservation coefficient, $\gamma_{d,i}^j$, is given by [134]

$$\begin{aligned} \gamma_{d,i}^j &= \gamma_{d0} \exp\left(\frac{-\overline{D}_{d,i}^{j\ 2}}{2\sigma_d^2}\right), \ and \\ \sigma_d &= \frac{1}{\sqrt{2 \ln 1/M^j}} \\ \forall j &= 1, 2, \ldots, m \end{aligned} \tag{7.17}$$

where the M^j is the total number of allowed values for the j^{th} (discrete) variable; and γ_{d0} is a user-defined parameter that represents the probability of position update for discrete variables.

Based on the value of $\gamma_{d,i}^j$ and a random real number r_4 between 0 and 1, the position of a candidate solution, x^j, is updated using the following rules:

i When r_4 is less than or equal to $\gamma_{d,i}^j$, x^j is randomly approximated to either $X^{max,j}$ or $X^{min,j}$.

ii When r_4 is greater than $\gamma_{d,i}^j$, x^j is approximated to $X^{min,j}$ if $|x^j - X^{min,j}| \leq |x^j - X^{max,j}|$; otherwise, x^j is approximated to $X^{max,j}$.

7.1.4 Roles of Diversity Preservation Coefficients

It is important to note that $\gamma_{c,i}$ is used to control the magnitude of a directional repulsion away from the location of $\vec{P}_i^g$. As more particles approach a particular global leader, the repulsion among the followers of this global leader increases, thus slowing down a potential premature clustering process. In addition, the scale parameter, γ_{c0}, determines the maximum magnitude of the repulsion; whereas the shape parameter, γ_{min}, determines the sensitivity of the repulsive force to the population diversity variation.

On the other hand, $\gamma_{d,i}^j$ is used to apply the stochastic update within the grid-like discrete variable space. In the context of MOO problems, this diversity preservation strategy facilitates convergence of the particles to different regions of the global Pareto frontier, which thereby helps to capture the full Pareto frontier. The probability threshold determining the stochastic update in the discrete space is based on the pre-defined value of γ_{d0}.

7.2 Numerical Experiments

Two different classes of popular benchmark MOO problems are considered to validate and investigate the performance of MO-MDPSO. These two classes are: (I) continuous unconstrained MOO problems, and (II) continuous constrained MOO problems. Table 7.1 lists the values of the user-defined parameters for these numerical experiments. Details of numerical experiments in Classes I and II are discussed in the following subsections.

7.2.1 Numerical Experiments with Continuous Benchmark Problems

First, the MO-MDPSO algorithm is validated using a series of well-known **unconstrained** (benchmark) test functions for bi-objective optimization problems (Class I), which include the second function used by Fonseca and Fleming in [145], the test function used by Coello et al. [146], two Schaffer functions [94], and five Zitzler Deb Thiele's (ZDT) functions [147]. The characteristics of these test problems and the corresponding allowed number of function evaluations are listed in Table 7.2. It is important to note that the Pareto frontiers of Coello, Shaffer 2, and ZDT 3 are disconnected, whereas those of Fonseca 2, ZDT 2, and ZDT 6 are nonconvex.

The maximum number of function evaluations allowed for the ZDT test problems in existing literature is $25,000$. To demonstrate and test the fast convergence feature of PSO, in this paper, the maximum allowable function evaluations for the five ZDT functions is deliberately set to $10,000$. For the rest of the test problems in Class I, 2000 function evaluations are allowed.

In Class II, we apply the MO-MDPSO algorithm to five continuous **constrained** (benchmark) MOO problems. Table 7.3 lists the characteristics of these five test problems and the corresponding allowed number of function evaluations. The maximum allowable function evaluations for each of these five test problems is set to $10,000$. A brief description of each constrained problem is provided below:

BNH This is the second test function used by Binh and Korn [148]. The Pareto frontier for this problem is connected and has a convex geometry.

CONSTR This problem was recommended by Deb [95]. The Pareto frontier of CONSTR is a concatenation of an unconstrained region and the boundary of the first constraint.

Table 7.2: Continuous unconstrained bi-objective optimization problems

Function name	Number of variables	Max. Function evaluations	Actual Pareto frontier
Coello	2	2,000	D
Fonseca 2	3	2,000	C/NV
Schaffer 1	1	2,000	C/V
Schaffer 2	1	2,000	D/V
ZDT 1	30	10,000	C/V
ZDT 2	30	10,000	C/NV
ZDT 3	30	10,000	D/V
ZDT 4	10	10,000	C/V
ZDT 6	10	10,000	C/NV

C: connected
D: disconnected
V: convex
NV: nonconvex

KITA This test problem was used by Kita et al. [149]. It includes three linear inequality constraints. The Pareto frontier in this case lies inside the feasible space.

SRN This problem was used in the study by Srinivas and Deb [150]. This test function includes two second-order nonlinear objectives, one linear inequality constraint, and one second-order nonlinear inequality constraint. The Pareto frontier of SRN comprises three subsets of the unconstrained region.

TNK This test problem was suggested by Tanaka et al. [151]. The design space of TNK is the same as the objective space. The Pareto frontier of TNK is disconnected, and lies along the boundary of the first constraint. The two anchor points are the intersection points of its two constraints.

Table 7.3: Continuous constrained bi-objective optimization problems

Function name	Number of variables	Max. Function evaluations	Actual Pareto frontier
BNH	2	10,000	C/V
CONSTR	2	10,000	C/V
KITA	2	10,000	D/V
SRN	2	10,000	D/V
TNK	2	10,000	D/NV

C: connected
D: disconnected
V: convex
NV: nonconvex

7.2.2 Performance Metrics

Two performance metrics introduced by Deb et al. [95] for multi-objective optimizers are used to evaluate the performance of MO-MDPSO. All distance parameters (d) considered in the two metrics are defined in the objective space. The first metric, Γ, is the accuracy metric, which measures the convergence or closeness of the computed Pareto optimal solutions to the analytical Pareto frontier (assumed known) of the MOO problem. It is given by

$$\begin{aligned} \Gamma &= \frac{\sum_{k=1}^{|\vec{S}^*|} \hat{d}_k}{|\vec{S}^*|} \\ \hat{d}_k &= \min \parallel \vec{x}_k^* - \vec{y}_l \parallel, \ \forall \vec{y}_l \in \vec{R}^*, \ l = 1, 2, \ldots, |\vec{R}^*| \\ &\text{where } \vec{x}_k^* \in \vec{S}^*, \ k = 1, 2, \ldots, |\vec{G}| \end{aligned} \tag{7.18}$$

In Eq. 7.18, $\vec{R}^*$ is the reference set of uniformly distributed solutions lying on the actual Pareto frontier, and $\vec{S}^*$ is the set of Pareto optimal solutions computed by MO-MDPSO; $\hat{d}_k$ represents the Euclidean distance between the k^{th} solution in $\vec{S}^*$ and its closest neighbor from the reference set $\vec{R}^*$. In this paper, 500 solutions are uniformly generated in $\vec{R}^*$ ($|\vec{R}^*| = 500$)

to evaluate Γ. Based on Eq. 7.18, a smaller value of Γ indicates a better accuracy.

The second metric, Δ, measures the uniformity of the obtained solutions in terms of their spatial distribution along the obtained Pareto frontier, which is given by

$$\Delta = \frac{d_f + d_l + \sum_{k=1}^{|\vec{S}^*|-1} \frac{|d_k - \bar{d}|}{|\vec{S}^*| - 1}}{d_f + d_l + (|S| - 1)\bar{d}} \tag{7.19}$$

In Eq. 7.19, d_f and d_l are the Euclidean distances between the two extreme solutions in $\vec{R}^*$ and $\vec{S}^*$, respectively; and $\bar{d}$ is the averaged inter-solution distance in $\vec{S}^*$, which is given by

$$\bar{d} = \frac{\sum_{k=1}^{|\vec{S}^*|-1} d_k}{|\vec{S}^*| - 1} \tag{7.20}$$

where d_k is the distance between two consecutive (the k^{th} and the $(k+1)^{th}$) Pareto optimal solutions in $\vec{S}^*$. Here, the solutions in $\vec{S}^*$ are sorted in the increasing order of one of the objectives. The closer the value of Δ to 0, the better the distribution of the obtained Pareto optimal solutions.

7.2.3 Results and Discussion

In this subsection, the results of the Classes I and II for MO-MDPSO are discussed. The Sobol's quasirandom sequence generator [143] is applied to prepare the initial population of particles for each test problem. Additionally, each test problem in Classes I and II is run 30 times to compensate for the impact of random parameters and then compared with the known analytical Pareto frontier both graphically and through the performance metrics, Γ and Δ.

7.2.3.1 Class I: Unconstrained Continuous Bi-objective Optimization Problems

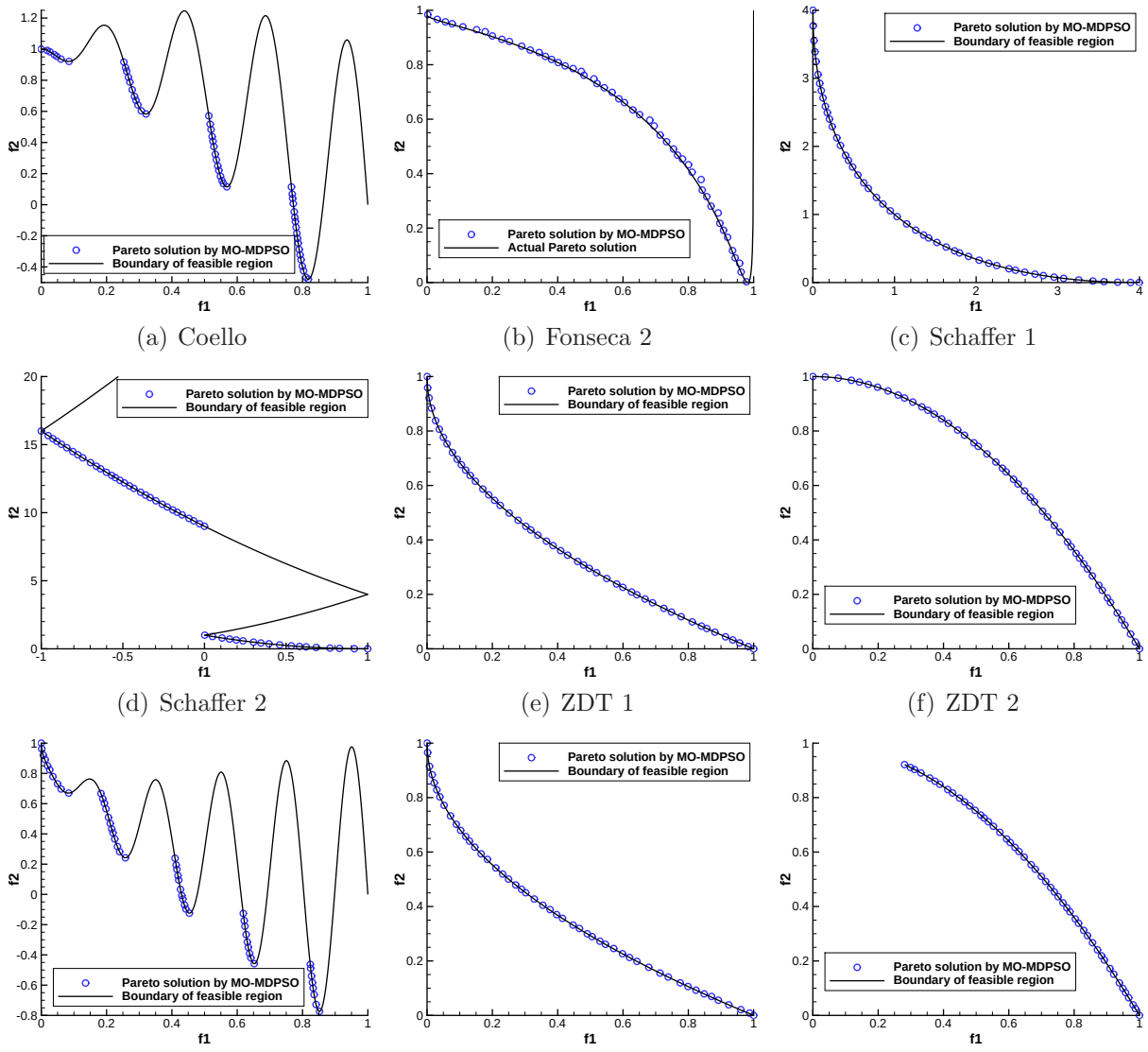

(a) Coello (b) Fonseca 2 (c) Schaffer 1

(d) Schaffer 2 (e) ZDT 1 (f) ZDT 2

(g) ZDT 3 (h) ZDT 4 (i) ZDT 6

Figure 7.2: Pareto optimal solutions obtained by MO-MDPSO for Class I problems

Figures 7.2(a) – 7.2(i) show the best Pareto optimal solutions (among the 30 runs) obtained for each test problem (blue circles), as well as the boundary of the feasible region (black curve)[2]. The results obtained using MO-MDPSO show promising agreement with the actual solutions in all the nine Class I test problems. Only in the case of Fonseca 2 problem, a few of the computed Pareto optimal solutions are not fully converged to the analytical

Table 7.4: Accuracy (Γ) metric for test problems in Class I

Test function		MO-MDPSO	NSGA-II Real-coded	NSGA-II Binary-coded	SPEA	PAES	MPP
Coello	μ_Γ	$8.2e-3$	N/A	N/A	N/A	N/A	$5.0e-2$
	σ_Γ	$1.2e-3$	N/A	N/A	N/A	N/A	N/A
Fonseca 2	μ_Γ	$4.4e-3$	$1.9e-3$	$2.6e-3$	$1.3e-1$	$1.5e-1$	$8.2e-3$
	σ_Γ	$4.6e-4$	0.0	0.0	$3.8e-5$	$9.1e-4$	N/A
Schaffer 1	μ_Γ	$9.0e-3$	$3.4e-3$	$2.8e-3$	$3.4e-3$	$1.3e-3$	N/A
	σ_Γ	$1.1e-3$	0.0	$1.0e-6$	0.0	$3.0e-6$	N/A
Schaffer 2	μ_Γ	$1.3e-2$	N/A	N/A	N/A	N/A	N/A
	σ_Γ	$1.1e-3$	N/A	N/A	N/A	N/A	N/A
ZDT 1	μ_Γ	**8.9e-4**	$3.3e-2$	$8.9e-4$	$1.8e-3$	$8.2e-2$	$4.5e-2$
	σ_Γ	$1.2e-4$	$4.7e-3$	0.0	$1.0e-6$	$8.7e-3$	N/A
ZDT 2	μ_Γ	**7.5e-4**	$7.2e-2$	$8.2e-4$	$1.3e-3$	$1.3e-1$	$1.2e-1$
	σ_Γ	**7.5e-3**	$3.2e-2$	0.0	0.0	$3.7e-2$	N/A
ZDT 3	μ_Γ	**4.2e-3**	$1.1e-1$	$4.3e-2$	$4.8e-2$	$2.4e-2$	$2.0e-2$
	σ_Γ	**4.0e-4**	$7.9e-3$	$4.2e-5$	$4.7e-5$	$1.0e-5$	N/A
ZDT 4	μ_Γ	1.4	$5.1e-1$	3.2	7.3	$8.5e-1$	$6.5e-1$
	σ_Γ	2.0	$1.2e-2$	7.3	6.6	$5.3e-1$	N/A
ZDT 6	μ_Γ	**4.6e-2**	$3.0e-1$	7.8	$2.2e-1$	$8.6e-2$	$2.3e-1$
	σ_Γ	$5.3e-2$	$1.3e-2$	$1.7e-3$	$4.0e-4$	$6.7e-3$	N/A

Table 7.5: Uniformity (Δ) metric for test problems in Class I

Test function		MO-MDPSO	NSGA-II Real-coded	NSGA-II Binary-coded	SPEA	PAES	MPP
Coello	μ_Δ	0.57	N/A	N/A	N/A	N/A	1.17
	σ_Δ	$2.9e-2$	N/A	N/A	N/A	N/A	N/A
Fonseca 2	μ_Δ	0.58	0.38	0.39	0.79	1.16	0.42
	σ_Δ	$1.5e-2$	$6.4e-4$	$1.3e-3$	$5.5e-3$	$8.9e-3$	N/A
Schaffer 1	μ_Δ	**0.21**	0.48	0.45	1.02	1.06	N/A
	σ_Δ	$1.2e-2$	$3.5e-3$	$2.1e-3$	$4.4e-3$	$2.9e-3$	N/A
Schaffer 2	μ_Δ	0.96	N/A	N/A	N/A	N/A	N/A
	σ_Δ	$2.9e-3$	N/A	N/A	N/A	N/A	N/A
ZDT 1	μ_Δ	**0.20**	0.39	0.46	0.78	1.23	0.59
	σ_Δ	$4.0e-2$	$1.9e-3$	$4.2e-2$	$4.4e-3$	$4.8e-3$	N/A
ZDT 2	μ_Δ	**0.20**	0.43	0.43	0.75	1.17	0.78
	σ_Δ	$4.0e-2$	$4.7e-3$	$2.5e-2$	$4.5e-3$	$7.7e-3$	N/A
ZDT 3	μ_Δ	**0.54**	0.74	0.58	0.67	0.79	0.73
	σ_Δ	$4.0e-2$	$2.0e-2$	$5.1e-3$	$3.6e-3$	$1.6e-3$	N/A
ZDT 4	μ_Δ	0.83	0.70	0.48	0.80	0.87	1.48
	σ_Δ	$1.6e-2$	$6.5e-2$	$9.8e-3$	$1.5e-2$	$1.0e-1$	N/A
ZDT 6	μ_Δ	**0.60**	0.67	0.64	0.85	1.15	0.71
	σ_Δ	$2.4e-2$	$9.9e-3$	$3.5e-2$	$2.7e-3$	$3.9e-3$	N/A

Pareto frontier. It is also observed that the Pareto optimal solutions are evenly distributed in all the Class I test problems.

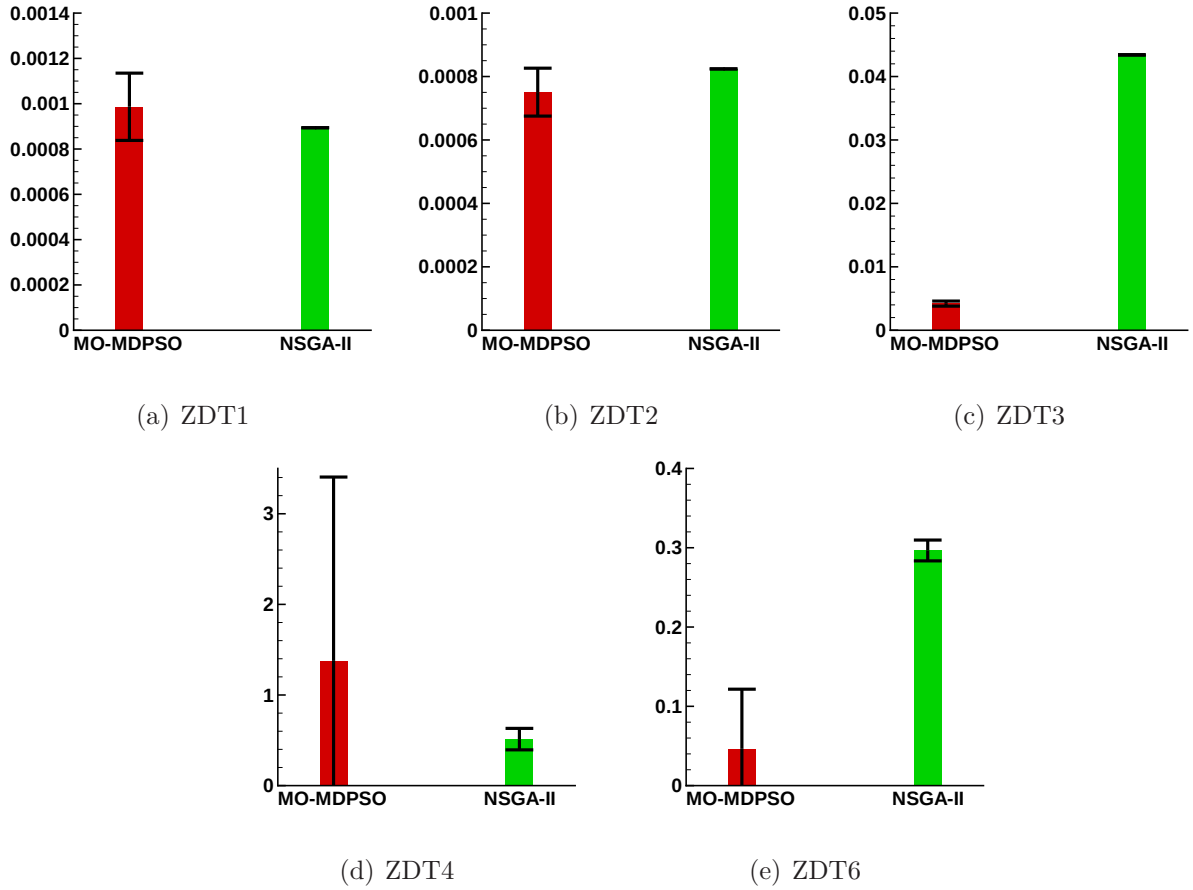

(a) ZDT1 (b) ZDT2 (c) ZDT3

(d) ZDT4 (e) ZDT6

Figure 7.3: Bar plot of accuracy metric for ZDT problems

Table 7.4 and Table 7.5 present the mean and standard deviation of Γ and Δ, respectively, estimated over 30 runs for each Class I test problem. The mean of the performance metrics represents the goodness and the standard deviation represents the robustness in the context of the respective performance metrics. The smaller the value, the better it is in all these cases. The performances of other powerful population-based MOO algorithms (as reported in the literature) are also included in this table for the purpose of explorative comparison. These algorithms are: (i) NSGA-II (real-coded and binary-coded) [95], (ii) SPEA [96], (iii) PAES [152], and (iv) MPP [100]. The performance metrics of these algo-

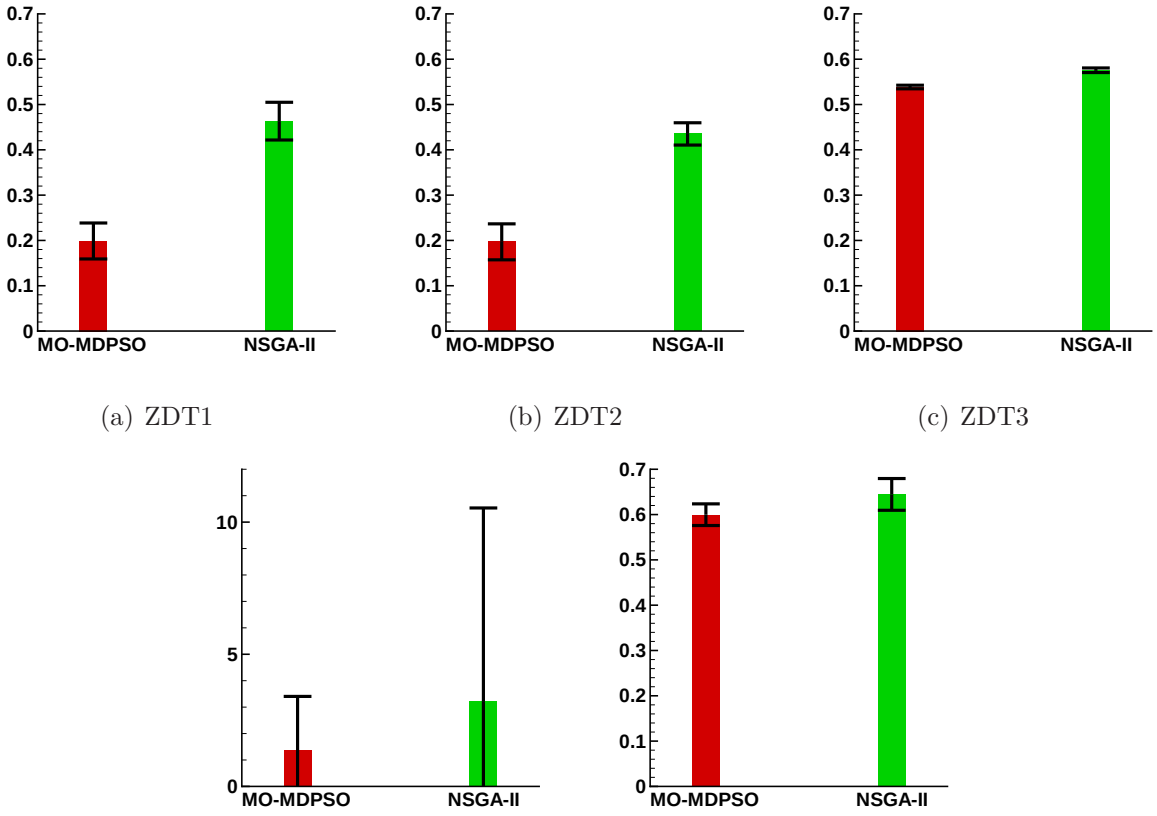

(a) ZDT1 (b) ZDT2 (c) ZDT3

(d) ZDT4 (e) ZDT6

Figure 7.4: Bar plot of uniformity metric for ZDT problems

rithms, as shown in Tables 7.4 and 7.5, are adopted from Deb et al. [95] and Chowdhury et al. [134]. Performance metrics information of SPEA, NSGA-II, and PAES for Schaffer 2 and Coello test functions, and that of MPP for Schaffer 1 and Schaffer 2 test functions, are however not readily available. The standard deviation values of Γ and Δ are also not provided by Chowdhury et al. [134], and hence not included here.

In addition, to better illustrate the comparison between MO-MDPSO and NSGA-II, Figs. 7.3 and 7.4 show the bar plots of Γ and Δ for the five ZDT test problems.

Compared to NSGA-II, SPEA, PAES, and MPP, MO-MDPSO provides better performance in terms of solution convergence and uniformity (mean values) for the Schaffer 1 and all the ZDT test functions except ZDT 4. The two versions of the NSGA-II algorithm

perform the best in the cases of Fonseca 2 and ZDT 4 test functions. However, it is important to note that the performance metrics of NSGA-II were obtained under 25,000 function evaluations, and both versions of NSGA-II were unable to converge to the analytical Pareto frontier of ZDT 4 in any of the test runs, whereas MO-MDPSO converged to the analytical Pareto frontier 10 times out of the 30 runs in this test problem. The standard deviation of the two performance metrics for MO-MDPSO is greater than that for the other algorithms in several cases, which can be attributed to the use of a relatively high number of random parameters in MO-MDPSO.

7.2.3.2 Class II: Constrained Continuous Bi-objective Optimization Problems

Table 7.6: Performance indicators for Class II

Function	Accuracy (Γ)		Uniformity (Δ)	
	μ_Γ	σ_Γ	μ_Δ	σ_Δ
BHN	0.1342	0.0157	0.3519	0.0221
CONSTR	0.0071	$7.6e-4$	0.5554	0.0397
KITA	0.0090	$8.1e-4$	0.2998	0.0239
SRN	0.5435	0.0844	0.7284	0.0040
TNK	0.0085	0.0010	0.7299	0.0835

The best Pareto optimal solutions obtained by MO-MDPSO (blue circles) and the boundary of the feasible region (black curve)[2] for Class II test problems are shown in Figs. 7.5(a) – 7.5(e). The Pareto optimal solutions are observed to be well distributed, and show promising agreement with the actual Pareto frontier. Only in the case of the TNK problem, some regions of the Pareto frontier are more sparsely covered than others (although the entire Pareto frontier has been adequately captured). The evenness of the distribution of the Pareto optimal solutions in TNK could be improved if the prescribed parameters are

[2]This is the boundary of the feasible region in the objective space also containing the actual Pareto frontier

Table 7.7: Mixed-integer constrained multi-objective optimization problems

Function property	MINLP
No. of design variables	6
No. of discrete variables	3
No. of constraints	9
Max. function evaluations	10,000

specifically tuned for this problem. Table 7.6 lists the mean and the standard deviation of Γ and Δ for the Class II test problems.

7.3 Numerical Experiment with Mixed Integer and Practical MOO Problems

In this section, we apply MO-MDPSO to solve a mixed-integer MOO problems: an analytical MINLP problem. Table 7.1 lists the prescribed parameters used for the mixed-discrete MOO problems. The characteristics of these problems and the corresponding allowed numbers of function evaluations are given in Table 7.7.

7.3.1 Results of Mixed-Integer MOO Problems

For the MINLP problems, no analytical Pareto frontier is available. Hence, to investigate the performance of MO-MDPSO, the computed Pareto optimal solutions are compared with those obtained using NSGA-II (binary-coded). The comparison is made between the best results of MO-MDPSO and NSGA-II, out of 10 runs of each algorithm.

The analytical MINLP problem, which is adapted from Dimkou [153], involves three continuous variables, x_1, x_2, x_3, and three binary variables, $y_1, y_2, y_3 \in \{0, 1\}$. The formula-

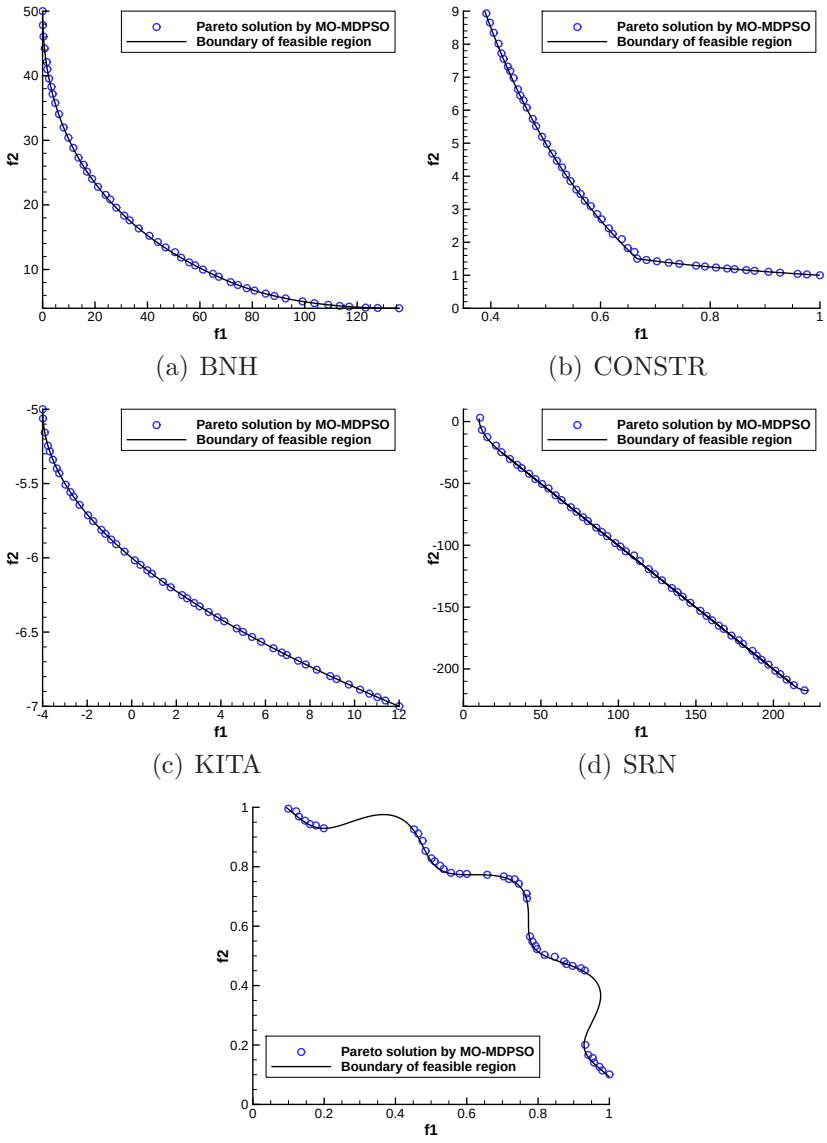

(a) BNH (b) CONSTR

(c) KITA (d) SRN

(e) TNK

Figure 7.5: Pareto optimal solutions obtained by MO-MDPSO for Class II problems

tion of this problem is given by

$$\begin{aligned} \min \quad & f_1 = x_1^2 - x_2 + x_3 + 3y_1 + 2y_2 + y_3 \\ \min \quad & f_2 = 2x_1^2 + x_2 - 3x_3 - 2y_1 + y_2 - 2y_3 \\ s.t. \quad & \\ & g_1 = 3x_1 - x_2 + x_3 + 2y_1 \leq 0 \\ & g_2 = 4x_1^2 + 2x_1 + x_2 + x_3 + y_1 + 7y_2 \leq 40 \\ & g_3 = -x_1 - 2x_2 + 3x_3 + 7y_3 \leq 0 \end{aligned} \tag{7.21}$$

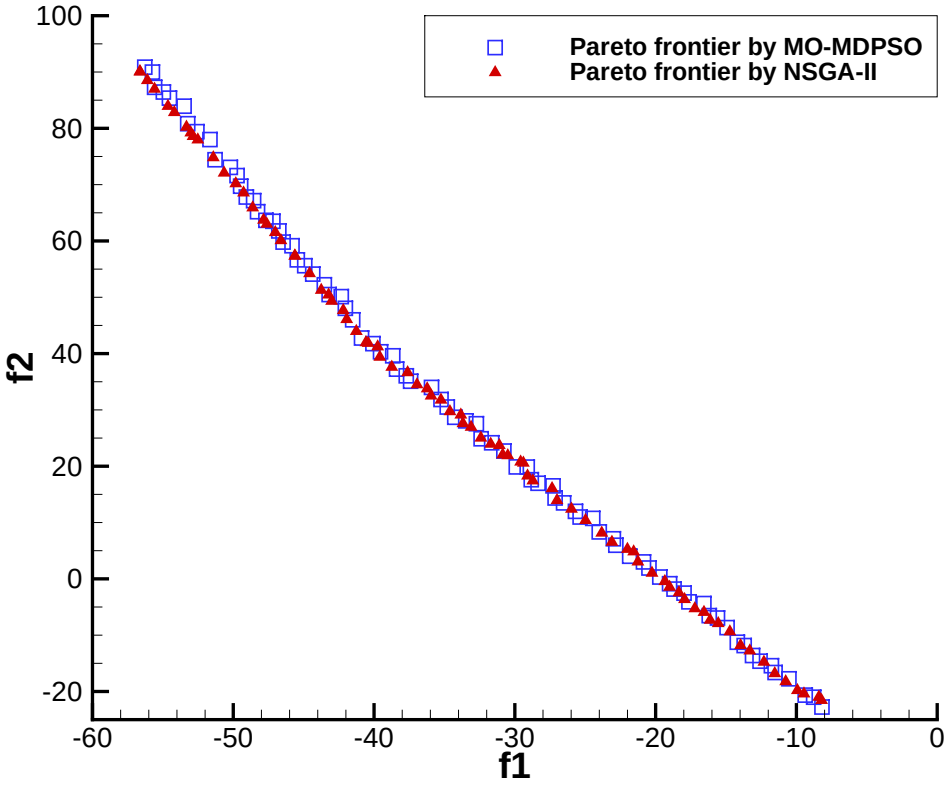

Figure 7.6: Pareto optimal solutions for the MINLP problem

Figure 7.6 shows the Pareto frontiers obtained using MO-MDPSO and NSGA-II. It is observed that the overall distribution of Pareto optimal solutions yielded by MO-MDPSO (blue squares) is practically similar to that yielded by NSGA-II (red triangles). Starting with the same initial population size (100), MO-MDPSO is able to obtain 100 Pareto optimal solutions, whereas NSGA-II obtained 78 Pareto optimal solutions (might be attributed to the prescribed parameter values).

7.4 Chapter Summary

In this chapter, we presented the development of a multi-objective advancement of the mixed-discrete PSO algorithm. This algorithm is designed to coherently address the

major attributes of complex engineering optimization problems, namely, **multiple objectives, high nonlinearity, non-convex Pareto frontier, constraints, and mixture of continuous and discrete design variables**.

MO-MDPSO has the following distinguished features from other variants of MOPSO:

1. The multi-domain diversity preservation technique coherently manages discrete variables and population diversity. Specifically, a dynamic control scheme is applied to each particle to explicitly adjust their motion, which involves (i) applying an increasing repulsion velocity away from the global leader of a particle when a greater number of particles appear to be clustering towards that particular global leader, and (ii) improving the evenness of the distribution of non-dominated solutions in the global set.

2. A special particle-sensitive concept for the selection of local and global leaders was developed and used to introduce multi-objective capabilities into the MDPSO algorithm. This concept allows MO-MDPSO to retain the original dynamics of the basic PSO, such that the fast convergence feature can be maintained. The overall crowding distance of the members in the concerned local/global set and a stochastic process are used to select the local/global leader based on the estimated population diversity.

Three classes of benchmark test problems were used to test the effectiveness of MO-MDPSO. For unconstrained and constrained continuous MOO problems, MO-MDPSO provided promising results, as evident from the successful convergence of its Pareto solutions to the analytical/exact Pareto front. Compared the results of MO-MDPSO with those yielded by five major MOO algorithms, MO-MDPSO comes out on top (in terms of accuracy and uniformity) in more than 35% of the cases. The MO-MDPSO was then tested on two MINLP problems, where the results obtained compare favorably with those yielded by NSGA-II.

CHAPTER 8

Practical Application using the Multi-Objective Mixed-Discrete Particle Swarm Optimization Algorithm

In this chapter, we apply MO-MDPSO to solve practical engineering multi-objective optimization problems, including (i) a disc brake design problem, (ii) multi-objective wind farm layout optimization problem, and (iii) multi-objective wind farm optimization considering different land plot availability

8.1 Disc Brake Design

In the disc brake design problem, reported by Osyczka and Kundu [154], there are two design objectives: minimize the mass of the brake and minimize the stopping time. Four design variables are considered, including the inner radius of the discs (x_1), the outer radius of the discs (x_2), the engaging force (x_3), and the number of friction surfaces (x_4), where x_4 is an integer variable. There are five inequality constraints that relate to the surface area, length of the brake, pressure, torque, and temperature. The optimization problem is

formulated as

$$
\begin{aligned}
\min \quad & f_1 = 4.9 \times 10^{-5}(x_2^2 - x_1^2)(x_4 - 1) \\
\min \quad & f_2 = \frac{9.82 \times 10^6 (x_2^2 - x_1^2)}{x_3 x_4 (x_2^3 - x_1^3)} \\
s.t. \quad & \\
& g1 = 20 - (x_2 - x_1) \leq 0 \\
& g2 = 2.5(x_4 + 1) - 30 \leq 0 \\
& g3 = \frac{x_3}{\pi(x_2^2 - x_1^2)} - 0.4 \leq 0 \\
& g4 = \frac{2.22 \times 10^{-3} x_3 (x_2^3 - x_1^3)}{(x_2^2 - x_1^2)^2} - 1 \leq 0 \\
& g5 = 900 - \frac{2.66 \times 10^{-2} x_3 x_4 (x_2^3 - x_1^3)}{(x_2^2 - x_1^2)} \leq 0
\end{aligned}
\tag{8.1}
$$

where

$$
\begin{aligned}
55 \leq \quad & x_1 \quad \leq 80 \\
75 \leq \quad & x_2 \quad \leq 110 \\
1000 \leq \quad & x_3 \quad \leq 3000 \\
2 \leq \quad & x_4 \quad \leq 20
\end{aligned}
$$

Figure 8.1 shows the Pareto optimal solutions for the disc brake design problem, obtained using MO-MDPSO and NSGA-II. Since the problem has a very small number of design variables, both algorithms finished (under the same number of function evaluations) within 1 minute. The Pareto optimal solutions yielded by MO-MDPSO and NSGA-II are observed to lie on the actual boundary of the feasible region in the objective space. On a detailed examination of the Pareto frontier (Fig. 8.1), it is found that NSGA-II does not capture the upper anchor point (the solution with the minimum stopping time). This ob-

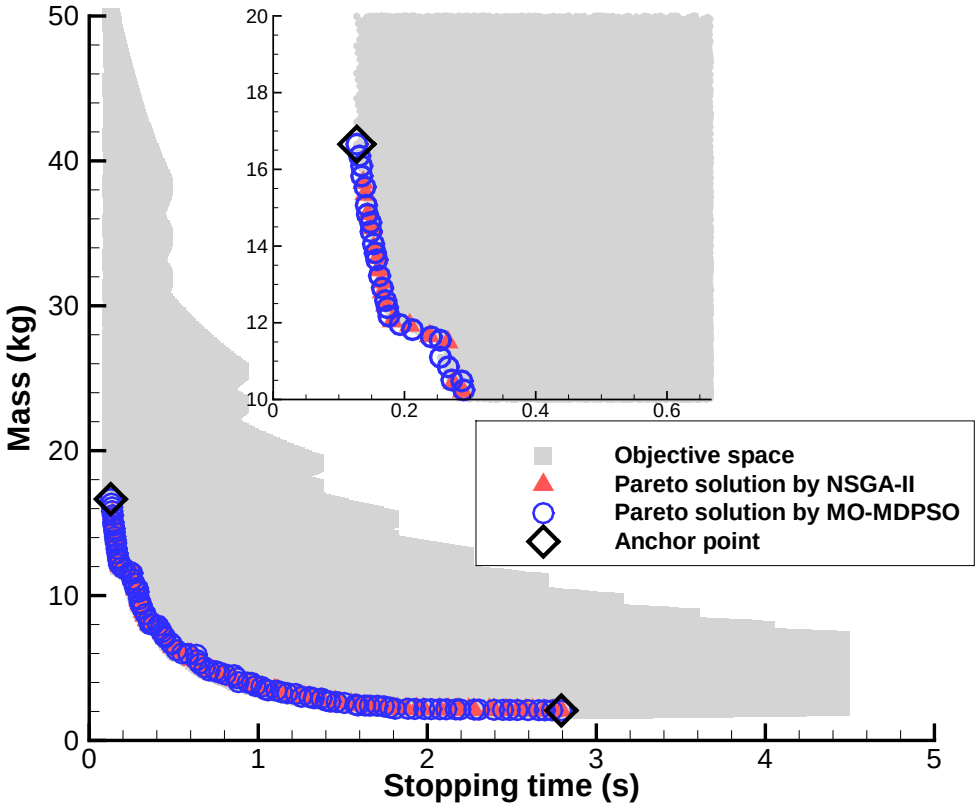

Figure 8.1: Pareto optimal solutions for disc brake design

servation might be due to the use of the original authors' prescribed values of NSGA-II parameters (with no dedicated tuning).

8.2 Multi-Objective Wind Farm Layout Optimization

The energy losses in a wind farm can be primarily attributed to the wake effects, which causes velocity deficits downstream of a turbine. In practice, WFLO can be applied to plan the arrangement of turbines, generally with the objective to minimize the wake-induced energy losses. On the other hand, the scope of layout design itself depends on the specified farm land usage, where the latter also regulates the net impact on surroundings (e.g., noise impact and impact on local wildlife) [155].

The WFLO problem considered here involves two objectives: (i) minimize the unit

Table 8.1: User-defined parameters in MO-MDPSO

Parameter	Wind farm optimization problem
w	0.5
C_1	1.5
C_2	1.5
γ_{c0}	3.0
γ_{min}	$1e-05$
γ_{d0}	1.5
λ	0.1
Capacity of local set $\|\vec{L}\|$	10
Capacity of global set $\|\vec{G}\|$	20
Population size N_p	500

Table 8.2: Mixed-integer constrained multi-objective optimization problems

Function property	Wind farm optimization
No. of design variables	150
No. of discrete variables	50
No. of constraints	300
Max. function evaluations	750,000

land footprint (denoted by the land area per MW installed) and (ii) maximize the wind farm capacity factor (CF), which is defined as the ratio of the actual energy production to the energy that could have been produced if the wind farm always operated at its rated capacity. The optimization problem is formulated as

$$\begin{aligned} & \min \left[CF(\vec{V}), A_{MW}(\vec{V})\right] \\ & \vec{V} = \{x_1, x_2, \ldots, x_{N_t}, y_1, y_2, \ldots, y_{N_T}, \\ & \qquad T_1, T_2, \ldots, T_{N_t}\} \\ s.t. & \\ & g(\vec{V}) \geq 1.5(D^{T_k} + D^{T_l}) \\ & k, l \in 1, 2, \ldots, N_T \end{aligned} \tag{8.2}$$

where A_{MW} is the land area per MW installed; N_T is the number of turbines; D is the turbine rotor diameter; and $\vec{V}$ represents the design vector, which includes $2N_t$ continuous variables representing turbine coordinates (x and y) and N_t integer variables representing turbine configurations (T). In this case study, $N_t = 25$, and 16 candidate turbine configurations are considered for selection. Figure 8.2(b) lists the principal features of these turbines, which are adopted from specifications reported by major turbine manufacturers. We implement MO-MDPSO to solve this multi-objective WFLO problem. The properties of the problem are listed in Table 8.2. Table 8.1 provides the user-defined parameters setup of the MO-MDPSO.

In Eq. 8.2, the capacity factor of the wind farm, CF, is computed using the power generation model and wind distribution model provided by the UWFLO framework [43]. This model estimates the wind farm power generation as a function of the incoming wind conditions, the turbine features, and the location of turbines. The land area per MW installed, A_{MW}, is determined by the land usage model [156], where the land area for any given layout of turbines can be estimated without prescribing the farm boundaries. The constraint $g(\vec{V})$ in Eq. 8.2 represents the minimum requirement for the inter-turbine spacing requirement, where the distance between any pair of turbines (Turbine-k and Turbine-l) must be no less than 1.5 times of the sum of their rotor diameters, i.e., $1.5(D^{T_k} + D^{T_l})$. Here, $g(\vec{V})$ can be expressed as

$$g(\vec{V}) = \sqrt{(x_k - x_l)^2 + (y_k - y_l)^2} \tag{8.3}$$

$$\forall k, l \in 1, 2, \ldots, N_t, \ \textit{and} \ k \neq l$$

where (x_k, y_k) and (x_l, y_l) respectively represent the coordinates of Turbine-k and Turbine-l.

The wind distribution considered in this case study is generated using the daily averaged data for wind speed and direction (from years 2000 to 2009) at the Baker station

in North Dakota [157]. The variation of wind conditions at this site is illustrated by the wind rose diagram in Fig. 8.2(a). The user-defined parameters in MO-MDPSO for this optimization problem are listed in Fig. 8.2(b).

Figure 8.2(c) shows the best tradeoffs between CF and A_{MW} obtained using MO-MDPSO. Based on the user-specified pruning of the global set, 20 Pareto optimal solutions are obtained, and are observed to be well-distributed in the objective space. From these results, the Pareto frontier for this WFLO problem appears to be non-convex. The solid lines and the dashed lines in Fig. 8.2(c) represent the averaged land usage of US commercial wind utilities in 2009 (34.5 ha/MW), and the standard deviation in land usage (22.4 ha/MW) [133]. It is observed from the Pareto optimal solutions that the wind farm capacity factor varies from 44.1% to 54.7%, at the cost of an increase in unit land footprint from 19.0 ha/MW to 83.5 ha/MW. This observation indicates that on average a 1.0% increase in capacity factor requires 6.1 ha/MW more land usage under optimal turbine selection and placement for the given wind conditions. At the same time, from the nature of the Pareto solutions, it can be inferred that increasing land area beyond 45 ha/MW provides diminishing returns in terms of capacity factor appreciation.

For 50 turbines MO-WFLO considering turbine type selection, the computational time using MO-MDPSO is approximately 3 minutes.

Figures 8.2(d) to 8.2(f) respectively illustrate the optimal wind farm layouts for Solution-A, Solution-B, and Solution-C, which are three widely distributed Pareto optimal solutions (as indicated in Fig. 8.2(c)).

These optimal layout designs provide the location of turbines, the selected turbine types, and the site orientation. The location of turbines is represented by square symbols with the turbine type number shown in the center of the symbol. The turbine symbols are

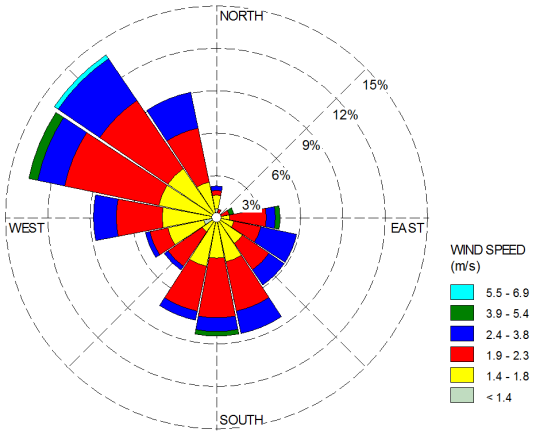

(a) Wind rose diagram for Baker state, ND (between years 2000 and 2009)

Turbine type	Rated power (MW)	Rotor diameter (m)	Hub height (m)
1	0.8	48.0	60.0
2	0.8	52.9	75.0
3	0.85	58.0	65.0
4	0.85	52.0	74.0
5	0.9	44.0	65.0
6	1.25	64.0	65.0
7	1.5	77.0	80.0
8	1.5	86.6	85.0
9	1.6	82.5	100.0
10	1.6	100.0	80.0
11	1.8	100.0	105.0
12	1.8	90.0	95.0
13	2.0	90.0	125.0
14	2.3	113.0	99.5
15	2.3	101.0	80.0
16	2.5	100.0	85.0

* : These features correspond to commercial turbines offered by major global manufacturers

(b) Major features of candidate turbines

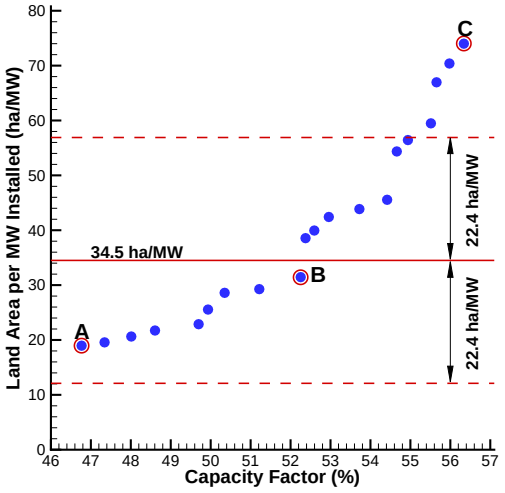

(c) Capacity factor – unit land footprint trade-off

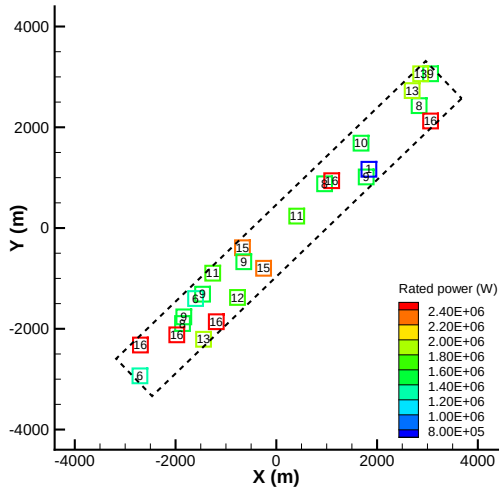

(d) Optimal layout for Solution-A (CF = 46.77%)

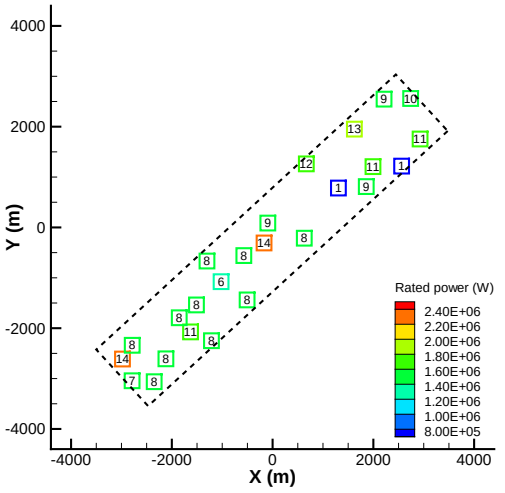

(e) Optimal layout for Solution-B (CF = 52.25%)

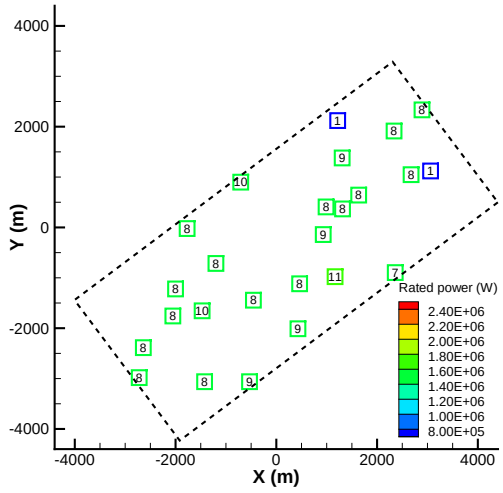

(f) Optimal layout for Solution-C (CF = 56.34%)

Figure 8.2: Results of multi-objective wind farm optimization

colored based on their rated power. The black dashed line represents the optimal layout-based wind farm boundary. It is observed that both Solution-A and Solution-B include 10 different types of turbines, while Solution-C includes 6 different types of turbines. Turbine types No.1 and No.7 − No.11 are selected by all three designs. No.8 is the most popularly chosen turbine type among the optimal layout designs.

It is interesting to note (from Figs. 8.2(a) to 8.2(c)) that, although the three optimal layout designs offer very different tradeoffs between CF and land area, they involve strikingly similar land orientation (NE-SW). Essentially, the farm site is stretched out along the direction that is approximately perpendicular to the dominating wind direction for this particular site (wind coming from NW as shown in Fig. 8.2(a)). The aspect ratio of the land (length/breath ratio) spanned by the optimal layout however varies significantly − decreases with increasing land usage.

In addition, the range of the predicted CF can be significantly improved if turbine type selection is enabled. Compared to the case study presented in Sec. 5.2, Chapter 5, where identical turbines (turbine Type-8) were considered, the predicted CF obtained from multiple-turbine case is approximately 10% better.

8.3 Multi-Objective Wind Farm Optimization Considering Different Land Plot Availability

Most onshore wind farms normally have turbines placed in discrete land plots due to imposed constraints. Landowner participation is one of the most commonly imposed constraints, which plays an important role in wind farm planning. During the early stage, in order to capture the wind above the associated land property, wind farm developers need to lease the land so as to have the right to install turbines. The landowner then receives the

lease payments from the concerned wind energy project through the lease term which may last for several decades. When wind farm developers make an offer to landowners, some of them may be much interested in participating in the project while others may not. Studies reported by Chen and MacDonald have shown how landowner participation affects the COE of a wind energy project [41, 158].

In practice, landowner participation is determined by many human involved uncertainties. For the sake of simplicity, this paper used a *binary participation scenario*, which indicates that a landowner is decided or undecided to participate in the concerned wind energy project. This scenario is based on the assumption of an initial survey on a representative farm site that has totally 16 landowners.

Table 8.3: Case study setup

Parameter	Case study 1	Case study 2	Case study 3
Number of turbines	50	50	50
Available types of turbines	16	16	16
Plots allowable to use	All 16 plots	8 specified plots	No more than arbitrary 6 plots

Three case studies will be conducted in this paper to implement the MOWFD methodology with/without the consideration of landowner participation. Table 8.3 lists the parameters setup of all case studies. Below are the assumptions applied to each of these three case studies:

1. The target farm site is uniformly owned by all the 16 landowners;
2. 16 types of turbines are available to select as provided in Fig. 8.2(b);
3. Identical turbines are considered;
4. A local wind distribution is considered as shown in Fig. 8.2(a); and

5. An onshore wind farm scenario is assumed, and the ambient turbulence (10%) is constant over the entire farm site.

8.3.1 Case Study 1

In Case study 1, we assume that all landowners are willing to participate. Since all land plots are available to install turbines, based on the observation of optimal layouts, the best portion (land plots) of the wind farm site which are suitable to install turbines can be found. The bi-objective WFLO problem of Case I then is defined as

$$
\begin{aligned}
&\min\left[\mathrm{COE}(V,T), A_{MW}(V,T)\right] \\
&V = \{x_1, x_2, \cdots, x_N, y_1, y_2, \ldots, y_N\} \\
&T \in \{1, 2, \ldots, 16\} \\
&\textit{subject to} \\
&g_1(V,T) \leq 0 \\
&X^{min} \leq x_i \leq X^{max} \\
&Y^{min} \leq y_i \leq Y^{max} \\
&\text{where} \\
&i = 1, 2, \ldots, N
\end{aligned}
\tag{8.4}
$$

In Eq. 8.4, N is the number of turbines installed; $\mathrm{COE}(V,T)$ and $A_{MW}(V,T)$ are the objectives functions considered; V and T are design variables, representing the location of turbines and the type of turbines, respectively; (X^{min}, X^{max}, Y^{min}), and Y^{max}) defines the boundary of the concerned wind farm; and $g_1(V,T)$ represents the inter-turbine spacing

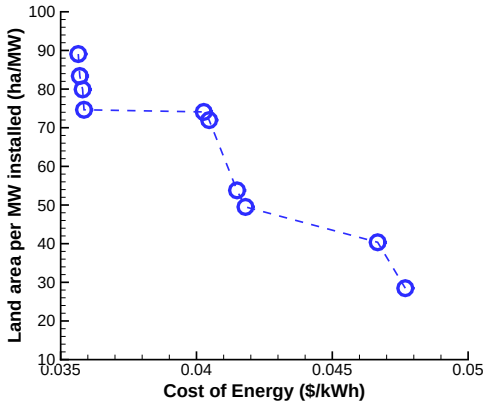

(a) Case I: The tradeoff between COE and unit land footprint

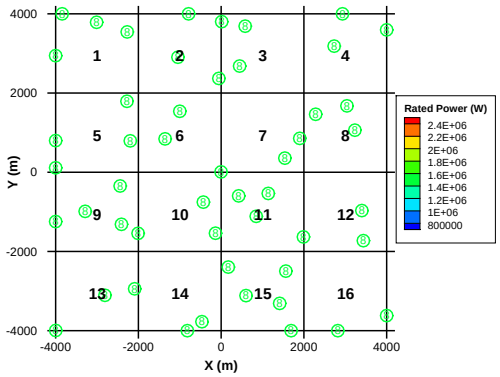

(b) The optimal solution with the minimum COE ($COE = 0.0356$\$/kWh, $A_{MW} = 89.07$ha/MW)

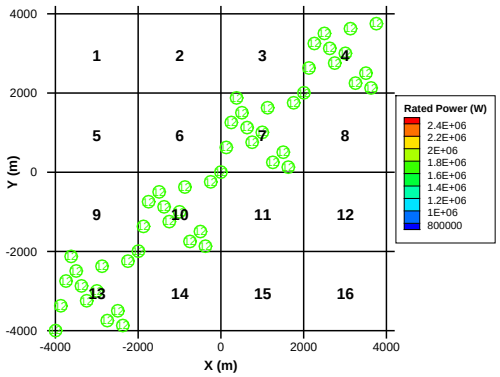

(c) The optimal solution with the minimum LAMI ($COE = 0.0477$\$/kWh, $A_{MW} = 28.48$ha/MW)

Figure 8.3: The optimization results of Case I (with all land plots available)

constraint between turbines, which is given by

$$g_1(V,T) = \sum_{i,j=1 \ and \ i \neq j}^{N} \max\left\{\left[1.5(D_{T_k} + D_{T_l}) - d_{ij}\right], 0\right\} \tag{8.5}$$

where

$$d_{ij} = \sqrt{(x_i - x_j)^2 + (y_i - y_j)^2}$$

Here D_T is the rotor diameter attribute to a certain type of turbine, T_k or T_l, and $k = l$ if identical turbines are assumed.

Figure 8.3 presents the WFLO results using **identical** turbines. It can be observed

from Fig. 8.3(b) that turbines are placed in all land plots, whereas in Fig. 8.3(c) turbines are mainly placed in the diagonal land plots. This is because that the former case has a relatively large inter-turbine spacing that causes less wake losses. Together with a relatively smaller turbine selection (Type 8), the minimum COE is then obtained. In contrast, the latter case has the minimum unit land footprint. However, to produce more energy with a relatively crowded turbine arrangement, the obtained layout is perpendicular to the dominant wind direction. This is the advantage of using the OL-based land usage model, in which the farm orientation can be automatically determined during the optimization process.

8.3.2 Case Study 2

In Case II, the location of turbines is restricted to those plots belonging to landowners who decided (to participate). Based on the results obtained from Case I, we assume that landowners 3, 4, 6, 7, 9, 10, 11, and 13 are willing to participate. The bi-objective WFLO problem of Case II is then defined as

$$
\begin{aligned}
&\min\left[\mathrm{COE}(V,T), A_{MW}(V,T)\right] \\
&V = \{x_1, x_2, \cdots, x_N, y_1, y_2, \ldots, y_N\} \\
&T \in \{1, 2, \ldots, 16\} \\
&\textit{subject to} \\
&g_1(V,T) \leq 0 \\
&g_2(V,T) \leq 0 \\
&X^{min} \leq x_i \leq X^{max} \\
&Y^{min} \leq y_i \leq Y^{max} \\
&\text{where} \\
&i = 1, 2, \ldots, N
\end{aligned}
\tag{8.6}
$$

It is noted that an additional constrained $g2(V,T)$, is added to Eq.(8.4), representing the restriction to the landowners who decided, which is given by

$$g_2(V,T) = \sum_{i=1}^{N}\sum_{p} \min\left\{\max[X_p^{min} - x_i, x_i - X_p^{max}, 0], \max[Y_p^{min} - y_i, y_i - Y_p^{max}, 0]\right\} \tag{8.7}$$

where $p = 3, 4, 6, 7, 9, 10, 11, 13$.

In Eq. 8.7, (X_p^{min}, X_p^{max}, Y_p^{min}, and Y_p^{max}) indicates the boundary of land plot belonging to the decided Landowner-p. Figure 8.4 shows the WFLO results of Case II. It can be observed that all turbines are strictly placed in the land plots belong to those landowners who decided. It is also noted that the obtained Pareto frontier in Case II (Fig. 8.4(a)) has a poor distribution, and a smaller variation of COE comparing to that in Case I. This can be attributed to the restrictions from the landowners, which makes the optimization problem highly constrained. Since the available land plots are limited, the inter-turbine space is relatively larger than the scenario in Case I. In addition, Type 2 and Type 7 turbines are respectively selected for the minimum COE and the minimum LAMI situations, of which scales are relatively smaller than those selected in Case I.

8.3.3 Case Study 3

In Figs. 8.4(b) and 8.4(c), we notice that land plots 6 and 11 are hardly used. To further explore the performance of the MOWFD methodology, the total number of plots to install turbines is limited to a maximum of 6 in Case III. In this case, the constrained

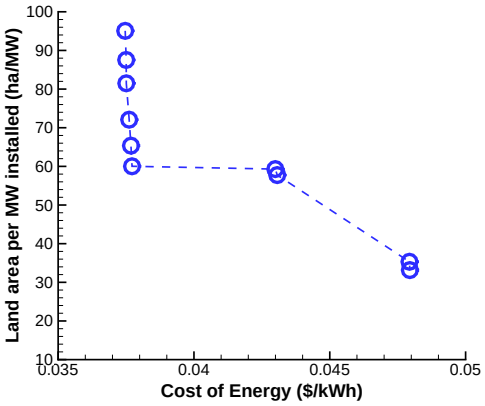

(a) Case II: The tradeoff between COE and unit land footprint

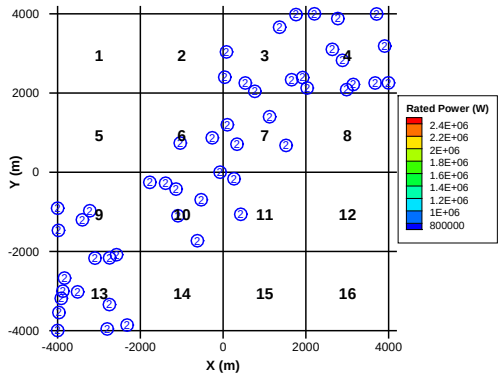

(b) The optimal solution with the minimum COE ($COE = 0.0375$\$/kWh, $A_{MW} = 95.07$ha/MW)

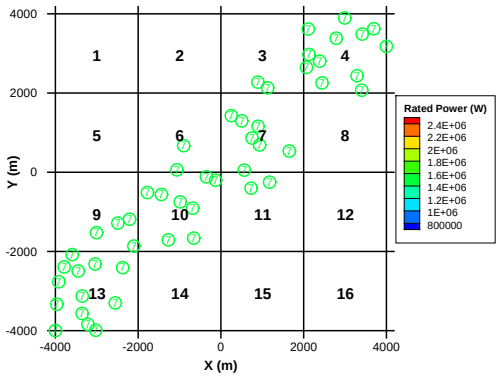

(c) The optimal solution with the minimum LAMI ($COE = 0.0479$\$/kWh, $A_{MW} = 33.17$ha/MW)

Figure 8.4: The optimization results of Case II (with 8 specified land plots available)

bi-objective optimization problem is formulated as

$$\begin{aligned} &\min\left[COE(V,T), A_{MW}(V,T)\right] \\ &V = \{x_1, x_2, \cdots, x_N, y_1, y_2, \ldots, y_N\} \\ &T \in \{1, 2, \ldots, 16\} \end{aligned}$$

subject to

$$\begin{aligned} &g_1(V,T) \leq 0 \\ &g_3(V,T) \leq 6 \\ &X^{min} \leq x_i \leq X^{max} \\ &Y^{min} \leq y_i \leq Y^{max} \end{aligned} \tag{8.8}$$

where

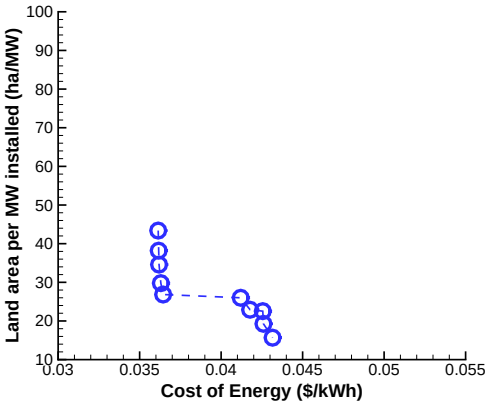

(a) Case III: The tradeoff between COE and unit land footprint

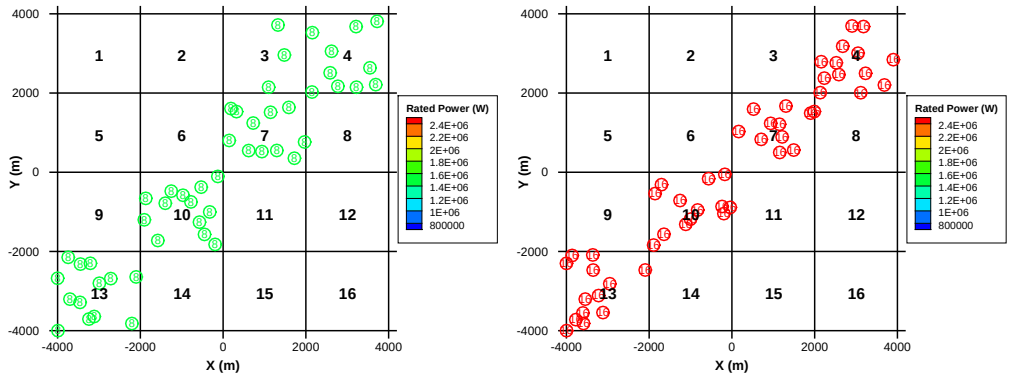

(b) The optimal solution with the minimum COE ($COE = 0.0361$\$/kWh, $A_{MW} = 43.39$ha/MW)

(c) The optimal solution with the minimum LAMI ($COE = 0.0432$\$/kWh, $A_{MW} = 15.67$ha/MW)

Figure 8.5: The optimization results of Case III (with the maximum of 6 arbitrary land plots available)

Here, $g_3(V)$ is the constraint of the maximum land usage, which is given by

$$\begin{aligned} &\forall p = 1, 2, \ldots, 16 \\ &g_3(V) = \sum_{i=1}^{N} \sum_{p=1}^{16} u(x_i) \end{aligned} \tag{8.9}$$

where

$$u(x_i) = \begin{cases} 1, & X_p^{min} \leq x_i \leq X_p^{max} \text{ and } Y_p^{min} \leq y_i \leq Y_p^{max}; \\ 0, & \text{otherwise} \end{cases}$$

The WFLO results of Case III are shown in Figure 8.5. Since fewer land plots are available to use, the spread (in the objective space) of the obtained Pareto frontier is significantly reduced, as shown in Fig. 8.5(a). It is very interesting to note that, with the maximum allowable number of land plots, all turbines are still placed in the diagonal land plots, which is similar to the scenario shown in Case II. Another interesting observation is that Type 8 and Type 16 are selected for the cases of extreme solutions in the Pareto frontier, of which scales are larger than the situations in Cases I and II.

It is important to note that both the numbers of land plots used (as shown in Figs. 8.5(b) and 8.5(c)) are fewer than the maximum allowable number. This is mainly because that we use the same parameters in all the optimization performances of the three case studies. The Pareto frontier of Case III could have further shifted to the left-bottom corner if we specifically tune the parameters for this case.

PART IV

Conclusion

CHAPTER 9

Conclusion and Future Work

This chapter summarizes the key observations and accomplishments of the research presented in this dissertation. In addition, we also present an overview of potential improvements to the algorithms and methods developed.

9.1 Conclusion

9.1.1 Multi-Objective Wind Farm Design

In this dissertation, the Multi-Objective Wind Farm Design (MOWFD) methodology was developed for the conceptual design of wind farms. Wind farm design is a complex process that involves many mutually-correlated factors affecting the quality of a wind energy project. The influence of these factors exists not only in different stages of wind farm development but also spans across the different scales in the entire wind farm system. The literature survey shows that there are significant gaps in the understanding of the intricate relationship among the different natural and design factors that affect the productivity, socio-economic, and environmental impact of a wind farm. Wind farm design problem is essentially multi-objective. However, a majority of the existing wind farm design frameworks focus on solving single objective optimizations. A major contribution of this dissertation is the sensitivity analysis-based investigation of the coupled role of the natural and design factors in wind farm design. The resulting increased understanding will allow wind farm developers and stakeholders are able to make time-efficient decisions that are associated with the benefits and impacts of the concerned wind energy project.

The complexity in the multi-objective wind farm design problems also demands the exploration of the tradeoffs between the primary performance criteria and the ability to systematically address a high-dimensional design space and highly nonlinear constraints. Due to the lack of information in the early stage, exploring the best tradeoffs is particularly important in the conceptual design phase of wind farm development.

In this dissertation, three primary performance objectives in wind farm design were considered and evaluated within the MOWFD methodology, including (i) the annual energy production, (ii) the cost of energy, and (iii) the unit land footprint. The tradeoffs between these objectives were also successfully explored.

Additionally, it is important to note that the distinguished funtions/features of MOWFD rely on the incorporated algorithms and models that have been published. For example, the current MOWFD methodology incorporates one of the most advanced energy production model offered by UWFLO framework; its multi-objective optimizations, MO-MDPSO, is capable of addressing most of the complex attributes in wind farm design. Because of that, MOWFD can also be implemented in other engineering fields, such as solar farms, which also have uncertain resource and generally large land usage.

Overall, MOWFD provides wind farm developers a comprehensive conceptual design tool. It helps reduce undesirable delays and facilitate the concept-to-installation process.

9.1.2 Consideration of Land Configuration

Land usage plays an important role in the early stage of wind farm planning. Many planning activities involve analysis and considerations directly related to the land usage (e.g., negotiation with local landowners, project sizing, and permitting). Conventional wind farm design frameworks generally prescribe the wind farm boundaries and/or the number of

turbines. In practice, wind farm siting should explore the maximum energy potential of the candidate sites under different land resource availability. Using prescribed conditions limits the exploration of feasible wind farm layout prospects, thus restricting the flexibility and efficiency of the planning process.

The layout-based land usage model, developed in this dissertation, enables the WFLO to be performed without limiting prescribed wind farm boundaries, and allows automatic determination of the best land area and land shape. This land usage model computes the land area of any given candidate layout during the optimization procedure. The Graham scan algorithm is applied to determine the 2D convex hull enclosing all turbines. The calipers algorithm is then applied to find the smallest bound rectangle to represent the wind farm land shape. By applying this land usage model in the case study (in Section 5.2, Chapter 5), it was observed that the wind farm site orientation can be automatically determined during the optimization procedure as well.

It should be noted that this land usage model can be used to represent the land shape of a wind farm in terms of any other geometric shape (e.g., triangle, circle, or polygon), as is compatible with the local distribution of land plots at the site.

9.1.3 Parameterization of Key Tradeoffs in Wind Farm Design

The Pareto shifting technique developed in this dissertation allows wind farm developers to study the impact of changes in site-scale decisions (e.g., installed capacity). A case study was used to illustrate this approach, in which regression models were used to fit the tradeoffs between the capacity factor and the unit land footprint. The coefficients of the best regression model are parameterized using the installed capacity, thus allowing an effective and efficient exploration of the best tradeoffs subject to different installed capacity decisions.

This readily allows determination and visualization of the best trade-offs at any site-scale decision within the range, at a reasonable computational expense. There are very few such computational tools in fundamental trade-off analysis.

Together with the land usage model, the MOWFD methodology can perform WFLO without limiting prescribed conditions, leading to a complete exploration of the best trade-offs in the feasible design space. Moreover, the Pareto shifting technique provides valuable insights to wind farm developers and significantly streamlines the wind farm planning process.

9.1.4 Multi-Objective Mixed-Discrete Particle Swarm Optimization

The major complex attributes addressed in the multi-objective wind farm design problems are: (i) high nonlinearity, (ii) high dimensional design domain, (iii) presence of nonlinear constraints, (iv) function multimodality, and (v) mixture of discrete and continuous variables. Depending on the characteristics of the performance objectives in a wind energy project (e.g., AEP), a significant amount of computational time is required to evaluate the candidate solutions, thereby also demanding a computationally efficient optimization process. To address these challenges, fundamental advancements were made to the powerful single-objective Mixed-Discrete PSO (MDPSO) algorithm:

1. *Multi-Objective Search Strategy*: the Pareto-dominance strategy was used, in which local sets were created for each particle to store local non-dominated solutions; whereas the global set was created and maintained by applying the Pareto filter to the stored solutions in all local sets.

2. *Leader Selection Mechanism*: the selection mechanism of local and global leaders was developed based on the overall crowding distance of the members in the concerned

local/global set. A stochastic process was developed to regulate the leader selection mechanism based on the estimated population diversity.

3. *Population Diversity Preservation*: the population diversity in multi-objective was measured based on the hypercube enclosing all particles. Considering the impact of outlier particles, multiple fractional domains were formed with respect to the positions of the corresponding global leaders. This multi-domain diversity preservation technique is essential to generate evenly distributed Pareto optimal solutions.

The performance of MO-MDPSO was investigated using a suite of benchmark problems and practical constrained mixed-discrete optimization problems. Comparison of MO-MDPSO with other popular multi-objective optimizers (e.g., NSGA-II) was also conducted. The results showed that MO-MDPSO is highly competitive with other popular algorithms (in terms of the accuracy and diversity). Overall, the important modifications described above illustrate the unique features of the developed MO-MDPSO algorithm, which makes influential contribution to the PSO family in solving complex MOO problems.

9.2 Future Work

This section further elaborates a number of issues that should be investigated based on the foundation provided by this dissertation and the potential future research directions.

9.2.1 Quantification of Wind Farm Performance

The quantification of energy production (or the power generation) of a wind energy project is one the most fundamental criteria. In this dissertation, we used the energy production model offered by the UWFLO framework to estimate the wake-induced energy losses. This model quantifies the energy production as a function of the incoming wind conditions,

the location of turbines, and turbine features. It also accounts for a variable induction factor, wake merging and overlapping, and wind shear effects. Future work should consider the impacts of topography and turbulence, which can be integrated into the UWFLO energy production model.

Owing to the high computational cost by high-fidelity wake models (CFD-based), the wake behaviors in this research was computed using analytical wake models (low-fidelity). However, a mid-fidelity wake model is desired in WFLO, which balances the accuracy and the computational efficiency. Surrogate modeling techniques and analyses of different wake model under various scenarios (e.g., single-turbine and multi-turbine) are necessary to develop such a wake model, which could provide an acceptable level of accuracy and computational cost.

The land usage model is capable of representing the wind farm boundaries in terms of different geometric shapes, such as circle, eclipse, triangle, and 2D convex polygon. Therefore, the land shape can be treated as a discrete design variable in WFLO. In addition, since the environmental impact is strongly regulated by land usage, dedicated models that quantitatively relate the different impact attributes (e.g., noise impact and impact on wildlife) to land usage should be developed.

9.2.2 Implementation of Parameterization of Tradeoffs

The Pareto shifting technique presented in this research suggests a promising research direction. Limitation(s) of this technique should be explored both practically and theoretically. Moreover, in the case study, the coefficients in the regression models (fitted using Pareto optimal solutions under different values of installed capacity) are quantified by a single variable (the installed capacity). Future research should seek multivariate implementations.

9.2.3 Multi-Domain Diversity Preservation in MO-MDPSO

The current version of the multi-domain diversity preservation technique measures the population diversity using the ratio of the volume of the smallest hypercube enclosing all particles to that of the design space. A fractional domain is created with respect to the position of each global leader, and its size is determined by a pre-defined parameter that is used to screen out outlier particles to the corresponding global leader. However, in multi-objective problems, the number of solutions "following" each global leader is also important. To better reflect the number of "followers" of each global leader, immediate future work is needed to develop a new population diversity measure with respect to each global leader. This development could also improve the robustness and increase the convergence speed of MO-MDPSO.

REFERENCES

[1] Global Wind Energy Council (GWEC), "Global wind report − annual market update 2013," www.gwec.net/publications/global-wind-report-2/global-wind-report-2013/, April 2014.

[2] American Wind Energy Association (AWEA), "Wind was largest source of new electricity in 2014," www.awea.org/MediaCenter/pressrelease.aspx?ItemNumber=7294, March 2015, last accessed Apr. 2015.

[3] U.S. Energy Information Administration (EIA), "Electric power monthly − with data for december 2014," www.eia.gov/electricity/monthly/pdf/epm.pdf, February 2015, last accessed Apr. 2015.

[4] U.S. Department of Energy (DOE), "20% Wind Energy by 2030: Increasing Wind Energy's Contribution to U.S. Electricity Supply," energy.gov/sites/prod/files/2013/12/f5/41869.pdf, July 2008, last accessed Apr. 2015.

[5] M. N. El-Kordy, M. A. Badr, K. A. Abed, and S. M. A. Ibrahim, "Economical evaluation of electricity generation considering externalities," *Renewable Energy*, vol. 25, no. 2, pp. 317–328, February 2002.

[6] International Renewable Energy Agency (IRENA), "Cost analysis of wind power," www.irena.org/DocumentDownloads/Publications/RE_Technologies_Cost_Analysis-WIND_POWER.pdf, June 2012, last accessed Apr. 2015.

[7] IRENA, "Renewable power generation costs in 2014," www.irena.org/

DocumentDownloads/Publications/IRENA_RE_Power_Costs_2014_report.pdf, January 2015, last accessed Apr. 2015.

[8] S. Krohn (editor), P.-E. Morthorst, and S. Awerbuch, "The economics of wind energy," The European Wind Energy Association (EWEA), Tech. Rep., March 2009.

[9] M. I. Blanco, "The economics of wind energy," *Renewable and Sustainable Energy Reviews*, vol. 13, no. 6-7, pp. 1372–1382, AugustSeptember 2009.

[10] Douglas-Westwood Ltd., "Offshore wind assessment for norway," The Research Council of Norway, Oslo, Norway, Tech. Rep., March 2010.

[11] U.S. Department Of Energy (DOE), "Revolution now: The future arrives for four clean energy technologies 2014 update," energy.gov/sites/prod/files/2014/10/f18/revolution_now_updated_charts_and_text_october_2014_1.pdf, October 2014, last accessed Apr. 2015.

[12] U.S. Energy Information Administration (EIA), "Annual energy outlook 2014 with projections to 2040," www.eia.gov/forecasts/aeo/pdf/0383(2014).pdf, April 2014, last accessed Apr. 2015.

[13] The European Wind Energy Association (EWEA), *Wind Energy - The Facts: A Guide to the Technology, Economics and Future of Wind Power*, 1st ed. Routledge, March 2009.

[14] J. S. Rodrigo, "State-of-the-art of wind resource assessment," Wind Resource Assessment Audit and Standardization (WAUDIT), Tech. Rep., March 2010.

[15] J. Zhang, "Hybrid and uncertainty-based surrogate modeling with applications to

wind energy," Ph.D. dissertation, Rensselaer Polytechnic Institute, Troy, New York, July 2012.

[16] Siting Subcommittee, National Wind Coordinating Committee (NWCC), "Permitting of wind energy facilities," nationalwind.org/wp-content/uploads/assets/publications/permitting2002.pdf, August 2002, last accessed Apr. 2015.

[17] Windustry, "The community wind toolbox," January 2008, last accessed Apr. 2015.

[18] U.S. Department of the Interior, Bureau of Land Management (BLM), "Final programmatic environmental impact statement on wind energy development on BLM-administered lands in the western United States," windeis.anl.gov/documents/fpeis/maintext/Vol1/Vol1Complete.pdf, June 2005, last accessed Apr. 2015.

[19] Committee on Environmental Impacts of Wind Energy Projects, National Research Council (NRC), *Environmental Impacts of Wind-Energy Projects*. Washington, DC: The National Academies Press, May 2007.

[20] International Energy Agency (IEA), "Technology roadmap: Wind energy," www.iea.org/publications/freepublications/publication/Wind_2013_Roadmap.pdf, October 2013, last accessed Apr. 2015.

[21] IEA, "How2guide for wind energy: Roadmap development and implementation," www.iea.org/publications/freepublications/publication/How2GuideforWindEnergyRoadmapDevelopementandImplementation.pdf, February 2014, last accessed Apr. 2015.

[22] S. Rynne, L. Flowers, E. Lantz, and E. Heller, Eds., *Planning for Wind Energy*.

Chicago, IL: American Planning Association (APA) Planning Advisory Service, November 2011.

[23] D. Christie and M. Bradley, "Optimising land use for wind farms," *Energy for Sustainable Development*, vol. 16, no. 4, pp. 471–475, December 2012.

[24] V. Nelson, *Introduction to Renewable Energy*. Boca Raton, FL: CRC Press, January 2011.

[25] Department for Business Enterprise and Regulatory Reform (BERR), UK, "Review of cabling techniques and environmental effects applicable to the offshore wind farm industry," webarchive.nationalarchives.gov.uk/+/http:/www.berr.gov.uk/files/file43527.pdf, January 2008, last accessed Apr. 2015.

[26] M. Ehrgott and X. Gandibleux, "A survey and annotated bibliography of multiobjective combinatorial optimization," *OR Spectrum*, vol. 22, no. 4, pp. 425–460, November 2000.

[27] W. Tong, S. Chowdhury, and A. Messac, "A multi-objective mixed-discrete particle swarm optimization with multi-domain diversity preservation," January 2015, submitted to Structural and Multidisciplinary Optimization.

[28] J. Kennedy and R. Eberhart, "Particle swarm optimization," in *Proceedings of the IEEE International Conference on Neural Networks*, vol. 4, Perth, WA, USA, November 27 - December 1 1995, pp. 1942–1948.

[29] M. Dorigo, "Optimization, learning and natural algorithms," Ph.D. dissertation, Politecnico di Milano, Milano, Italy, 1992.

[30] D. Karaboga, "An idea based on honey bee swarm for numerical optimization," Erciyes University, Kayseri, Turkey, Tech. Rep. TR06, October 2005.

[31] Environmental Audit Committee, *Keeping the Lights On: Nuclear, Renewables and Climate Change*, ser. Sixth Report of Session 200506. London, UK: House of Commons, March 2006, vol. 1, no. HC 584-I.

[32] J. Annoni, P. Seiler, K. Johnson, P. Fleming, and P. Gebraad, "Evaluating wake models for wind farm control," in *Proceedings of the American Control Conference (ACC)*, Portland, OR, June 4-6 2014.

[33] N. O. Jensen, "A note on wind generator interaction," Risø National Laboratory, Roskilde, Denmark, Tech. Rep. Risø-M-2411, 1983.

[34] I. Katic, J. Højstrup, and N. O. Jensen, "A simple model for cluster efficiency," in *Proceedings of European Wind Energy Conference and Exhibition*, vol. 1, Rome, Italy, October 6-8 1986, pp. 407–410.

[35] J. N. Sørensen and A. Myken, "Unsteady actuator disc model for horizontal axis wind turbines," *Journal of Wind Engineering and Industrial Aerodynamics*, vol. 39, no. 1-3, pp. 139–149, 1992.

[36] G. C. Larsen, H. A. Madsen, F. Bingöl, J. Mann, S. Ott, J. N. Sørensen, V. Okulov, N. Troldborg, M. Nielsen, K. Thomsen, T. J. Larsen, and R. Mikkelsen, "Dynamic wake meandering modeling," Risø National Laboratory, Roskilde, Denmark, Tech. Rep. Risø-R-1607, 2007.

[37] M. Churchfield and S. Lee, "High-fidelity analysis of wind plant and wind turbine fluid physics and structural response using computational fluid dynamics (CFD) and

FAST," wind.nrel.gov/designcodes/simulators/SOWFA/, 2012, last accessed Apr. 2015.

[38] P. Fleming, P. Gebraad, M. Churchfield, S. Lee, K. Johnson, J. Michalakes, and J.-W. van Wingerden, "SOWFA+ super controller users manual," National Renewable Energy Laboratory, Golden, CO, Tech. Rep. NREL/TP-5000-59197, 2013.

[39] A. Kusiak and Z. Song, "Design of wind farm layout for maximum wind energy capture," *Renewable Energy*, vol. 35, no. 3, pp. 685–694, March 2010.

[40] B. L. Du Pont and J. Cagan, "An extended pattern search approach to wind farm layout optimization," *Journal of Mechanical Design*, vol. 134, no. 8, pp. 081 002–18, August 2012.

[41] L. Chen and E. MacDonald, "Considering landowner participation in wind farm layout optimization," *Journal of Mechanical Design*, vol. 134, no. 8, pp. 084 506–6, July 2012.

[42] J. S. González, A. G. G. Rodriguez, J. C. Mora, J. R. Santos, and M. B. Payan, "Optimization of wind farm turbines layout using an evolutive algorithm," *Energy Procedia*, vol. 35, no. 8, pp. 1671–1681, August 2010.

[43] S. Chowdhury, J. Zhang, A. Messac, and L. Castillo, "Optimizing the arrangement and the selection of turbines for wind farms subject to varying wind conditions," *Renewable Energy*, vol. 52, pp. 273–282, 2013.

[44] M. Gaumond, P.-E. Réthoré, A. Bechmann, S. Ott, G. C. Larsen, A. Pena Diaz, and K. S. Kurt, "Benchmarking of wind turbine wake models in large offshore

windfarms," in *Proceedings of the Science of Making Torque from Wind*, Oldenburg, Germany, October 9-11 2012.

[45] P. Beaucage, M. Brower, N. Robinson, and C. Alonge, "Overview of six commercial and research wake models for large offshore wind farms," in *Proceedings of the European Wind Energy Associate (EWEA)*, Copenhagen, Denmark, 2012.

[46] R. Barthelmie and S. C. Pryor, "An overview of data for wake model evaluation in the virtual wakes laboratory," *Applied Energy*, vol. 104, pp. 838–844, 2013.

[47] J. F. Herbert-Acero, O. Probst, P.-E. Réthoré, G. C. Larsen, and K. K. Castillo-Villar, "A review of methodological approaches for the design and optimization of wind farms," *Energies*, vol. 7, no. 11, pp. 6930–7016, 2014.

[48] J. Garza, A. Blatt, R. Gandoin, and S.-Y. Hui, "Evaluation of two novel wake models in offshore wind farms," in *Proceedings of the European Wind Energy Associate Offshore Conference*, Amsterdam, The Netherlands, November 29-December 1 2011.

[49] S. Ott, J. Berg, and M. Nielsen, "Linearised CFD models for wakes," Risø National Laboratory, Roskilde, Denmark, Tech. Rep. Risø-R-1772, 2011.

[50] R. J. Barthelmie, K. Hansen, S. Frandsen, O. Rathmann, J. G. Schepers, W. Schlez, J. Phillips, K. Rados, A. Zervos, E. S. Politis, and P. K. Chaviaropoulos, "Modelling and measuring flow and wind turbine wakes in large wind farms offshore," *Wind Energy*, vol. 12, no. 5, pp. 431–444, 2009.

[51] S. Frandsen, R. Barthelmie, S. Pryor, O. Rathmann, S. Larsen, J. Højstrup, and M. Thøgersen, "Analytical modelling of wind speed deficit in large offshore wind farms," *Wind Energy*, vol. 9, no. 2, pp. 39–53, 2006.

[52] R. J. Barthelmie, L. Folkerts, G. C. Larsen, K. Rados, S. C. Pryor, S. T. Frandsen, B. Lange, and G. Schepers, "Comparison of wake model simulations with offshore wind turbine wake profiles measured by sodar," *Journal of Atmospheric and Oceanic Technology*, vol. 23, no. 7, pp. 888–901, 2006.

[53] G. C. Larsen, "A simple wake calculation procedure," Risø National Laboratory, Roskilde, Denmark, Tech. Rep. Risø-M-2760, 1988.

[54] J. W. M. Dekker and J. T. G. Pierik, Eds., *European Wind Turbine Standards II*. ECN Solar & Wind Energy, 1999.

[55] T. Ishihara, A. Yamaguchi, and Y. Fujino, "Development of a new wake model based on a wind tunnel experiment," windeng.t.u-tokyo.ac.jp/ishihara/proceedings/2004-5_poster.pdf, 2004, last accessed Apr. 2015.

[56] G. Crasto, A. R. Gravdahl, F. Castellani, and E. Piccioni, "Wake modeling with the actuator disc concept," *Energy Procedia*, vol. 24, pp. 385–392, 2012.

[57] G. Mosetti, C. Poloni, and B. Diviacco, "Optimization of wind turbine positioning in large windfarms by means of a genetic algorithm," *Journal of Wind Engineering and Industrial Aerodynamics*, vol. 51, no. 1, pp. 105–116, January 1994.

[58] S. Grady, M. Hussaini, and M. Abdullah, "Placement of wind turbines using genetic algorithms," *Renewable Energy*, vol. 30, no. 2, pp. 259–270, February 2005.

[59] I. Mustakerov and D. Borissovah, "Wind turbines type and number choice using combinatorial optimization," *Renewable Energy*, vol. 35, no. 9, p. 18871894, September 2010.

[60] C. N. Elkinton, "Offshore wind farm layout optimization," Ph.D. dissertation, University of Massachusetts Amherst, Amherst, MA, September 2007.

[61] J. Castro Mora, J. M. C. Barón, J. M. R. Santos, and M. B. Payán, "An evolutive algorithm for wind farm optimal design," *Neurocomputing*, vol. 70, no. 16-18, pp. 2651–2658, October 2007.

[62] G. Marmidis, S. Lazarou, and E. Pyrgioti, "Optimal placement of wind turbines in a wind park using Monte Carlo simulation," *Renewable Energy*, vol. 33, no. 7, pp. 1455–1460, July 2008.

[63] A. Mittal, "Optimization of the layout of large wind farms using a genetic algorithm," Master's thesis, Case Western Reserve University, Cleveland, OH, May 2010.

[64] S. Şişbot, özgü Turgut, M. Tunç, and Ünal Çamdalı, "Optimal positioning of wind turbines on g¨kçeada using multi-objective genetic algorithm," *Wind Energy*, vol. 13, no. 4, pp. 297–306, May 2010.

[65] A. Emami and P. Noghreh, "New approach on optimization in placement of wind turbines within wind farm by genetic algorithms," *Renewable Energy*, vol. 35, no. 7, pp. 1559–1564, July 2010.

[66] M. Bilbao and E. Alba, "Simulated annealing for optimization of wind farm annual profit," in *Proceedings Of the 2nd International Symposium on Logistics and Industrial Informatics (LINDI)*, Linz, Austria, September 10-12 2009, pp. 1–5.

[67] B. P. Rašuo and A. Č. Bengin, "Optimization of wind farm layout," *FME Transactions*, vol. 38, no. 3, pp. 107–114, 2010.

[68] R. Archer, G. Nates, S. Donovan, and H. Waterer, "Wind turbine interference in a wind farm layout optimization mixed integer linear programming model," *Advanced Materials Research*, vol. 35, no. 2, pp. 165–175, October 2011.

[69] Y.-K. Wu, C.-Y. Lee, C.-R. Chen, K.-W. Hsu, and H.-T. Tseng, "Optimization of the wind turbine layout and transmission system planning for a large-scale offshore wind farm by AI technology," in *Proceedings of 2012 IEEE Industry Applications Society Annual Meeting (IAS)*. Las Vegas, NV: IEEE, October 7-11 2012, pp. 1–9.

[70] J. S. González, M. B. Payán, A. G. G. Rodriguez, and J. R. Santos, "Optimization of wind farm turbine layout including decision making under risk," *IEEE Systems Journal*, vol. 6, no. 1, pp. 94–102, March 2012.

[71] S. Salcedo-Sanz, D. Gallo-Marazuela, A. Pastor-Sáncheza, L. Carro-Calvoa, A. Portilla-Figuerasa, and L. Prieto, "Evolutionary computation approaches for real offshore wind farm layout: A case study in northern Europe," *Expert Systems with Applications*, vol. 40, no. 16, pp. 6292–6297, November 2013.

[72] W. Y. Kwong, P. Y. Zhang, D. Romero, J. Moran, M. Morgenroth, and C. Amon, "Multi-objective wind farm layout optimization considering energy generation and noise propagation with NSGA-II," *Journal of Mechanical Design*, vol. 136, no. 9, p. 091010, July 2014.

[73] U. A. Ozturk and B. A. Norman, "Heuristic methods for wind energy conversion system positioning," *Electric Power Systems Research*, vol. 30, no. 2, pp. 179–185, August 2004.

[74] M. A. Lackner and C. N. Elkinton, "An analytical framework for offshore wind farm layout optimization," *Wind Engineering*, vol. 31, no. 1, pp. 17–31, January 2007.

[75] S. Chowdhury, J. Zhang, A. Messac, and L. Castillo, "Unrestricted wind farm layout optimization (UWFLO): Investigating key factors influencing the maximum power generation," *Renewable Energy*, vol. 38, no. 1, pp. 16–30, February 2012.

[76] C. Vezyris, "Offshore wind farm optimization: Investigation of unconventional and random layouts," Master's thesis, Delft University of Technology, Delft, The Netherlands, June 2012.

[77] Y. Eroğlu and S. U. Seçkiner, "Design of wind farm layout sing ant colony algorithm," *Renewable Energy*, vol. 44, pp. 53–62, August 2012.

[78] C. Wan, J. Wang, G. Yang, H. Gu, and X. Zhang, "Wind farm micro-siting by Gaussian particle swarm optimization with local search strategy," *Renewable Energy*, vol. 48, pp. 276–282, December 2012.

[79] M. Song, K. Chen, Z. He, and X. Zhang, "Bionic optimization for micro-siting of wind farm on complex terrain," *Renewable Energy*, vol. 50, p. 551557, February 2013.

[80] M. Wagner, J. Day, and F. Neumann, "A fast and effective local search algorithm for optimizing the placement of wind turbines," *Renewable Energy*, vol. 51, pp. 64–70, March 2013.

[81] B. Pérez, R. Mnguez, and R. Guanche, "Offshore wind farm layout optimization using mathematical programming techniques," *Renewable Energy*, vol. 53, pp. 389–399, May 2013.

[82] J. E. G. Martínez, "Layout optimisation of offshore wind farms with realistic constraints and options," Ph.D. dissertation, Delft University of Techonology, Delft, The Netherlands, June 2014.

[83] D. Wilson, S. Cussat-Blanc, K. Veeramachaneni, U.-M. O'Reilly, and H. Luga, "A continuous developmental model for wind farm layout optimization," in *Proceedings Of the 2014 Conference on Genetic and Evolutionary Computation (GECCO)*, New York, NY, USA, July 12-16 2014, pp. 745–752.

[84] J. F. H.-A. 1, O. Probst, P.-E. Réthoré, G. C. Larsen, and K. K. Castillo-Villar, "A review of methodological approaches for the design and optimization of wind farms," *Energies*, vol. 7, no. 1, pp. 6930–7016, October 2014.

[85] A. Kusiak, Z. Zhang, and M. Li, "Optimization of wind turbine performance with data-driven models," *IEEE Transactions on Sustainable Energy*, vol. 1, no. 2, pp. 66–76, June 2010.

[86] K. Veeramachaneni, M. Wagner, U.-M. OReilly, and F. Neumann, "Optimizing energy output and layout costs for large wind farms using particle swarm optimization," in *Proceedings Of the 2012 IEEE World Congress on Computational Intelligence (WCCI)*, Brisbane, QLD, Australia, June 10-15 2012, pp. 1–7.

[87] J. S. González, M. B. Payán, A. G. G. Rodriguez, and J. R. Santos, "A new and efficient method for optimal design of large offshore wind power plants," *IEEE Transactions on Power Systems*, vol. 28, no. 3, pp. 3075–3084, August 2013.

[88] S. Chowdhury, J. Zhang, W. Tong, and A. Messac, "Modeling the influence of

land-shape on the energy production potential of a wind farm site," *Journal of Energy Resources Technology*, vol. 136, no. 1, p. 011203, February 2014.

[89] A. Banks, J. Vincent, and C. Anyakoha, "A review of particle swarm optimization. Part II: Hybridisation, combinatorial, multicriteria and constrained optimization, and indicative applications," *Natural Computing*, vol. 7, no. 1, pp. 109–124, March 2008.

[90] S. Kirkpatrick, C. D. Gelatt, and M. P. Vecchi, "Optimization by simulated annealing," *Science*, vol. 220, no. 4598, pp. 671–680, May 1983.

[91] R. A. Rivas, J. Clausen, K. S. Hansen, and L. E. Jensen, "Solving the turbine positioning problem for large offshore wind farms by simulated annealing," *Wind Engineering*, vol. 33, no. 3, pp. 287–297, May 2009.

[92] G. C. Larsen and P.-E. Réthoré, "TOPFARM − a tool for wind farm optimizationt," *Energy Procedia*, vol. 35, p. 317324, 2013.

[93] J. D. Schaffer, "Some experiments in machine learning using vector evaluated genetic algorithms," Ph.D. dissertation, Vanderbilt University, Nashville, TN, USA, 1984.

[94] J. D. Schaffer, "Multiple objective optimization with vector evaluated genetic algorithms," in *Proceedings of the 1st International Conference on Genetic Algorithms*, Pittsburgh, PA, USA, July 24-26 1985, pp. 93–100.

[95] K. Deb, A. Pratap, S. Agarwal, and T. Meyarivan, "A fast and elitist multiobjective genetic algorithm: NSGA-II," *IEEE Transactions on Evolutionary Computation*, vol. 6, no. 2, pp. 182–197, 2002.

[96] E. Zitzler and L. Thiele, "Multiobjective evolutionary algorithms: a comparative case

study and the strength Pareto approach," *IEEE Transactions on Evolutionary Computation*, vol. 3, no. 4, pp. 257–271, 1999.

[97] E. Zitzler and L. Thiele, "An evolutionary algorithm for multiobjective optimization: the strength Pareto approach," Computer Engineering and Communication Networks Lab (TIK), Swiss Federal Institute of Technology (ETH), Zürich, Switzerland, Tech. Rep. TIK-Report 43, 1998.

[98] E. Zitzler, M. Laumanns, and L. Thiele, "SPEA2: Improving the Strength Pareto Evolutionary Algorithm," in *Proceedings of the International Conference on Evolutionary Methods for Design, Optimisation, and Control with Applications to Industrial Problems*, Athens, Greece, 2001, pp. 95–100.

[99] M. Laumanns, G. Rudolph, and H.-P. Schwefel, "A spatial predator-prey approach to multi-objective optimization: A preliminary study," in *Proceedings of the 5th International Conference on Parallel Problem Solving from Nature*, Amsterdam, The Netherlands, September 2730 1998, pp. 241–249.

[100] S. Chowdhury, G. S. Dulikravich, and R. J. Moral, "Modified predator-prey algorithm for constrained and unconstrained multi-objective optimisation," *Int. J. of Mathematical Modelling and Numerical Optimisation*, vol. 1, no. 1/2, pp. 1–38, 2009.

[101] S. Lalwani, S. Singhal, R. Kumar, and N. Gupta, "A comprehensive survey: Applications of multi-objective particle swarm optimization (MOPSO) algorithm," *Transactions on Combinatorics*, vol. 2, no. 1, pp. 39–101, 2013.

[102] K. E. Parsopoulos and M. N. Vrahatis, "Particle swarm optimization method in

multiobjective problems," in *Proceedings of the ACM Symposium on Applied Computing (SAC)*, 2002, pp. 603–607.

[103] C. Coello, G. Pulido, and M. Lechuga, "Handling multiple objectives with particle swarm optimization," *IEEE Transactions on Evolutionary Computation*, vol. 8, no. 3, pp. 256–279, 2004.

[104] X. Hu and R. Eberhart, "Multiobjective optimization using dynamic neighborhood particle swarm optimization," in *Proceedings of the Congress on Evolutionary Computation (CEC)*, vol. 2, Honolulu, HI, May 12-17 2002, pp. 1677–1681.

[105] X. Hu, R. Eberhart, and Y. Shi, "Particle swarm with extended memory for multiobjective optimization," in *Proceedings of the IEEE Swarm Intelligence Symposium (SIS)*, Indianapolis, Indiana, USA, April 24-26 2003, pp. 193–197.

[106] X. Li, "A non-dominated sorting particle swarm optimizer for multiobjective optimization," in *Proceedings of the International Conference on Genetic and Evolutionary Computation (GECCO): Part I*, Chicago, IL, USA, July 1216 2003, pp. 37–48.

[107] C. R. Raquel and P. C. Naval, Jr., "An effective use of crowding distance in multiobjective particle swarm optimization," in *Proceedings of the 7th Annual Conference on Genetic and Evolutionary Computation (GECCO '05)*, 2005, pp. 257–264.

[108] H. Javanshir, S. Ebrahimnejad, and S. Nouri, "Bi-objective supply chain problem using MOPSO and NSGA-II," *International Journal of Industrial Engineering Computations*, vol. 3, no. 4, pp. 681–694, 2012.

[109] J. Chen, G. Chen, and W. Guo, "A discrete PSO for multi-objective optimization in VLSI floorplanning," in *Proceedings of the 4th International Symposium on Intelligence Computation and Applications (ISICA)*, Huangshi, China, Ocotober 23-25 2009, pp. 400–410.

[110] A. B. de Carvalho and A. Pozo, "Non-ordered data mining rules through multi-objective particle swarm optimization: Dealing with numeric and discrete attributes," in *Proceedings of the 8th International Conference on Hybrid Intelligent Systems (HIS)*, Barcelona, Spain, 2008, pp. 495–500.

[111] M. Rahimi and H. Iranmanesh, "Multi objective particle swarm optimization for a discrete time, cost and quality trade-off problem," *World Applied Sciences Journal*, vol. 4, no. 2, pp. 270–276, 2008.

[112] A. M. Sharaf and A. A. El-Gammal, "A novel discrete multi-objective particle swarm optimisation (MOPSO) technique for optimal hybrid power filter compensator schemes," *International Journal of Power and Energy Conversion*, vol. 1, no. 2/3, pp. 157–177, 2009.

[113] S. P. Venkatesan and S. Kumanan, "A multi-objective discrete particle swarm optimisation algorithm for supply chain network design," *International Journal of Logistics Systems and Management*, vol. 11, no. 3, pp. 375–406, 2012.

[114] W. Ren, Y. Xiong, and X. Hongmei, *Study on Warship Combat System Design Using DMOPSO Algorithm*. Trans. Tech. Publications, Switzerland, 2012, vol. Advanced Materials Research (482-484), ch. 9: Processing and Manufacturing, Properties and Performance, pp. 1963–1968.

[115] J. C. F. Cabrera and C. A. C. Coello, "Micro-MOPSO: A multi-objective particle swarm optimizer that uses a very small population size," in *Multi-Objective Swarm Intelligent Systems*, ser. Studies in Computational Intelligence. Springer Berlin Heidelberg, 2010, vol. 261, pp. 83–104.

[116] E. J. S. Pires, J. A. T. Machado, and P. B. de Moura Oliveira, "Entropy diversity in multi-objective particle swarm optimization," *Entropy*, vol. 15, pp. 5475–5491, 2013.

[117] M. Reyes-Sierra and C. A. C. Coello, "Multi-objective particle swarm optimizers: A survey of the state-of-the-art," *International Journal of Computational Intelligence Research*, vol. 2, no. 3, pp. 287–308, 2006.

[118] K. E. Parsopoulos and M. N. Vrahatis, *Multi-Objective Optimization In Computational Intelligence: Theory and Practice*. IGI Global, 2008, ch. II. Multi-objective Particle Swarm Optimization Approaches, pp. 20–42.

[119] U. Baumgartner, C. Magele, and W. Renhart, "Pareto optimality and particle swarm optimization," *IEEE Transactions on Magnetics*, vol. 40, no. 2, pp. 1172–1175, 2004.

[120] K. E. Parsopoulos, D. K. Tasoulis, and M. N. Vrahatis, "Multiobjective optimization using parallel vector evaluated particle swarm optimization," in *Proceedings of the IASTED International Conference on Artificial Intelligence and Applications (AIA)*, 2004, pp. 823–828.

[121] T. Ray and K. M. Liew, "A swarm metaphor for multiobjective design optimization," *Engineering Optimization*, vol. 34, no. 2, pp. 141–153, 2002.

[122] GE Energy, "GE 1 .5MW wind turbine series," geosci.uchicago.edu/~moyer/

GEOS24705/Readings/GEA14954C15-MW-Broch.pdf, March 2009, last accessed Apr. 2015.

[123] M. O. L. Hansen, *Aerodynamics of Wind Turbines*, 2nd ed. Earthscan, 2008.

[124] B. Sanderse, "Aerodynamics of wind turbine wakes," Energy research Centre of the Netherlands, Tech. Rep. ECN-06-016, 2009.

[125] L. Fingersh, M. Hand, and A. Laxson, "Wind turbine design cost and scaling model," National Renewable Energy Laboratory, Golden, CO, Tech. Rep. NREL/TP-500-40566, December 2006.

[126] E. Rosenbloom, "A Problem With Wind Power," www.aweo.org/ProblemWithWind.pdf, September 2006, last accessed Apr. 2015.

[127] R. A. McEowen, "Wind energy production: Legal issues and related liability concerns for landowners," www.calt.iastate.edu/briefs/CALT%20Legal%20Brief%20-%20Wind%20Energy%20Production.pdf, June 2011, last accessed Apr. 2015.

[128] the International Organization for Standardization (ISO), *Acoustics – Attenuation of Sound during Propagation Outdoors*, 1st ed., ser. Part 2: General Method of Calculation, Geneva, Switzerland, December 1996, no. ISO 9613-2.

[129] NWCC, "Wind turbine interactions with birds, bats, and their habitats: A summary of research results and priority questions," nationalwind.org/wp-content/uploads/assets/publications/Birds_and_Bats_Fact_Sheet_.pdf, last accessed Apr. 2015 2010.

[130] R. Graham, "An efficient algorithm for determining the convex hull f a finite planar set," *Information Processing Letters*, vol. 1, pp. 132–133, 1972.

[131] G. Toussaint, "Solving geometric problems with the rotating calipers," in *n Proceedings of IEEE Mediterranean Electrotechnical Conference (MELECON)*, Athens, Greece, May 24-26 1983.

[132] S. Chowdhury, J. Zhang, A. Messac, and L. Castillo, "Characterizing the influence of land area and nameplate capacity on the optimal wind farm performance," in *Proceedings of the ASME 6th International Conference on Energy Sustainability*, San Diego, July 23-26 2012, pp. 1349–1359.

[133] P. Denholm, M. Hand, M. Jackson, and S. Ong, "Land-use requirements of modern wind power plants in the United States," National Renewable Energy Laboratory, Golden, CO, Tech. Rep. NREL/TP-6A2-45834, August 2009.

[134] S. Chowdhury, W. Tong, A. Messac, and J. Zhang, "A mixed-discrete particle swarm optimization algorithm with explicit diversity-preservation," *Structural and Multidisciplinary Optimization*, vol. 47, no. 3, pp. 367–388, 2013.

[135] A. Saltelli and R. Bolado, "An alternative way to compute Fourier amplitude sensitivity test (FAST)," *Computational Statistics & Data Analysis*, vol. 26, no. 4, pp. 445–460, 1998.

[136] R. I. Cukier, C. M. Fortuin, K. E. Shuler, A. G. Petschek, and J. H. Schaibly, "Study of the sensitivity of coupled reaction systems to uncertainties in rate coefficients. I Theory," *Journal of Chemical Physics*, vol. 59, no. 8, pp. 3873–3878, 1973.

[137] J. H. Schaibly and K. E. Shuler, "Study of the sensitivity of coupled reaction systems to uncertainties in rate coefficients. II. Applications," *Journal of Chemical Physics*, vol. 59, no. 8, pp. 3879–3888, 1973.

[138] R. I. Cukier, H. B. Levine, and K. E. Shuler, "Study of the sensitivity of coupled reaction systems to uncertainties in rate coefficients. III. Analysis of the approximations," *Journal of Chemical Physics*, vol. 63, no. 3, 1975.

[139] R. I. Cukier, "Nonlinear sensitivity analysis of multiparameter model systems," *Journal of Computational Physics*, vol. 26, no. 1, pp. 1–42, 1978.

[140] A. Saltelli, K. Chan, and E. M. Scott, *Sensitivity Analysis*, ser. probability and statistics. Wiley, 2009.

[141] IEC-61400-1, *Wind turbines - Part 1: Design requirements*, 3rd ed., International Electrotechnical Commission, August 2005.

[142] W. Tong, S. Chowdhury, A. Mehmani, A. Messac, and J. Zhang, "Modeling the influence of land-shape on the energy production potential of a wind farm site," *Journal of Energy Resources Technology*, no. 2015, February 2015.

[143] I. M. Sobol, "On the distribution of points in a cube and the approximate evaluation of integrals," *USSR Computational Mathematics and Mathematical Physics*, vol. 7, no. 4, pp. 86–112, July 6-9 1967.

[144] A. Messac, A. Ismail-Yahaya, and C. A. Mattson, "The normalized normal constraint method for generating the Pareto frontier," *Structural and Multidisciplinary Optimization*, vol. 25, no. 2, pp. 86–98, 2003.

[145] C. M. Fonseca and P. J. Fleming, "Multiobjective genetic algorithms made easy: Selection sharing and mating restriction," in *Proceedings of the 1st International Conference on Genetic Algorithms in Engineering Systems: Innovations and Applications*, Sheffield, UK, September 12-14 1995, pp. 45–52.

[146] C. C. Coello, G. Lamont, and D. van Veldhuizen, *Evolutionary Algorithms for Solving Multi-Objective Problems*, 2nd ed. Springer US, 2007.

[147] E. Zitzler, K. Deb, and L. Thiele, "Comparison of multiobjective evolutionary algorithms: Empirical results," *Evolutionary Computation*, vol. 8, no. 2, pp. 173–195, 2000.

[148] T. T. Binh and U. Korn, "MOBES: A multiobjective evolution strategy for constrained optimization problems " in *Proceedings of the 3rd International Conference On Genetic Algorithms (MENDEL97)*, vol. 1, Brno, Czech Republic, June 1997, pp. 176–182.

[149] H. Kita, Y. Yabumoto, N. Mori, and Y. Nishikawa, "Multi-objective optimization by means of the thermodynamical genetic algorithm," in *Proceedings of the 4th International Conference on Parallel Problem Solving from Nature*, Berlin, Germany, September 2226 1996, pp. 504–512.

[150] N. Srinivas and K. Deb, "Muiltiobjective optimization using nondominated sorting in genetic algorithms," *Evolutionary Computation*, vol. 2, no. 3, pp. 221–248, September 1994.

[151] M. Tanaka, H. Watanabe, Y. Furukawa, and T. Tanino, "GA-based decision support system for multicriteria optimization," in *Proceedings of the IEEE International Conference on Systems, Man and Cybernetics*, vol. 2, Vancouver, BC, Canada, October 22-25 1995, pp. 1556–1561.

[152] J. D. Knowles and D. W. Corne, "The Pareto archived evolution strategy : A new baseline algorithm for Pareto multiobjective optimisation," in *Proceedings of the*

IEEE Congress on Evolutionary Computation (CEC), vol. 1, Washington, DC, USA, July 6-9 1999.

[153] T. I. Dimkou and K. P. Papalexandri, "A parametric optimization approach for multiobjective engineering problems involving discrete decisions," *Computers and Chemical Engineering*, vol. 2, no. Supplement 1, pp. S951–S954, March 1998.

[154] A. Osyczka and S. Kundu, "A genetic algorithm-based multicriteria optimization method," in *Proceedings of the 1st World Congress of Structural and Multidisciplinary Optimization*, Goslar, Germany, May 1995, pp. 909–914.

[155] W. Tong, S. Chowdhury, A. Mehmani, and A. Messac, "Multi-objective wind farm design: Exploring the trade-off between capacity factor and land use," in *Proceedings of the 10th World Congress on Structural and Multidisciplinary Optimization*, Orlando, FL, USA, May 19 - 24 2013.

[156] W. Tong, S. Chowdhury, and A. Messac, "A consolidated visualization of wind farm energy production potential and optimal land shapes under different land area and nameplate capacity decisions," in *Proceedings of 2014 AIAA Science and Technology Forum and Exposition*, National Harbor, MA, USA, January 13-17 2014.

[157] NDSU, "North Dakota agricultural weather network," ndawn.ndsu.nodak.edu/, 2009, last accessed Apr. 2015.

[158] L. Chen and E. MacDonald, "A system-level cost-of-energy wind farm layout optimization with landowner modeling," *Energy Conversion and Management*, vol. 77, pp. 484–494, January 2014.

WEIYANG TONG

EDUCATION

SYRACUSE UNIVERSITY, Syracuse, NY, USA

Sep 2011 – May 2015 PhD in Mechanical & Aerospace Engineering

Jan 2010 – Aug 2011 MS in Mechanical & Aerospace Engineering

BEIHANG UNIVERSITY (BUAA), Beijing, China

Sep 2006 – Jan 2009 MS in Aerospace Propulsion Theory & Engineering

Sep 2001 – Jul 2005 BE in Aerospace Power Engineering

PROFESSIONAL EXPERIENCE

September 2013 – April 2015	*Research Associate I,* Department of Aerospace Engineering Mississippi State University, Mississippi State, MS
September 2011 – August 2013	*Teaching Assistant,* Department of Mechanical & Aerospace Engineering Syracuse University, Syracuse, NY
September 2006 – January 2009	*Research Assistant,* Department of Aerospace Engineering Beihang University, Beijing, China

TEACHING EXPERIENCE

January 2015 – May 2015	Engineering Design Optimization *Instructor:* Achille Messac
January 2013 – May 2013	Senior Design Course (Mechanical Engineering) *Instructor:* Frederick J. Carranti
September 2012 – December 2012	Advanced Practical Design Optimization *Instructor:* Achille Messac
January 2012 – May 2012	Senior Design Course (Aerospace Engineering) *Instructor:* John F. Dannenhoffer, III
September 2011 – December 2011	Introduction to Practical Design Optimization *Instructor:* Achille Messac

JOURNAL ARTICLES

[1]. **Tong, W.,** Chowdhury, S., and Messac, A., Sensitivity of Wind Farm Output to Wind Conditions, Land Configuration, and Installed Capacity, Under Different Wake Models. *Journal of Mechanical Design*, doi:10.1115/1.4029892 (*In Press)*

[2]. **Tong, W.,** Chowdhury, S., and Messac, A., A Multi-objective Mixed-discrete Particle Swarm Optimization Algorithm with Multi-domain Diversity Preservation. *Structural and Multidisciplinary Optimization* (*Accepted)*

[3]. Mehmani, A., Chowdhury, S., **Tong, W.,** and Messac, A., Adaptive Switching of Variable-Fidelity Models in Population-based Optimization Algorithm. *Engineering and Applied Sciences Optimization* (*In Press*)

[4]. Victor Maldonado, Chowdhury, S., Messac, A., and **Weiyang Tong**. A New Modular Product Platform Planning Approach to Design Macro-scale Reconfigurable Unmanned Aerial Vehicles (UAVs). *Journal of Aircraft* (*Accepted*)

[5]. Chowdhury, S., Zhang, Jie, **Tong, W.,** and Messac, A., Modeling the Influence of Land-Shape on the Energy Production Potential of a Wind Farm Site. *Journal of Energy Resources Technology*, ***136***(1): 011203 (10 pages), 2013

[6]. Chowdhury, S., **Tong, W.,** Messac, A., and Zhang, Jie. A Mixed-Discrete Particle Swarm Optimization Algorithm with Explicit Diversity-Preservation. *Structure and Multidisciplinary Optimization*, ***47***(3): pp. 367-388, 2013

PEER-REVIEWED CONFERENCE PAPERS

[1]. **Tong, W.,** Chowdhury, S., and Messac, A., "Multi-Domain Diversity Preservation to Mitigate Particle Stagnation and Enable Better Pareto Converge in Mixed-Discrete Particle Swarm Optimization", Proceedings of the AIAA Aviation and Aeronautics Forum and Exposition, Dallas, Texas, USA, June 22-26, 2015

[2]. Chowdhury, S., **Tong, W.,** Mehmani, A., and Messac, A., "Visualizing Model Uncertainties in Multi-Objective Wind Farm Layout Optimization", Proceedings of the 11th World Congress on Structural and Multidisciplinary Optimization, Sydney, Australia, June 7-12, 2015

[3]. Mehmani, A., **Tong, W.,** Chowdhury, S., and Messac, A., "A Visually-Informed Decision-Making Platform for Wind Farm Layout Optimization", Proceedings of the 11th World Congress on Structural and Multidisciplinary Optimization, Sydney, Australia, June 7-12, 2015

[4]. **Tong, W.,** Chowdhury, S., and Messac, A., "Multi-Objective WindFarm Optimization Simultaneously Optimizing COE and Land Footprint of Wind Farms under Different Land Plot Availability", Proceedings of the AIAA 2015 Science and Technology Forum and Exposition, Paper No. AIAA2015-1802, Kissimmee, Florida, USA, January 5-9, 2015

[5]. **Tong, W.,** Chowdhury, S., and Messac, A., "A New Multi-Objective Mixed-Discrete Particle Swarm Optimization Algorithm", Proceedings of the ASME 2014 International Design Engineering Technical Conference (IDETC) & Computers and Information in Engineering Conference (CIE), Paper No. DETC2014-35572, Buffalo, NY, USA, August 17-20, 2014

[6]. **Tong, W.,** Chowdhury, S., and Messac, A., "A Consolidated Visualization of Wind Farm Energy Production Potential and Optimal Land Shapes under Different Land Area and Nameplate Capacity Decisions", Proceedings of the AIAA 2014 Science and Technology Forum and Exposition, Paper No. AIAA2014-0998, National Harbor, Maryland, USA, August 13-17, 2014

[7]. Chowdhury, S., Mehmani, A., **Tong, W.,** and Messac, A., "A Visually-Informed Decision-Making Platform for Model-based Design of Wind Farms", AIAA Aviation and Aeronautics Forum and Exposition, Paper No. AIAA2014-2727, Atlanta, Georgia, June 16-20, 2014

[8]. **Tong, W.,** Chowdhury, S., Mehmani, A., Zhang, Jie, and Messac, A., "Sensitivity of Array-like and Optimized Wind Farm Output to Key Factors and Choice of Wake Models", Proceedings of the ASME 2013 International Design Engineering Technical Conference (IDETC) & Computers and Information in Engineering Conference (CIE), Paper No. DETC2013-13196, Portland, OR, USA, August 4-7, 2013

[9]. Chowdhury, S., Victor Maldonado, **Tong, W.,** and Messac, A., "Comprehensive Product Platform

Planning (CP^3) for a Modular Family of Unmanned Aerial Vehicles", Proceedings of the ASME 2013 International Design Engineering Technical Conference (IDETC) & Computers and Information in Engineering Conference (CIE), Paper No. DETC2013-13181, Portland, OR, USA, August 4-7, 2013

[10]. **Tong, W.,** Chowdhury, S., Mehmani, A., and Messac, A., "Multi-Objective Wind Farm Design: Exploring the Trade-off between Capacity Factor and Land Use", Proceedings of the 10th World Congress on Structural and Multidisciplinary Optimization, Paper No. 5590, Orlando, FL, USA, May 19-24, 2013

[11]. Chowdhury, S., Victor Maldonado, **Tong, W.,** and Messac, A., "Macro-scale Reconfigurable Unmanned Aerial Vehicles for Civilian Offshore Applications", Proceedings of the 10th World Congress on Structural and Multidisciplinary Optimization, Orlando, Paper No., 5597, FL, USA, May 19-24, 2013

[12]. Mehmani, A., Chowdhury, S., Zhang, Jie, **Tong, W.,** and Messac, A., "Model Selection based on Regional Error Estimation of Surrogates", Proceedings of the 10th World Congress on Structural and Multidisciplinary Optimization, Orlando, Paper No., 5447, FL, USA, May 19-24, 2013

[13]. Mehmani, A., Chowdhury, S., Zhang, Jie, **Tong, W.,** and Messac, A., "Quantifying Regional Error in Surrogates by Modeling its Relationship with Sample Density", 54th AIAA/ASME/ASCE/AHS/ASC Structures, Structural Dynamics and Materials Conference, Paper No. AIAA 2013-1751, Boston, Massachusetts, April 8-11, 2013

[14]. **Tong, W.,** Chowdhury, S., Zhang, Jie, and Messac, A., "Impact of Different Wake Models on the Estimation of Wind Farm Power Generation", Proceedings of the 12th AIAA Aviation Technology, Integration, and Operations (ATIO) Conference and 14th AIAA/ISSMO Multidisciplinary Analysis and Optimization Conference, Paper No. AIAA2012-5430, Indianapolis, IN, USA, September 17-19, 2012

[15]. Zhang, Junqiang, Chowdhury, S., Zhang, Jie, **Tong, W.,** and Messac, A., "Optimal Preventive Maintenance Time Windows for Offshore Wind Farms Subject to Wake Losses", Proceedings of the 12th AIAA Aviation Technology, Integration, and Operations (ATIO) Conference and 14th AIAA/ISSMO Multidisciplinary Analysis and Optimization Conference, Indianapolis, IN, US, September 17-19, 2012